

**Understanding Process Performance Parameters in a Two-Step Monoclonal Antibody  
Chromatographic Purification Process**

---

**A Dissertation**

**Presented to  
the faculty of the School of Engineering and Applied Science  
University of Virginia**

---

**in partial fulfillment  
of the requirements for the degree**

**Doctor of Philosophy**

**by**

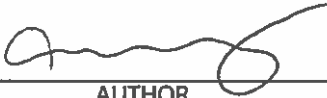
**Shaojie Zhang**

**December**

**2016**

APPROVAL SHEET

The dissertation  
is submitted in partial fulfillment of the requirements  
for the degree of  
Doctor of Philosophy

  
\_\_\_\_\_  
AUTHOR

The dissertation has been read and approved by the examining committee:

Giorgio Carta

\_\_\_\_\_  
Advisor

Kyle Lample

\_\_\_\_\_  
Geoffrey M. Geise

\_\_\_\_\_  
Ammasi Periasamy

\_\_\_\_\_  
Stacey Criswell

Accepted for the School of Engineering and Applied Science:



Craig H. Benson, Dean, School of Engineering and Applied Science

December

2016

## **Abstract**

Chromatography is used extensively to purify monoclonal antibodies (mAbs) at process scale. This work examines key performance parameters that affect the separation of such process using a two-step purification approach including Protein A (PA) capture followed by weak partitioning chromatography (WPC) with anion-exchange (AEX) resins.

The first part of this work focuses on understanding the fouling mechanism of the Protein A MabSelect resin. A fouling mechanism was proposed based on both macroscopic and microscopic studies. The structural and performance characterization of the cycled resin was studied by chromatographic and batch adsorption/desorption experiments.

Microscopic studies including transmission electron microscopy (TEM) and confocal scanning laser microscopy (CLSM) was used to determine the nature and spatial distribution of the foulants and to understand protein conformational change when bound to PA resin. The second part of this work focuses on understanding the relationship between AEX resin structure and protein properties in WPC. Chromatographic experiments were used to determine protein partition and diffusion and to obtain the pore size distribution of AEX resin under WPC conditions. Microscopic experiments were performed with both TEM and CLSM. TEM was used to understand the architecture and pore structure of the AEX resin and CLSM was used to observe mAb and impurity adsorption profile and to understand the mass transfer mechanism under WPC conditions.

## **Acknowledgements**

I would like to express my greatest gratitude to my advisor, Dr. Giorgio Carta, for his guidance, patience and support during the course of my Ph.D. study. I could not achieve this without your continuous encouragement and instruction.

I would also like to thank my advisory committee members: Dr. Kyle Lampe, Dr. Geoffrey Geise, Dr. Ammasi Periasamy and Dr. Stacey Criswell for their valuable inputs and inspiring discussions.

I would also like to thank Pfizer Inc. for providing the financial and material support for my research and industrial insights.

I would like to thank all the current and previous members of Carta lab, especially Yige, Mimi, Jing, Arch, Jason and Yiran, for their help and companion. It was a great pleasure to work with you all.

I also appreciate the help from Vickie, Teresa, Jenifer and Ricky, for smoothing things including scheduling, purchasing and building experimental apparatus.

Finally, I would like to thank my family and friends for their continuous love and support for all the years. Thanks for being with me through all the good and bad times.

## Table of Contents

<b>1 Chapter 1. Motivations, Background and Theory</b> .....	1
<b>1.1 Motivations</b> .....	1
<b>1.2 Background</b> .....	2
1.2.1 Protein A Capture.....	3
1.2.2 Weak Partitioning Chromatography.....	4
<b>1.3 Theory</b> .....	6
1.3.1 Intraparticle porosity and distribution coefficient.....	6
1.3.2 Protein binding.....	7
1.3.3 Mass transfer effects.....	11
<b>1.4 References</b> .....	11
<b>2 Chapter 2. Structural and Functional Characteristics of Virgin and Fouled Protein A MabSelect Resin Cycled in a Monoclonal Antibody Purification Process</b> .....	16
<b>2.1 Introduction</b> .....	16
<b>2.2 Materials and Methods</b> .....	19
2.2.1 Materials.....	19
2.2.2 Methods.....	19
<b>2.3 Results</b> .....	24
2.3.1 Structural characterization.....	24
2.3.2 Batch adsorption and desorption results.....	24
2.3.3 CLSM results.....	32
<b>2.4 Discussion and conclusions</b> .....	37
<b>2.5 References</b> .....	41

<b>3 Chapter 3. Nature of Foulants and Fouling Mechanism in the Protein A</b>	
<b>MabSelect Resin Cycled in a Monoclonal Antibody Purification Process .....</b>	<b>45</b>
<b>3.1 Introduction .....</b>	<b>45</b>
<b>3.2 Materials and Methods .....</b>	<b>47</b>
3.2.1 Materials .....	47
3.2.2 Methods .....	50
<b>3.3 Results.....</b>	<b>52</b>
3.3.1 Resin cycled with conditioned CHO cell culture supernatant.....	52
3.3.2 Resin cycled with purified mAb A and with null cell culture supernatant...	59
3.3.3 Virgin resin saturated with purified mAb A.....	59
3.3.4 Resin cycled with conditioned CHO cell culture supernatant spiked with labeled mAb A and labeled BSA .....	65
3.3.5 Discussion and conclusions .....	65
<b>3.4 References.....</b>	<b>70</b>
<b>4 Chapter 4. Structural and Performance Characteristics of Representative Anion</b>	
<b>Exchange Resins Used for Weak Partitioning Chromatography.....</b>	<b>73</b>
<b>4.1 Introduction .....</b>	<b>73</b>
<b>4.2 Materials and Methods .....</b>	<b>76</b>
4.2.1 Materials .....	76
4.2.2 Methods .....	78
<b>4.3 Results.....</b>	<b>82</b>
4.3.1 Resin Structure .....	82
4.3.2 Isocratic Elution Behavior .....	87

4.3.3	Adsorption Isotherms .....	91
4.3.4	CLSM Imaging.....	93
<b>4.4</b>	<b>Conclusions.....</b>	<b>97</b>
<b>4.5</b>	<b>Reference .....</b>	<b>99</b>
<b>5</b>	<b>Chapter 5. Conclusions and Recommendations .....</b>	<b>103</b>

## List of Figures

**Figure 2.1.** Recovery of mAb during the first 19 manufacturing process cycles conducted with the protocol described in the Materials and Methods section. .... 18

**Figure 2.2.** Representative TEM images of: (a) virgin resin; (b) cycled resin from top 2/3 of column; and (c) and (d) cycled resin from bottom 1/3 of column. Images (a)-(c) are taken near the outer edge of a bead. (d) is taken near the center of the bead. White circular areas in (c) are artifacts resulting from incomplete infiltration with the embedding polymer, or from the sectioning and imaging processes. Magnification was 20k for all four images. Scale bar is 0.5  $\mu\text{m}$ . .... 26

**Figure 2.3.** mAb adsorption isotherms for virgin and cycled resin samples in PBS. .... 27

**Figure 2.4.** Batch adsorption from 2 mg/mL mAb solution in PBS (a) and batch desorption in 50 mM sodium acetate at pH 3.5 for resin samples initially saturated with 5 mg/mL mAb in PBS (b). The inset in (a) shows the batch uptake rates for short times. . 29

**Figure 2.5.** Representative CLSM images of virgin resin particles during adsorption of 2 mg/mL mAb in PBS. The actual particle diameter is shown in each image. The graph on the right hand side shows the position of the adsorption front vs. reduced time  $Ct / q^* r_p^2$ . The solid line is based on eq. 4 with  $D_e = 6.1 \times 10^{-8} \text{ cm}^2/\text{s}$  and  $1/Bi = 0$ . .... 33

**Figure 2.6.** Representative CLSM images of particles from the cycled resin sample (bottom 1/3) during adsorption of 2 mg/mL mAb in PBS. Pairs of beads with comparable size at the same adsorption time are shown in each panel. The graph on the right hand side shows the position of the adsorption front vs. reduced time  $Ct / q^* r_p^2$ . The solid line is for the virgin resin based on eq. 4 with  $D_e = 6.1 \times 10^{-8} \text{ cm}^2/\text{s}$  and  $1/Bi = 0$ . .... 34

**Figure 2.7.** Representative CLSM images of a virgin resin bead (a) and of a bead from the bottom 1/3 sample of the cycled resin (b) during desorption at pH 3.5 following incubation with 5 mg/mL mAb in PBS. The bead diameters are 72 and 85  $\mu\text{m}$  for the virgin and cycled bead, respectively. The graphs on the right show the digitized fluorescence intensity at the bead centerline from the bead surface to the bead center. ... 36

**Figure 2.8.** TEM images of cycled resin from: (a) the top 2/3; and (b) the bottom 1/3 of a column after 40 cycles used with the protocol described in the Materials and Methods section but with an improved 3-step cleaning procedure. Magnification was 15k. Scale bar is 1  $\mu\text{m}$ . No stain was used. .... 40

**Figure 3.1.** TEM images of beads taken from the bottom 1/3 of the column cycled with conditioned CHO cell culture supernatant after incubation with gold-labeled Protein A. Both images were taken near the resin bead surface. The larger box shown in each image is an enlarged view of the smaller box of (a) near the heavily fouled bead surface and (b) inside the bead. Arrows highlight some of the gold nanoparticles for better clarity. .... 53

**Figure 3.2.** TEM image of a bead taken from the bottom 1/3 of the column cycled with conditioned CHO cell culture supernatant after incubation with gold-labeled BSA. The image was taken near the outside surface of the bead. The larger box is the enlarged view of the smaller box in the image. Arrows highlight some of the gold nanoparticles for better clarity. .... 55

**Figure 3.3.** CLSM images of three different beads taken from the bottom 1/3 of the column cycled with clarified cell culture supernatant after incubation with a mixture of rhodamine green-labeled Protein A and rhodamine red-labeled BSA. The actual diameter of each bead is shown in each image. Arrows indicate for clarity some of the areas of

concentrated fluorescence at the two wavelengths used to detect the rhodamine green and red dyes. .... 56

**Figure 3.4.** CLSM images of a virgin resin bead (a) and three different beads taken from the bottom 1/3 of the column cycled with conditioned cell culture supernatant (b, c, d) following incubation with rhodamine green-labeled anti-CHO-HCP antibodies. Actual particle diameters were 73, 78, 88, and 53  $\mu\text{m}$  in a, b, c, and d, respectively. The dashed lines show the outline of each bead. Arrows indicate for clarity some of the areas of concentrated fluorescence. .... 58

**Figure 3.5.** Images of beads taken from a column cycled with (a) the purified mAb A and (b) the column cycled with the null cell culture supernatant. (a) shows a TEM image (left) and CLSM images with the corresponding optical images of the beads (right) for resin samples incubated in RG-PA (top) and in RG-BSA (bottom). (b) shows CLSM and optical images for two beads incubated in RG-BSA. The diameter of each bead is indicated in each image. .... 60

**Figure 3.6.** CLSM images of beads from virgin resin samples pre-saturated with a mixture of unlabeled and rhodamine red-labeled mAb A in PBS and then incubated in rhodamine green-labeled BSA. (a) MabSelect and (b) SP-Sepharose-FF. Actual bead diameters were 80 and 57  $\mu\text{m}$ , for (a) and (b) respectively. Identical CLSM settings were used in both cases. .... 62

**Figure 3.7.** CLSM images of beads from virgin resin samples pre-saturated with three different mAbs in PBS and then incubated in rhodamine green-labeled BSA. Actual bead diameters were 64, 73, and 79  $\mu\text{m}$  for mAb A, B, and C, respectively. Identical CLSM settings were used in all three cases. .... 64

**Figure 3.8.** CLSM images of two resin beads taken from the MabSelect column that was cycled 30 times with mAb A conditioned CHO cell culture supernatant spiked with rhodamine red-labeled mAb A and rhodamine green-labeled BSA. The molar ratios of labeled mAb and labeled BSA to the mAb contained in the cell culture supernatant were 1:240 and 1:20, respectively. Actual particle diameters are 71 and 65  $\mu\text{m}$  for (a) and (b) respectively. The dashed circles show the outline of each bead. Arrows indicate for clarity some of the areas of concentrated fluorescence. .... 66

**Figure 3.9.** Proposed fouling mechanism of MabSelect resin by mAb A. When the mAb molecules bind to the Protein A ligands, a fraction of the mAb molecules undergo a conformational change, which exposes the hydrophobic patches at the surface of mAb molecules. Lipophilic proteins associate with these mAb molecules. During elution, most of these complexes are detached from the Protein A ligand in part refolding to the native form and in part precipitating out on and within the resin under the combined conditions of low pH and high local concentration. Once formed, unless remove by aggressive cleaning, these precipitates continue to grow as a result of cycling. .... 69

**Figure 4.1.** Transmission electron micrographs of TMAE (a), QFF (b), and POROS (c) resins. The arrow point to different structural characteristics as indicated in the text..... 83

**Figure 4.2.**  $K_D$ -values obtained from dextran standards in the mAbB WPC buffer (open symbols) and for mAb monomer and dimer species under non-binding conditions in 2 M NaCl (filled symbols). Lines are based on eq. 3 with  $n=1$  for TMAE and QFF and  $n=2$  for POROS. Parameter values are given in Table 4.1. .... 85

**Figure 4.3.** Chromatographic elution profiles obtained under WPC conditions (squares) and non-binding conditions in 2 M NaCl (circles) for mAbA and mAbB monomers and

mAbB dimer. Note the different CV-axis scale in (a), (b), and (c) for the mAbA monomer data..... 88

**Figure 4.4.** Adsorption isotherms for BSA in the buffers selected for WPC of mAbA (open squares) and WPC of mAbB (filled squares). Lines are based on the Langmuir isotherm. Note the different  $q$ -axis scale in (a)..... 92

**Figure 4.5.** CLSM images of particles of TMAE (a), QFF (b) and POROS (c) during adsorption of 0.5 mg/mL BSA in the mAbB WPC buffer (top row in each panel) and in the mAbA WPC buffer (bottom row in each panel). The time and actual particle diameter are shown in each image..... 94

**Figure 4.6.** CLSM images of particles of TMAE (a), QFF (b) and POROS (c) during co-adsorption of 0.5 mg/mL BSA and 0.5 mg/mL of mAbB multimeric species in the mAbB WPC buffer. The top row in each panel shows the multimeric species while the bottom row in each panel shows BSA for the same particle at the time indicated. The actual particle diameter is shown in each image..... 95

## List of Tables

<b>Table 2.1.</b> Properties of virgin and cycled resin samples.....	25
<b>Table 2.2.</b> Biot number and diffusivities obtained from batch adsorption and batch desorption experiments. ....	30
<b>Table 4.1.</b> Structural properties of the resins used in this work. ....	86
<b>Table 4.2.</b> $K_p$ -values, based on the resin particle volume, and effective pore diffusivities, $D_e$ in $10^{-8}$ cm <sup>2</sup> /s, obtained from isocratic elution experiments under non-binding conditions and under WPC conditions as defined in the text. Error margins for the $K_p$ -values are $\pm 10\%$ . ....	90

# 1 Chapter 1

## Motivations, Background and Theory

---

### 1.1 Motivations

This work focuses on a two-step downstream purification process of monoclonal antibodies (mAb). The mAb purification process consists a capture step using a Protein A column and a polishing step using an anion-exchange column. The capture step can remove up to 95% of the impurities [1]. The second column is used in weak partitioning chromatography (WPC) to remove the remaining impurities from the Protein A elution pool.

Protein A capture has been the "gold standard" for mAb purification because of its high specificity. Due to the very high cost and relatively low binding capacity, cycling the Protein A resin is often desired. As a result of cycling, substantial performance losses are sometimes observed and are attributed to the accumulation of foulants on the resin beads in as few as 20 cycles. Therefore, understanding the fouling mechanism of the Protein A resin is critical.

Weak portioning chromatography (WPC) was introduced by Kelley et al. in 2008 [2] as an operating mode intermediate between "flow through (FT)", where the product does not bind at all, and "bind-elute (B/E)", where the product is initially strongly bound and then elutes. It has been shown that different anion-exchange (AEX) resins exhibit different WPC performance even though the ligand is chemically the same or very similar, suggesting that the resin physical structure may have a greater effect than the ligand chemistry itself. There have also been cases where an AEX resin may work well in

WPC mode for one mAb, but poorly for another, suggesting that protein properties also play an important role in WPC. Therefore, understanding the relationships between protein properties and WPC performance will be helpful.

## 1.2 Background

Monoclonal antibodies (mAbs), whose use as therapeutic applications emerged in the mid-1990s', have risen in importance dramatically in recent years and now occupy a large portion of the biopharmaceuticals that are currently in clinical trials [3][4][5][6]. Many successful multi-million dollar mAbs already exist on the market and many more are expected to be licensed in the future [7][8].

The industrial scale production of mAbs remains challenging mainly because of the following three reasons. First, unlike small molecules that might be synthesized by *in-vitro* methods, mAbs are exclusively produced by recombinant DNA technology [9][10]. Due to the complexity of mAb structures, which consist of more than 1,000 amino acids, and because of glycosylation requirements, mAbs are almost exclusively produced either in yeast cells or, more commonly, in mammalian cells, including Chinese Hamster Ovary (CHO) and baby hamster kidney (BHK-21) cells [11]. The complexity of the cell cultivation media used in these systems requires purification processes that can deal with various impurities including host cell protein (HCP), lipids, and DNA, which have vastly different biophysical attributes [12]. Second, due to the potential toxicity of these impurities, therapeutic mAbs need to be of purity usually higher than 95% chemically and 99% conformationally even at the end of shelf-life [13]. Third, the biological function of mAbs depends highly on their molecular conformation, which, typically, is affected by harsh conditions such as extreme temperature and pH. Based on all these

facts, currently, chromatography and membrane filtration are the main tools used in the industrial purification of mAb.

### **1.2.1 Protein A Capture**

Protein A is a protein originally derived from prokaryotic organisms, notably *Staphylococcus aureus*, with the ability to bind immunoglobulins with high specificity. This ability to bind immunoglobulin explains, for example, the aggressiveness of so-called “Staph infections”. Once these organisms enter the blood stream, they recruit antibodies on their surface becoming virtually “invisible” to the host immune system [14]. This property is used to develop so-called Protein A adsorbents where their native or recombinantly produced Protein A is immobilized on a solid matrix. Engineered forms of Protein A, having, for example, improved chemical stability, are also available [15]. In either case, since the Protein A binding site is located in the constant region of antibody molecules and is not affected by glycosylation, Protein A adsorbents are ideally suited for so-called platform processes, which can be rapidly deployed to purify different antibody products [1][16][17][18][19]. A basic Protein A cycle consists of feed loading, normally at or near physiological pH and ionic strengths conditions, followed by wash with the load buffer, elution with a low pH buffer, typically acetate at pH 3 to 4, strip, typically at even lower pH values, clean-in-place (CIP), most commonly with dilute NaOH, and re-equilibration with the load buffer.

The acidic eluate from the Protein A column is usually further purified, following pH and salt concentration adjustment, with either one or two polishing columns [20]. For cases where only one polishing step is used, an AEX resin is normally used and the operating conditions are chosen to bind the impurities while the mAb flows through. For cases

where two polishing steps are used, after the AEX step, an additional cation exchange or ceramic hydroxyapatite or hydrophobic interaction column [2] is operated in bind/elute mode usually with the mAb binding and the impurities flowing through.

With the demand of therapeutic mAbs approaches the one ton per year level [19], and because of their high cost and relatively low capacity, Protein A resins are almost always used over multiple cycles. In such cases, consideration of the resin lifetime under cycling process conditions is critical [15][21][22].

In a case recently reported by Pfizer [23], a MabSelect Protein A column used in a mAb manufacturing process exhibited substantial performance losses in as few as 20 cycles, characterized by rapidly declining product recovery accompanied by a rapidly increasing strip peak. Changes in the chromatographic elution profile also resulted in increased product pool volume with each subsequent cycle. Since such losses are unlikely to have been caused by ligand degradation over the limited number of cycles used, resin fouling was suspected as the culprit. Although improved cleaning protocols could be developed empirically, for example, on high throughput screening studies, understanding the nature of fouling is desirable.

### **1.2.2 Weak Partitioning Chromatography**

Weak partitioning chromatography was developed as a way to replace the two polishing steps routinely used in mAb purification with a single step. If only one polishing column can be used, substantial cost savings can be obtained. Because both leached Protein A and most of the HCPs have low pI [24][25] and DNA is usually negatively charged at or above neutral pH, an AEX column is typically used as the single polishing step.

WPC is defined as an isocratic chromatographic process performed under mobile phase conditions where both target product and impurities bind to the resin but where the impurities bind much more strongly than the product. While a significant amount of the product protein binds to the resin, well in excess of typical FT operations, the amount bound is much less than in a typical B/E process [2]. A partition coefficient,  $K_p$ , defined as:

$$K_p = \frac{\text{target protein concentration in resin}}{\text{target protein concentration in solution}}$$

is often used to define WPC conditions. Values of  $K_p$  between 0.2 and 20 (preferably between 1 and 3) are usually chosen for WPC [2]. Kelley et al. [2] showed that for these conditions, removal of impurities from the Protein A pool elution pool was more effective. The potential product loss caused by the high  $K_p$  can usually be mitigated by incorporating a short wash step [2][26]. The WPC operating conditions are usually determined by high throughput screening (HTS) methods to identify, empirically, the combination of pH, salt concentration, and resin type that yield  $K_p$ -values in the desired range [27][28]. Although an extensive database has been established defining conditions where WPC is effective for different resins and mAbs, the relationship between the physical structure of the AEX resin and performance is not known. It is noted that although the functional ligand is chemically the same or very similar among many AEX resins, their WPC performance can be dramatically different. Moreover, there have been cases where a certain AEX resin worked well for one mAb but poorly for another. These situations indicate that the physical structure of the AEX resin and the protein properties play important roles in WPC. Therefore, understanding these relationships is thought to be helpful in choosing AEX resins for novel proteins.

### 1.3 Theory

#### 1.3.1 Intraparticle porosity and distribution coefficient

In columns packed with porous particles, there are three easily definable porosities: the intraparticle porosity,  $\varepsilon_p$ , the extraparticle porosity,  $\varepsilon$ , and the total porosity  $\varepsilon_t$ , which is related to  $\varepsilon_p$  and  $\varepsilon$  by:

$$\varepsilon_t = \varepsilon + (1 - \varepsilon)\varepsilon_p \quad (1)$$

The distribution coefficient,  $K_D$ , is usually defined as the ratio of a molecule concentration in the resin bead and the molecule concentration in solution at equilibrium. For a non-bound molecule,  $K_D$  can be obtained from the retention volume in the column according to the following equation:

$$K_D = (\overline{CV} - \varepsilon) / (1 - \varepsilon) \quad (2)$$

where  $\overline{CV}$  is the mean retention volume divided by the column volume.  $K_D$  depends on the size of the molecules and that of the pores. If the pores are treated as long cylinders of uniform radius  $r_{pore}$ ,  $K_D$  is given by the following equation [29]:

$$K_D = \varepsilon_p \left( 1 - \frac{r_m}{r_{pore}} \right)^2 \quad (3)$$

where  $r_m$  is the molecular radius.

In WPC, the distribution coefficient  $K_p$ , defined as [2]:

$$K_p = \frac{Q}{C} \quad (4)$$

where  $Q$  is the amount of protein partitioned into the resin divided by the settled resin volume and  $C$  is the protein concentration in solution at equilibrium, is conventionally

used instead of  $K_D$ . The settled resin volume includes both the volume of particles (including the intraparticle pores) and the volume of the solution surrounding the particles.  $\bar{q}$  is defined here as the amount of mAb partitioned in the resin per unit of particle volume without extraparticle solution, and can be written as

$$\bar{q} = q + K_D C \quad (5)$$

where  $q$  is the amount of protein bound per unit particle volume. Accordingly,

$$Q = (1 - \varepsilon)\bar{q} = (1 - \varepsilon)(q + K_D C) \text{ or}$$

$$K_p = (1 - \varepsilon)\left(\frac{q}{C} + K_D\right) \quad (6)$$

If there is no protein binding,  $K_p$  is at a minimum and is given by

$$K_{p,\min} = (1 - \varepsilon)K_D. \quad (7)$$

Since  $K_D < 1$  and  $\varepsilon \sim 0.5$ , according to eq. (6),  $K_p$  values between 1 and 3 correspond to values of  $q$  that are comparable to  $C$ . Thus both protein bound and protein held in the pores need to be considered for such conditions.

### 1.3.2 Protein binding

Two different cases are considered here. The first pertains to the B/E conditions of the initial capture step. Binding of antibodies to Protein A resins occurs as a result of the strong affinity of the Protein A ligand for the Fc region of human IgG1, IgG2 and IgG4 at neutral pH [30]. This interaction is typically described by an association constant,  $K_a$ , or by its reciprocal,  $K_d$ . Since the number of Protein A ligands immobilized in the resin is finite, the following relationship is obtained:

$$q = \frac{q_m K_a C}{1 + K_a C} = \frac{q_m C}{K_d + C}. \quad (8)$$

The value of  $K_d$  usually varies between  $5 \times 10^{-9}$  and  $2 \times 10^{-8}$  mol/L [31]. Since the molecular mass of antibodies is around 150,000, the  $K_d$  values, in g/L units, are between  $7.5 \times 10^{-4}$  and  $3.3 \times 10^{-3}$ . In practical cases,  $C$  is on the order of 0.1 to 5 g/L. As a result,  $q \sim q_m$  implying that at neutral pH the adsorption isotherm is essentially rectangular.

The value of  $K_d$  is, however, a strong function of pH increasing dramatically under acidic conditions. In practice  $K_d$  is very large at pH<4 indicating that there is essentially no mAb binding for the conditions used in the elution step.

The kinetics of mAb binding to Protein A resins at neutral pH is controlled by pore diffusion [32]. Since the adsorption isotherm is essentially rectangular owing to the small  $K_d$ -values, the kinetics for these conditions is described by the so-called shrinking core model. Accordingly, the position of the protein adsorption front in a single bead,  $r_s$ , is given by [33]:

$$2\rho_s^3 - 3\rho_s^2 + 1 = \frac{6D_e C}{q^* r_p^2} t \quad (9)$$

where  $\rho_s = r_s / r_p$ ,  $D_e$  is the effective pore diffusivity,  $C$  is the protein solution concentration,  $q^*$  is the binding capacity and  $r_p$  is the bead radius.

Since  $q_m$  is usually large ( $\sim 50$ - $100$  g/L for modern Protein A resins [34]),  $\bar{q} \sim q_m$ . The values  $D_e$  found experimentally fall in the range  $3.0 \times 10^{-8}$  to  $4.0 \times 10^{-7}$  cm<sup>2</sup>/s dependent on protein concentration, resin pore size and porosity [35].

Less is known about the kinetics of mAb desorption from Protein A resins when a mAb-loaded resin bead is exposed to a low pH buffer. For these conditions, assuming that detachment of the mAb molecules from the Protein A ligands is fast, the mAb concentration in the resin pore is expected to approach, rapidly, values near the neutral

pH binding capacity. Further, assuming that the time needed for the low pH buffer to diffuse in the particle is short and that negligible diffusion of the mAb out of the particle occurs during that time, the following equation is obtained [33]:

$$F = 1 - \frac{6}{\pi^2} \sum_{n=1}^{\infty} \frac{1}{n^2} \exp\left(-n^2 \pi^2 \frac{D_e t}{K_D r_p^2}\right) \quad (10)$$

where  $F$  is the fractional amount of protein desorbed.

Taking into account the particle size distribution, by [36]:

$$\bar{F} = \sum_{i=1}^M f_i \left[ 1 - \frac{6}{\pi^2} \sum_{n=1}^{\infty} \frac{1}{n^2} \exp\left(-n^2 \pi^2 \frac{D_e t}{K_D r_{p,i}^2}\right) \right] \quad (11)$$

where  $\bar{F}$  is the average value of  $F$  and  $f_i$  is the volume fraction of particles of radius  $r_{p,i}$  and  $M$  is the number of fractions in the particle size distribution. Both eqs. 10 and 11 assume that desorption occurs in a large volume of desorbent so that the concentration of the mAb in the solution surrounding the particle remains close to zero.

The second case pertains to the WPC polishing step. In this case, protein binding is expected to depend on the stoichiometric exchange with counterions such as chloride.

Accordingly, the so-called Steric Mass Action (SMA) model [37] can be used to describe binding:

$$q_i = \frac{K_{e,i} [q_0 - \sum (z_i + \sigma_i) q_i]^{z_i} C_i}{(C_{Cl^-})^{z_i}} \quad (12)$$

where  $K_{e,i}$  is the equilibrium constant for the exchange of a protein  $i$  with chloride,  $q_0$  is the resin charge density,  $\sigma_i$  is the number of ligands blocked by the protein  $i$ ,  $C_{Cl^-}$  is the counterion ( $Cl^-$ ) concentration and  $z_i$  is the effective charge of the protein  $i$ . The protein effective charge is used instead of protein net charge because the former considers only

the charged residues that directly interact with resin ligands. If the chloride concentration is relatively high and a single protein  $i$  is present, eq. (12) yields [10]:

$$q_i \sim \frac{K_{e,i} q_0^{\bar{z}_i} C_i}{(C_{Cl^-})^{\bar{z}_i}} = m_i C_i \quad (13)$$

which corresponds to a linear isotherm. For these conditions, protein retention for a pulse injection in a column under isocratic conditions is given by [10]:

$$\overline{CV} = \varepsilon(1 + k'_i) \quad (14)$$

where

$$k'_i = k'_{i,\infty} + A_i (C_{Cl^-})^{-\bar{z}_i} \quad (15)$$

In this equation,  $k'_{i,\infty} = \frac{1-\varepsilon}{\varepsilon} K_{D,i}$  and  $A_i = \frac{1-\varepsilon}{\varepsilon} K_{e,i} q_0^{\bar{z}_i}$ .

Predicting retention of the mAb in the column for conditions where proteins are strongly bound is obviously more complicated. Consider, for example, the case of a weakly bound mAb product (A) together with a strongly bound impurity (B). In this case, eq. 12 yields:

$$q_A = \frac{K_{e,A} [q_0 - (z_B + \sigma_B) q_B]^{\bar{z}_A} C_A}{(C_{Cl^-})^{\bar{z}_A}} = f(C_A, C_B, C_{Cl^-}) \quad (16)$$

$$q_B = \frac{K_{e,B} [q_0 - (z_B + \sigma_B) q_B]^{\bar{z}_B} C_B}{(C_{Cl^-})^{\bar{z}_B}} = f(C_B, C_{Cl^-}) \quad (17)$$

Since, under practical WPC conditions, binding of the impurities is not expected to be affected by the presence of the mAb product, the model parameters for binding of the impurity (eq. 17) can be determined independently of the mAb. If the term  $(z_B + \sigma_B) q_B$  is close to  $q_0$ , little if any mAb binding will occur where the impurity is present. For these conditions in a column process, mAb binding will occur only in the region of the column downstream of the impurity adsorption front.

### 1.3.3 Mass transfer effects

Due to the size of the pores typically encountered in porous resin media, protein adsorption and desorption processes are usually controlled by diffusion. Therefore diffusional mass transfer is expected to be another important aspect that characterizes resin-protein interaction in WPC to an extent that depends on the resin structure. For example, macroporous or polymer-grafted resins should have different effects on protein diffusion. Under high salt conditions, protein has little interaction with ligands.

According to Carta and Jungbauer [10], the height equivalent to the theoretical plate (*HETP*) is correlated to the effective diffusivity by the following equation:

$$HETP = a + \frac{2u}{1-\varepsilon} \left( \frac{k'}{1+k'} \right)^2 \frac{r_p^2}{15D_e} \quad (18)$$

where  $a$  is a constant.

### 1.4 References

- [1] Hober, S., Nord, K., Linhult, M. Protein A chromatography for antibody purification. *J. Chromatogr. B*, 848 (2007) 40-47.
- [2] Kelley, B.D., Tobler, S.A., Brown, P., Coffman, J.L., Godavarti, R., Iskra, T., Switzer, M., Vunnum, S. Weak partitioning chromatography for anion exchange purification of monoclonal antibodies. *Biotechnol. Bioeng.*, 101.3 (2008) 553-566.
- [3] Stockwin, L.H., Holmes, S. Antibodies as therapeutic agents: Vive la renaissance! *Expert Opin. Biol. Ther.*, 3 (2003) 1133–1152.
- [4] Walsh, G. Modern antibody-based therapeutics. *Biopharm.*, 17 (2004) 18-25.
- [5] Gottschalk, U. Downstream processing of monoclonal antibodies: from high dilution to high purity. *Biopharm.*, 18 (2005) 42

- [6] van Dijk, M.A., van de Winkel, J.G. Human antibodies as next generation therapeutics. *Curr. Opin. Chem. Boil.*, 5 (2001) 368-374.
- [7] Norman, P. Monoclonal antibodies in the pipeline: a segment of major growth. *Insight Pharma. Reports*, (2011) 173.
- [8] Pharmaceutical Research and Manufacturers of America, *Pharmaceutical Industry Profile 2012*.
- [9] Nelson, A.L., Dhimolea, E., Reichert, J. M. Development trends for human monoclonal antibody therapeutics. *Nat. Rev. Drug Discov.*, 9 (2010) 767-774.
- [10] Carta, G., Jungbauer, A. *Protein Chromatography: Process Development and Scale-Up*, Wiley-VCH, Weinheim, Germany (2010).
- [11] Chen, S., Gray, D., Ma, J., Subramanian, S. Production of Recombinant Proteins in Mammalian Cells. *Curr. Protoc. Protein Sci.*, (2001) 5-10.
- [12] Flatman, S., Alam, I., Gerard, J., Mussa, N. Process analytics for purification of monoclonal antibodies. *J. Chromatogr. B*, 848 (2007) 79-87.
- [13] Randolph, T.W., John F.C. Engineering challenges of protein formulations. *AIChE journal*, 53.8 (2007) 1902-1907.
- [14] Kutateladze, M., Adamia, R. Bacteriophages as potential new therapeutics to replace or supplement antibiotics. *Trends Biotechnol.*, 28 (2010) 591-595.
- [15] Hahn, R., Shimihara, K., Steindl, F. Jungbauer, A. Comparison of Protein A affinity sorbents. III Life time study. *J. Chromatogr. A*, 1102 (2006) 224-231.
- [16] Gagnon, P. *Purification tools for monoclonal antibodies. Validated Biosystems*, Tucson, AZ (1995).

- [17] Fahrner, R.L., Whitney, D.H., Vanderlaan, M., Blank, G.S. Performance comparison of Protein A affinity-chromatography sorbents for purifying recombinant monoclonal antibodies. *Biotechnol. Appl. Biochem.*, 30 (1999) 121-128.
- [18] Shukla, A.A., Hubbard, B., Tressel, T., Guhan, S., Low, D. Downstream processing of monoclonal antibodies: application of platform approaches. *J. Chromatogr. B*, 848 (2007) 28-39.
- [19] Kelley, B. Very large scale monoclonal antibody purification: The case for conventional unit operations. *Biotechnol. Progr.*, 23 (2007) 995–1008.
- [20] Fahrner, R.L., Knudsen, H.L., Basey, C.D., Galan, W., Feuerhelm, D., Vanderlaan, M., Blank, G.S. Industrial purification of pharmaceutical antibodies: development, operation, and validation of chromatography processes. *Biotechnol. Genet. Eng. Rev.*, 18.1 (2001), 301-327.
- [21] Jiang, C., Liu, J., Rubacha, M., Shukla, A.A. A mechanistic study of Protein A chromatography resin lifetime. *J. Chromatogr. A*, 1216 (2009) 5849-5855.
- [22] Grönberg, A., Eriksson, M., Ersoy, M., Johansson H.J. A tool for increasing the lifetime of chromatography resins. *MABS*, 3 (2011) 192–202.
- [23] Daniels, W. MabSelect resin lifetime presentation. Personal communication. January 2013.
- [24] Horisberger, M., Clerc, M.F. Labelling of colloidal gold with protein A. *Histochemistry*, 82 (1985) 219-223.

- [25] Jin, M., Szapiel, N., Zhang, J., Hickey, J., Ghose, S. Profiling of host cell proteins by two-dimensional difference gel electrophoresis (2D-DIGE): Implications for downstream process development. *Biotechnol. Bioeng.*, 105 (2010) 306-316.
- [26] Liu, H.F., Ma, J., Winter, C., Bayer, R. Recovery and purification process development for monoclonal antibody production. *MAbs*, 2 (2010) 480-499.
- [27] Coffman, J.L., Kramarczyk J.F., Kelley B.D. High-throughput screening of chromatographic separations: I. Method development and column modeling. *Biotechnol. Bioeng.*, 100.4 (2008) 605-618.
- [28] Kelley, B.D., Switzer, M., Bastek, P., Kramarczyk, J.F., Molnar, K., Yu, T., Coffman, J.L. High-throughput screening of chromatographic separations: IV. Ion-exchange. *Biotechnol. Bioeng.*, 100.5 (2008) 950-963.
- [29] Hagel, L., Ostberg, M., Andersson, T. Apparent pore size distributions of chromatography media. *J. Chromatogr. A*, 743 (1996) 33-42.
- [30] Jendeborg, L., Nilsson, P., Larsson, A., Denker, P., Uhlén, M., Nilsson, B., Nygren, P. Å. Engineering of Fc 1 and Fc 3 from human immunoglobulin G to analyse subclass specificity for staphylococcal protein A. *J. Immunol. Methods*, 201 (1997) 25-34.
- [31] Langone, J. J. Applications of immobilized protein A in immunochemical techniques. *J. Immunol. Methods*, 55 (1982) 277-296.
- [32] Horstmann, B.J., Chase, H.A.. Modeling the affinity adsorption of immunoglobulin G to Protein A immobilised to agarose matrices. *Chem. Eng. Res. Des.*, 67 (1989) 243-254.

- [33] Ruthven, D.M. Principles of adsorption and adsorption processes. Wiley, New York (1985).
- [34] Hahn, R., Schlegel, R., Jungbauer, A. Comparison of protein A affinity sorbents. *J. Chromatogr. B*, 790 (2003) 35-51.
- [35] Hahn, R., Bauerhansl P., Shimara K., Wiznieski C., Tscheliessnig A., Jungbauer A. Comparison of Protein A affinity sorbents. II. Mass transfer properties. *J. Chromatogr. A*, 1093 (2005) 98-110.
- [36] Ubiera, A.R., Carta G. Particle-size distribution effects in batch adsorption. *AIChE J.*, 49 (2003) 3066-3073.
- [37] Brooks, C.A., Cramer, S.M. "Steric mass-action ion exchange: displacement profiles and induced salt gradients." *AIChE J.*, 38.12 (1992) 1969-1978.

## 2 Chapter 2

### Structural and Functional Characteristics of Virgin and Fouled Protein A

#### MabSelect Resin Cycled in a Monoclonal Antibody Purification Process

---

##### 2.1 Introduction

Protein A resins are used extensively in the purification of monoclonal antibodies and Fc-fusion proteins [1][2][3][4][5]. Because of their high cost and relatively low capacity, these resins are almost always used over multiple cycles, requiring consideration of the resin lifetime under cycling process conditions [6][7][8].

The potential for degradation of resin performance as a function of cycling is well documented [5][6]. However, less is known about the underlying mechanisms. Several potential causes can be considered including chemical alteration of the Protein A ligand, leakage of the ligand, loss of structural integrity of the resin beads and/or the packed bed, and accumulation of strongly held impurities and/or residual product resulting in reduced access to the binding sites within the resin. Jiang et al. [7] examined the effects of cycling the Protein A resin MabSelect for the capture of an Fc-fusion protein and concluded that the primary factor leading to loss of performance was ligand degradation due to the harsh conditions used for cleaning. Significant improvement in resin lifetime performance could be obtained in their case by using milder cleaning conditions or adding stabilizing excipients to the cleaning solution. Other authors, however, have observed fouling of Protein A resins due to accumulation of protein impurities. Grönberg et al. [8], using a high throughput screening methodology, found that the Protein A resin MabSelect SuRe

was extensively fouled by proteinaceous material which could be extracted from the cycled resin with an SDS buffer at 95 °C and analyzed by SDS-PAGE.

In our own experience, we have observed substantial performance losses for the Protein A resin MabSelect with certain monoclonal antibodies in as few as 20 cycles. Figure 2.1 gives an example for manufacturing-scale mAb production process showing a significant decline in product yield. Additionally, an increased strip peak and changes in the chromatographic elution profile resulting in increased pool volume were noted with each subsequent cycle. Since such losses are unlikely to have been caused by ligand degradation over the limited number of cycles used, resin fouling was suspected as the culprit. Upon unpacking the column used for these studies, the cycled resin was found to be highly agglomerated, especially for samples collected from the bottom third of the column, near the exit. Attempts to re-suspend this resin in buffer and repack it in the column resulted in very poor packing quality. Although improved cleaning protocols could be developed empirically, understanding the nature of fouling was thought to be desirable.

The objective of this work is thus four-fold: (i) to determine what, if any, structural changes occur in the resin during cycling; (ii) to determine what intrinsic performance characteristics are affected by cycling, including binding capacity and kinetics during both adsorption and desorption; (iii) to obtain an understanding of the mechanisms leading to fouling; and (iv) to show how some of the techniques developed to study the resin's structural properties can be used to assess the effectiveness of alternative cleaning strategies. The tools used in this study comprise both macroscopic and microscopic techniques and include: inverse size exclusion chromatography (iSEC) to determine any

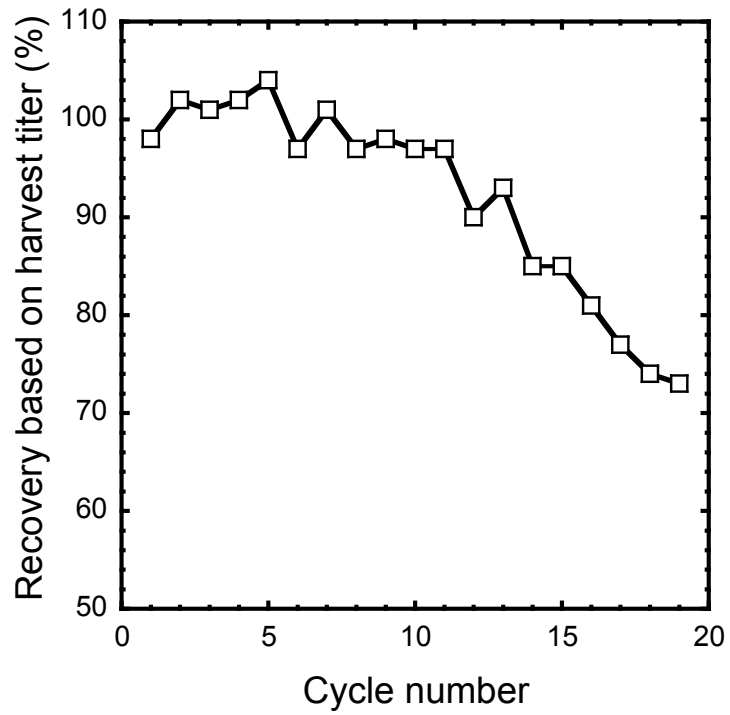


Figure 2.1. Recovery of mAb during the first 19 manufacturing process cycles conducted with the protocol described in the Materials and Methods section.

effects on pore accessibility; transmission electron microscopy (TEM) to determine any effects on internal resin structure; equilibrium isotherms to determine any effects on binding capacity; batch adsorption/desorption and confocal microscopy (CLSM) to determine any effects on rates and transport mechanisms.

## **2.2 Materials and Methods**

### **2.2.1 Materials**

The Protein A resin used in this work, MabSelect, was obtained from GE Healthcare (Piscataway, NJ) and is based on a crosslinked agarose matrix. It should be noted that, compared to other resins such as, for example, MabSelect SuRe, also from GE Healthcare, MabSelect has more limited base stability, which prevents use of harsh cleaning conditions that would result in rapid degradation of the Protein A ligand [5]. The resin's particle size distribution was determined from microphotographs (data not shown) and ranged from 44 to 122  $\mu\text{m}$  with a volume-average particle diameter of 86  $\mu\text{m}$ . The mAb used in this work was provided by Pfizer (St. Louis, MO) and is a glycosylated IgG2 antibody with a molecular mass around 160 kDa. Rhodamine Red<sup>TM</sup>-X succinimidyl ester amine-reactive dye was purchased from Invitrogen Corporation (Carlsbad, CA). Other chemicals were from Fisher Scientific (Pittsburgh, PA) and Sigma-Aldrich (St. Louis, MO). All experiments were conducted at room temperature ( $22\pm 2$  °C).

### **2.2.2 Methods**

#### **2.2.2.1 Process cycle**

The MabSelect resin was packed in a 60 cm diameter, 20 cm long column from Pall Life Sciences (Resolute® Chromatography Column, Port Washington, NY). Packing was done according to the resin manufacturer specifications using a compression factor

(defined as the settled bed height divided by the packed bed height) of 1.16. The packed columns was then used in an antibody manufacturing campaign over multiple cycles according to the following protocol:

Equilibration: Tris buffer with high NaCl at pH 7.5 for 5 CV

Load: Conditioned CHO cell culture supernatant with a mAb load of 25 to 38 mg/mL of column volume

Wash: First equilibration buffer for 3 CV, then Tris buffer with low NaCl at pH 7.5 for 3 CV

Elute: 25 mM sodium acetate at pH 3.5 for 4 CV

Strip: 250 mM acetic acid and 250 mM NaCl for 4 CV

Clean: 50 mM NaOH with 1 M NaCl for 4 CV

All steps were operated in the downflow direction. No product breakthrough was observed during cycling. However, as shown in Fig. 2.1, a steady decline in product recovery occurred after the first 10-11 cycles. This decline was accompanied by obvious changes in the elution profile requiring increasingly larger pool volumes (data not shown).

After 20 cycles, the resin was removed from the column and two fractions of the cycled resin were collected – one corresponding to the bottom 1/3 of the column (near the exit), and the other corresponding to the top 2/3 (near the entrance). Since the amount of mAb loaded during each cycle was also on the order of 2/3 of the column equilibrium binding capacity (which was about 59 mg/mL), the top 2/3 resin sample represents resin that was saturated with mAb to a significant extent prior to wash and elution steps. Unlike the virgin resin, the particles in the samples from these two resin fractions have an

agglomerated appearance and a strong tendency to stick to each other, which may indicate the presence of hydrophobic foulants on the bead surface. Dispersion of these particles in PBS required vigorous shaking. Using this particular mAb feedstream in the process cycle described above, MabSelect resin fouling was found to occur independent of the load storage or handling conditions.

#### **2.2.2.2 Inverse size exclusion chromatography**

Inverse size exclusion chromatography (iSEC) was used to determine accessible porosity and pore radius using glucose dextran standards. Values of the distribution coefficient,  $K_D$ , were calculated for each standard as  $K_D = (\overline{CV} - \varepsilon) / (1 - \varepsilon)$  where  $\overline{CV}$  is the mean retention volume divided by the column volume. Intraparticle porosity,  $\varepsilon_p$ , and pore radius,  $r_{pore}$ , were calculated by fitting the  $K_D$ -values to the following equation [9]:

$$K_D = \varepsilon_p \left( 1 - \frac{r_m}{r_{pore}} \right)^2 \quad (1)$$

where  $r_m$  is the molecular radius of each standard.

#### **2.2.2.3 Transmission electron microscopy**

Transmission electron microscopy (TEM) was performed with a JEOL 1230 instrument (JEOL Ltd., Tokyo, Japan) after dehydrating the resin samples by washing them with increasing ethanol concentrations from 0 to 100% anhydrous ethanol. Each sample was then embedded in LR-White resin (London Resin Company, Ltd., London, UK) following the procedure outlined by Corbett et al. [10] and ultramicrotomed into 80 nm sections. For better contrast, sections of the virgin resin samples were stained with lead citrate followed by uranyl acetate, while sections of the cycled samples were viewed unstained. Images were taken by a SIA CCD camera with 4K×4K resolution.

#### **2.2.2.4 Adsorption isotherms and batch adsorption/desorption kinetics**

Adsorption isotherms were obtained by first equilibrating the resin samples with PBS with vigorous shaking and then filtering them in a microcentrifuge filter for 15 min at 5,000 rpm to remove the extraparticle solution. Weighed resin samples were then added to 1.5 mL microcentrifuge tubes containing 1.5 mL of mAb solutions at different initial concentrations in PBS. After rotating the tubes end-over-end at 20 rpm for 20 h, the supernatant concentration in each tube was measured with a NanoVue spectrophotometer (GE Healthcare, Piscataway, NJ) and the adsorbed protein concentration was calculated by mass balance. The hydrated resin densities, obtained with a pycnometer and used to convert the adsorbed concentrations to units of mg per mL of hydrated bead volume, were all in the range  $1.04 \pm 0.01$  g/mL.

The batch adsorption kinetics was determined as described by Carta et al. [11]. Briefly, the resin particles were first dispersed in PBS. This was immediate for the virgin resin but required vigorous shaking for the fouled samples. PBS-equilibrated resin samples (each containing 0.22 to 0.23 g of resin) were then added to 20 mL of 2.0 mg/mL mAb in PBS in amounts estimated to adsorb about one half of the mAb. The solution was agitated with a small paddle stirrer and a stream was continuously recirculated through a UV detector. The amount of protein adsorbed was obtained by mass balance based on the UV readings. The batch desorption kinetics was determined by first mixing a 0.25 g resin sample with an excess amount of 5 mg/mL purified mAb in PBS for 1 to 3 h. The resin sample was then washed with PBS and centrifuged in a microcentrifuge filter. The resin particles were then re-suspended in 0.7 mL of PBS buffer and added to a vial containing 19 mL of the elution buffer (25 mM sodium acetate at pH 3.5). UV absorbance readings of the

supernatant were collected over time and used to calculate by mass balance the amount of mAb desorbed.

#### **2.2.2.5 Confocal microscopy**

Confocal laser scanning microscopy (CLSM) was performed with Rhodamine Red-labeled mAb as described by Perez-Almodovar et al. [12] and Tao et al. [13]. Briefly, the mAb was mixed with Rhodamine Red<sup>TM</sup>-X dye in a 3:1 ratio and incubated in 500 mM sodium bicarbonate buffer at pH 8.5 for 1 h. A desalting column was then used to separate the labeled mAb from unreacted dye. A labeling ratio of 0.2 was determined spectrophotometrically. The labeled protein mixture was further diluted with unlabeled protein in a 1:40 ratio yielding a final ratio of labeled to unlabeled protein of 1:200. CLSM experiments were conducted with a Zeiss LSM 510 microscope with a Plan-Apochromat 63 ×/1.4 NA oil objective (Carl Zeiss MicroImaging, LLC, Thornwood, NY). The excitation wavelength was 561 nm and emission wavelength greater than 575 nm was collected. All images were taken at the equator of the beads. Batch measurements were made to determine the adsorption kinetics by adding 10 mg of resin to a tube containing 10 mL of the labeled protein at a total concentration of 2.0 mg/mL, periodically pipetting out 300 µL samples of the slurry, and rapidly filtering them in a microcentrifuge filter to remove the extraparticle solution. The particles were then re-suspended in PBS and imaged. Since the time scale for desorption is much shorter than for adsorption, a microfluidics flow-cell was used instead of batch measurements. The cell was constructed by cutting a 5-mm long, 5-mm wide slit in a 280 µm-thick polydimethylsiloxane (PDMS) film and laser etching a small recessed area, 40 µm deep, in the film at one end of the slit. The film was then sandwiched between a glass cover slip

and a piece of 1-mm thick Corning glass with glued tubing connectors providing a 280  $\mu\text{m}$  channel with the 40  $\mu\text{m}$  deep area serving as a weir to retain the particles in the channel under flow. A model 11V-0150H multiport valve from Valco Instruments Co. Inc. (Houston, TX), connected to model 11 Plus syringe pumps (Harvard Apparatus, Holliston, MA), was used to feed load, wash, and elution buffers at a flow rate of 3 mL/h, which corresponds to an average velocity of 214 cm/h past the particles.

## **2.3 Results**

### **2.3.1 Structural characterization**

Table 2.1 shows the porosity and pore radii obtained from the iSEC data. As seen from this table, the cycled samples have lower accessible intraparticle porosity and smaller pore size compared to the virgin sample. However, the differences between resin samples from the top and bottom of the column appear to be statistically insignificant.

Figure 2.2 shows representative TEM images of virgin resin (a, stained) and cycled resin samples (b, c, d, unstained). In all four images, the uniform light grey areas are the embedding material, while the darker grey is the MabSelect resin backbone. Very dark areas are also visible in the cycled resin samples both near the bead outer surface as a roughly continuous film (b and c), as well as in the particle's interior (d) as dense globules that are generally less than about 0.1  $\mu\text{m}$  in size. Only small differences are seen between the top 2/3 and bottom 1/3 samples.

### **2.3.2 Batch adsorption and desorption results**

Figure 2.3 shows the mAb adsorption isotherms. The virgin resin isotherm is highly favorable and consistent with prior equilibrium measurements for other mAbs (e.g. Hahn et al., [14]; Bankston et al., [15]). The isotherms for the cycled samples are also highly

Table 2.1. Properties of virgin and cycled resin samples.

Resin sample	Total column porosity, $\varepsilon_t$	Intraparticle porosity, $\varepsilon_p$	Apparent pore radius, $r_{pore}$ (nm)
Virgin	0.899	0.851	36.2±2.3
Cycled, top sample	0.871	0.811	31.7±1.8
Cycled, bottom sample	0.870	0.805	27.7±2.9

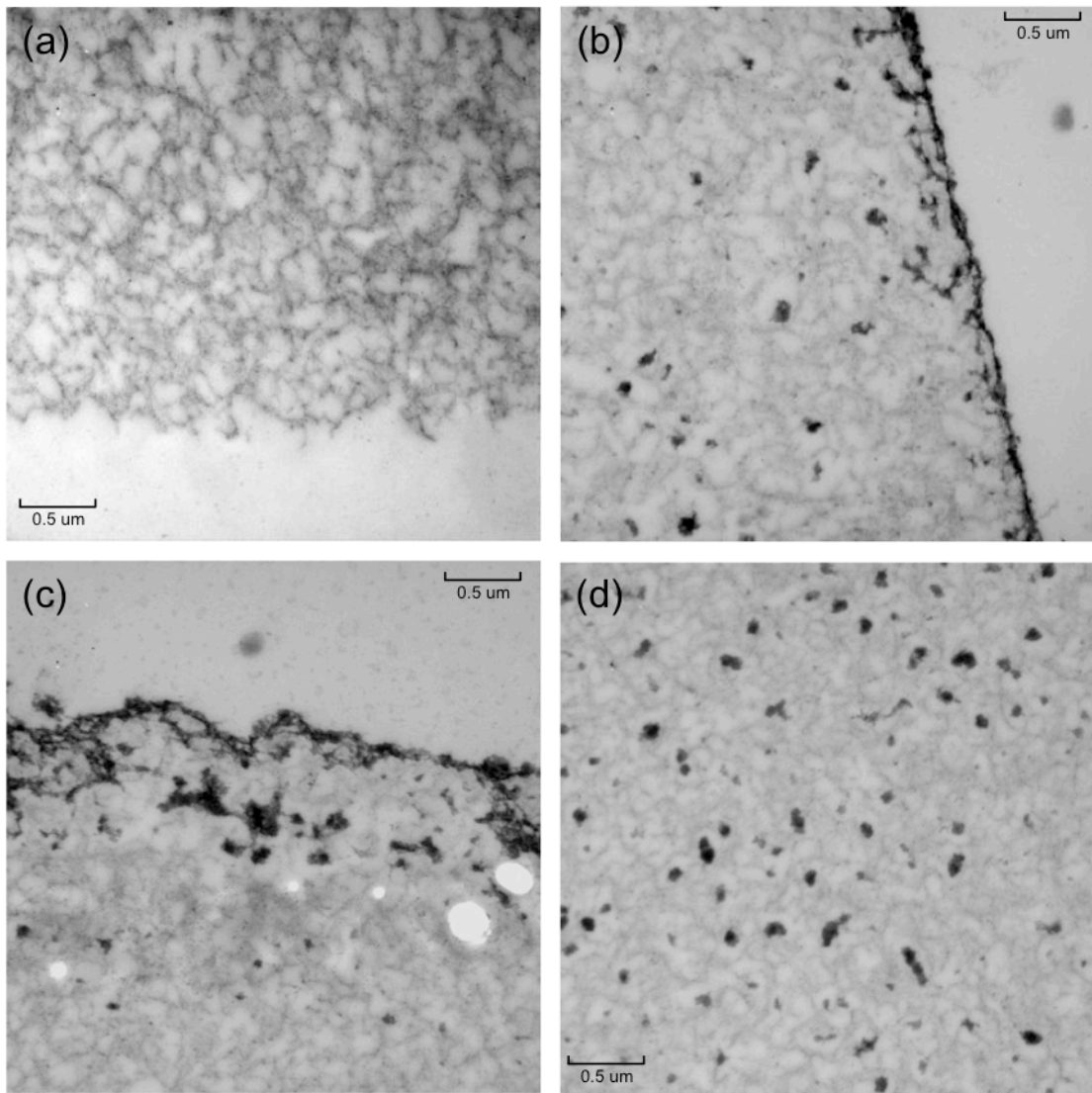


Figure 2.2. Representative TEM images of: (a) virgin resin; (b) cycled resin from top 2/3 of column; and (c) and (d) cycled resin from bottom 1/3 of column. Images (a)-(c) are taken near the outer edge of a bead. (d) is taken near the center of the bead. White circular areas in (c) are artifacts resulting from incomplete infiltration with the embedding polymer, or from the sectioning and imaging processes. Magnification was 20k for all four images. Scale bar is 0.5  $\mu\text{m}$ .

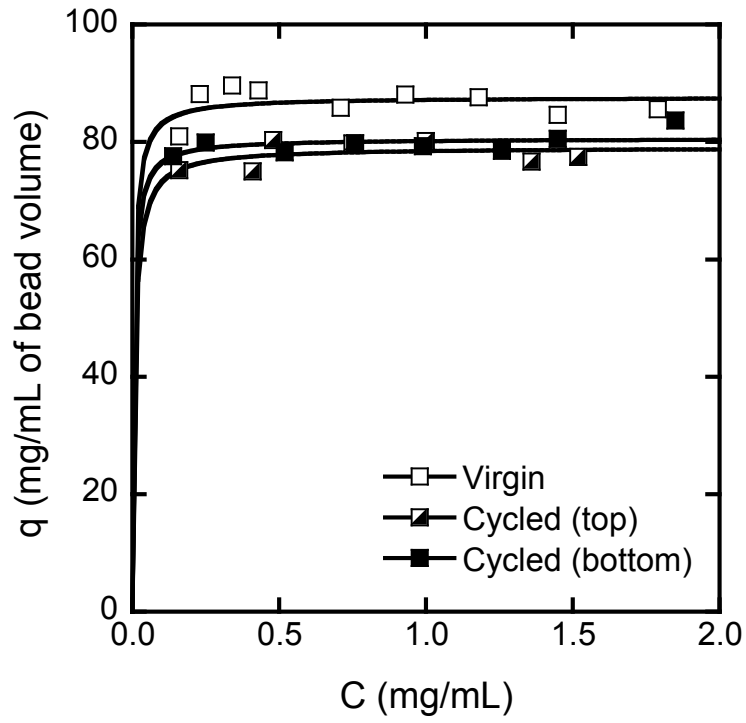


Figure 2.3. mAb adsorption isotherms for virgin and cycled resin samples in PBS.

favorable, but show lower capacity compared to the virgin resin. The corresponding maximum capacities, estimated by regressing the Langmuir isotherm to the data, are  $91.1 \pm 1.4$  mg/mL for the virgin resin and  $82.2 \pm 1.0$  and  $83.8 \pm 0.9$  mg/mL for top and bottom samples, respectively, all per mL of bead volume. The reasons for the decline in binding capacity with cycling are likely to be in part degradation of the Protein A ligand and in part accumulation of foulants that block or hinder access to a portion of the ligands. Since the total number of cycles was small, it is likely that the latter is more important. In practice, the approximately 10% drop had little effect on process performance since the protein loads were substantially below these capacity values. As a result, no breakthrough of the mAb was seen during cycling.

Figure 2.4 shows the batch adsorption and desorption curves. The time scale in the two panels is different (4000 s for adsorption and 60 s for desorption) according to the time needed to approach equilibrium in each case. As seen in Fig. 2.4a, similar uptake curves are obtained for virgin and cycled resin samples. Except for the fact that a higher value of  $q$  is attained for the virgin resin, significant differences are only seen for short times (<500 s) which show that the initial rate of adsorption is smaller for the cycled resin samples. Since the isotherm is very favorable, the shrinking core model taking into account a film resistance as well as the resin particle size distribution was used to determine the best fit values of the effective pore diffusivity,  $D_e$ , and Biot number  $Bi = k_f r_p / D_e$ , where  $k_f$  is a film mass transfer coefficient and  $r_p$  is the particle radius. The relevant equations are given by Stone and Carta [16]. Table 2.2 gives the best fit values of these parameters. For virgin MabSelect resin, based on similar measurements, Hahn et al. [14] obtained effective pore diffusivities varying between  $3.0 \times 10^{-8}$  and  $40.0 \times 10^{-8}$

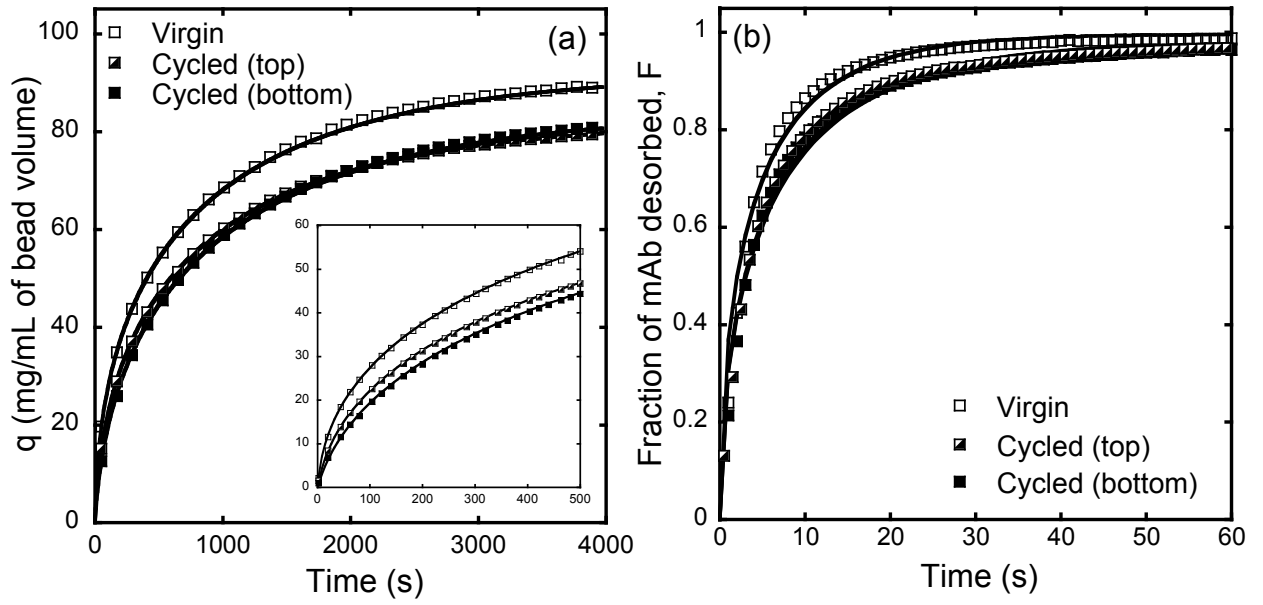


Figure 2.4. Batch adsorption from 2 mg/mL mAb solution in PBS (a) and batch desorption in 50 mM sodium acetate at pH 3.5 for resin samples initially saturated with 5 mg/mL mAb in PBS (b). The inset in (a) shows the batch uptake rates for short times.

Table 2.2. Biot number and diffusivities obtained from batch adsorption and batch desorption experiments.

	Batch adsorption		Batch desorption	
	$Bi$	$D_e$ ( $10^{-8}$ $\text{cm}^2/\text{s}$ )	$D_e/K_D$ ( $10^{-7}$ $\text{cm}^2/\text{s}$ )	$D_e$ ( $10^{-8}$ $\text{cm}^2/\text{s}$ )
Resin				
Virgin	102	5.9	2.6	15.9
Cycled, top sample	39	5.4	1.9	10.5
Cycled, bottom sample	25	4.9	1.8	9.3

$\text{cm}^2/\text{s}$  for protein concentrations varying from 3 to 0.05 mg/mL. Bankston et al. [15], on the other hand, based on a microscopic technique, obtained a nearly constant  $D_e$ -value of  $(7.7 \pm 0.7) \times 10^{-8} \text{ cm}^2/\text{s}$  independent of protein concentration in the range from 0.1 to 1.8 mg/mL. The  $D_e$ -values obtained in this work are closer to those of Bankston et al. The free solution diffusivity of the mAb, obtained by dynamic light scattering with a Wyatt Nanostar instrument (Santa Barbara, CA), is  $D_0 = 3.7 \times 10^{-7} \text{ cm}^2/\text{s}$ , which corresponds to a molecular radius  $r_m = 5.4 \text{ nm}$ . Using a value of  $K_D = 0.612$  for the mAb calculated from eq. 1 and our value of  $D_e = 5.9 \times 10^{-8} \text{ cm}^2/\text{s}$ , the tortuosity factor for diffusion in the virgin resin is  $\tau = D_0 K_D / D_e = 3.9$ , which falls in the range of tortuosity factors typically encountered for transport in macroporous media [17]. As seen from Table 2.2, cycling has a relatively large effect on the  $Bi$ -value but only a small effect on  $D_e$ . Since the actual boundary layer mass transfer coefficient, being dependent only on hydrodynamic factors, is expected to be the same for virgin and cycled samples, the trend observed suggests that the lower  $Bi$ -values are connected with the fouled film at the bead outer surface. The somewhat smaller  $D_e$ -values also seen for the cycled samples compared to the virgin resin are also an indication that fouling affects protein transport, consistent with the reduction of accessible pore size observed by iSEC.

As seen in Fig. 2.4b, desorption occurs on a much shorter time scale compared to adsorption. Even though the final mAb recovery is nearly complete for all three samples (about 100% and 98% for virgin and cycled resins, respectively), the desorption rate is significantly slower for the cycled resins. Neglecting the time needed for the desorption buffer to diffuse in the particles and assuming that desorption is controlled by diffusion of

the unbound mAb in the particle pores, the following equation can be used to describe the fractional amount,  $F$ , of protein desorbed from a resin sample [18][19]:

$$F = \sum_{i=1}^M f_i \left[ 1 - \frac{6}{\pi^2} \sum_{n=1}^{\infty} \frac{1}{n^2} \exp\left(-n^2 \pi^2 \frac{D_e t}{K_D r_{p,i}^2}\right) \right] \quad (2)$$

where  $K_D$  is the distribution coefficient for the unbound mAb (based on eq. 1),  $f_i$  is the volume fraction of particles of radius  $r_{p,i}$ , and  $M$  the number of fractions in the particle size distribution. This equation assumes that desorption occurs in a large volume of desorbent so that the concentration of the mAb in the solution surrounding the particle remains close to zero. Since, in each case, whether virgin or fouled resin samples were used, the particles were initially fully dispersed in PBS by vigorous agitation and did not appear to re-agglomerate, the values of  $f_i$  used in eq. 2 were those obtained for the virgin resin. Table 2.2 gives the values of  $D_e/K_D$  obtained by fitting eq. 2 to the data. As shown by this table,  $D_e/K_D$  is significantly lower for the cycled resins, likely as a result of the accumulation of foulants that block or restrict some of the pores. The corresponding  $D_e$ -values, obtained using  $K_D$  from eq. 1, also decrease with cycling, but still remain about twice as large as the  $D_e$ -values obtained from the batch adsorption experiments suggesting that diffusion under adsorption conditions is hindered by the bound mAb molecules [20]. For the cycled resin, the effect on  $D_e$  during adsorption appears to be a combination of diffusional hindrance due to the bound mAb and the additional hindrance caused by the foulants accumulated in the cycled resins.

### 2.3.3 CLSM results

Figure 2.5 and 2.6 show representative CLSM images for the adsorption of 2 mg/mL mAb on virgin and cycled resin particles, respectively. The virgin particles (Fig. 2.5)

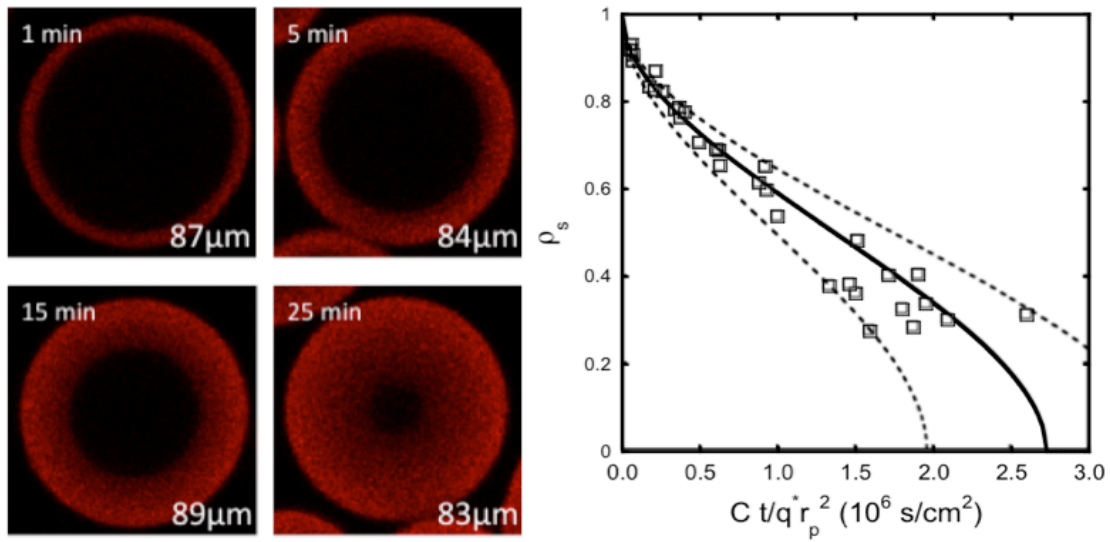


Figure 2.5. Representative CLSM images of virgin resin particles during adsorption of 2 mg/mL mAb in PBS. The actual particle diameter is shown in each image. The graph on the right hand side shows the position of the adsorption front vs. reduced time  $Ct/q_p^* r_p^2$ . The solid line is based on eq. 4 with  $D_e = 6.1 \times 10^{-8} \text{ cm}^2/\text{s}$  and  $1/Bi = 0$ . The dashed lines bracket all data points with  $D_e = 4.8 \times 10^{-8} \text{ cm}^2/\text{s}$  and  $8.5 \times 10^{-8} \text{ cm}^2/\text{s}$ .

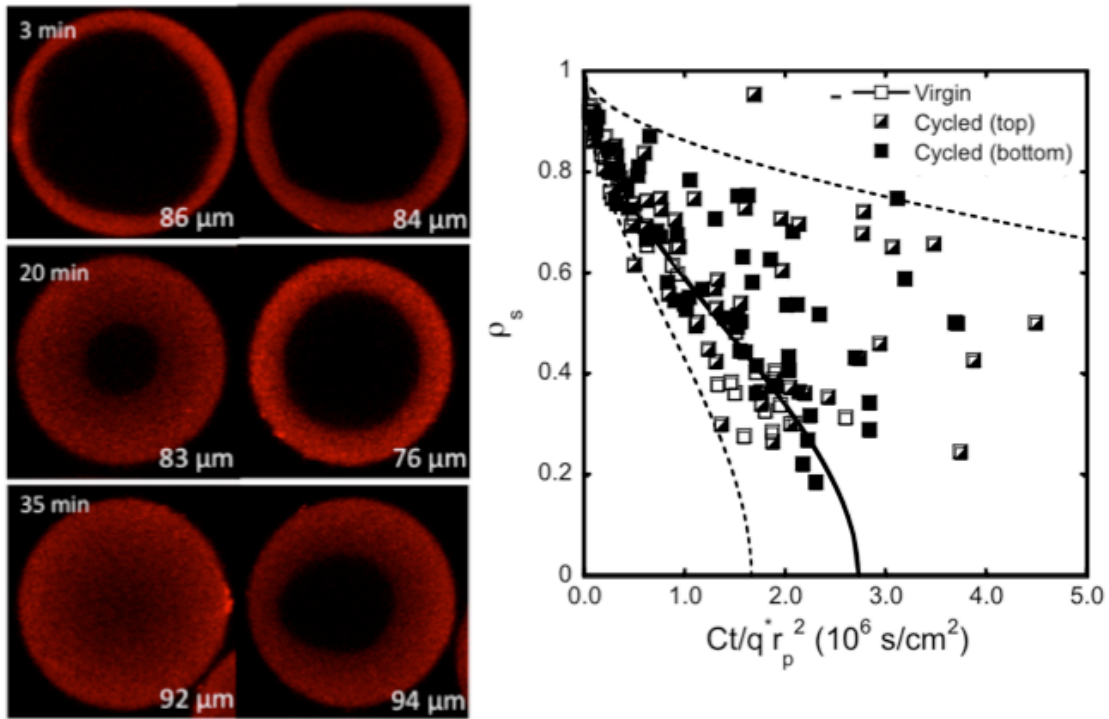


Figure 2.6. Representative CLSM images of particles from the cycled resin sample (bottom 1/3) during adsorption of 2 mg/mL mAb in PBS. Pairs of beads with comparable size at the same adsorption time are shown in each panel. The graph on the right hand side shows the position of the adsorption front vs. reduced time  $Ct/q_p^* r_p^2$ . The solid line is for the virgin resin based on eq. 4 with  $D_e = 6.1 \times 10^{-8} \text{ cm}^2/\text{s}$  and  $1/Bi = 0$ . The dashed lines bracket all data points with  $D_e = 0.86 \times 10^{-8} \text{ cm}^2/\text{s}$  and  $10.0 \times 10^{-8} \text{ cm}^2/\text{s}$ .

show sharp and circular adsorption fronts consistent with the shrinking core model.

Accordingly, the front position,  $r_s$ , is related to time by the following equation [17][18]:

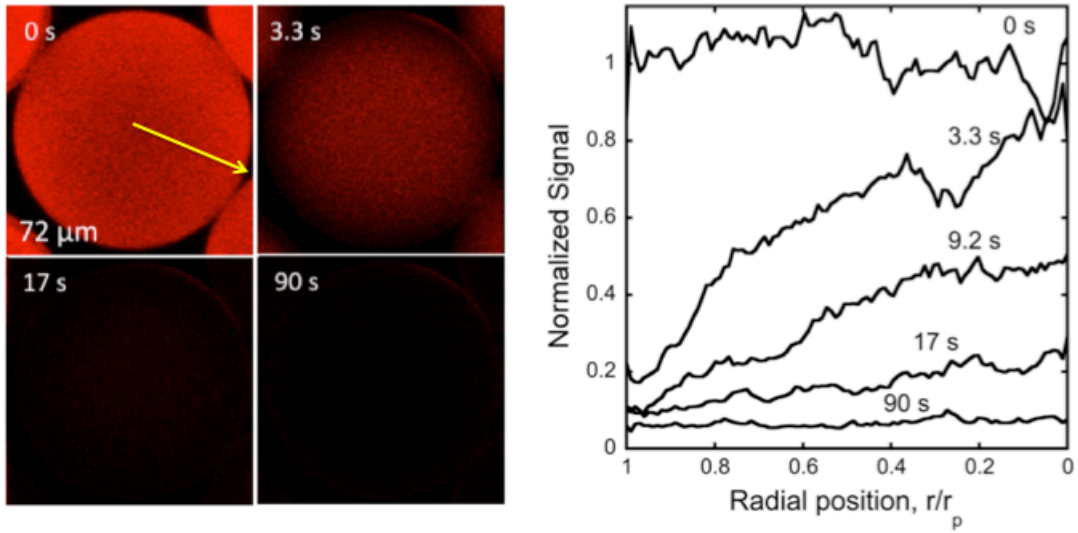
$$3(1 - \rho_s^2) - 2\left(1 - \frac{1}{Bi}\right)(1 - \rho_s^3) = \frac{6D_e C t}{q^* r_p^2} \quad (3)$$

where  $\rho_s = r_s / r_p$ ,  $C$  is the protein solution concentration, and  $q^*$  is the binding capacity.

A high value of  $Bi$  is expected based on the batch adsorption measurements. A comparison of this equation taking  $1/Bi=0$  with the data is shown in Fig. 2.5. The regressed value of  $D_e = (6.1 \pm 0.2) \times 10^{-8} \text{ cm}^2/\text{s}$  is in good agreement with the value obtained from the batch adsorption experiments.  $D_e$  is bracketed by  $4.8 \times 10^{-8} \text{ cm}^2/\text{s}$  and  $8.5 \times 10^{-8} \text{ cm}^2/\text{s}$  as shown in Fig 2.5. All beads examined in this sample behaved in a consistent manner. However, this was not the case for the cycled samples. As seen in Fig. 2.6, not only is the progress of the adsorption front in the particles generally slower than for the virgin resin, but, as seen from the plot of the average value  $\rho_s$  included in Fig. 2.6, different beads in the same sample show drastically different rates for samples collected either from the top or from the bottom of the column.  $D_e$  in this case is bracketed by  $0.86 \times 10^{-8} \text{ cm}^2/\text{s}$  and  $10.0 \times 10^{-8} \text{ cm}^2/\text{s}$  as shown in Fig 2.6. Moreover, for several particles in each sample, the front did not exhibit the circular pattern expected for homogenous diffusion.

The observed variations from particle to particle in the cycled samples suggest that the degree of fouling and its effects on protein adsorption are different for different particles. Additionally, it is apparent that fouling is also not uniformly distributed on the bead surface, probably being dependent on the physical contact with other beads in the column used for the process cycle. Based on the CLSM observations about 12% of the beads in

(a) Virgin bead



(b) Cycled bead

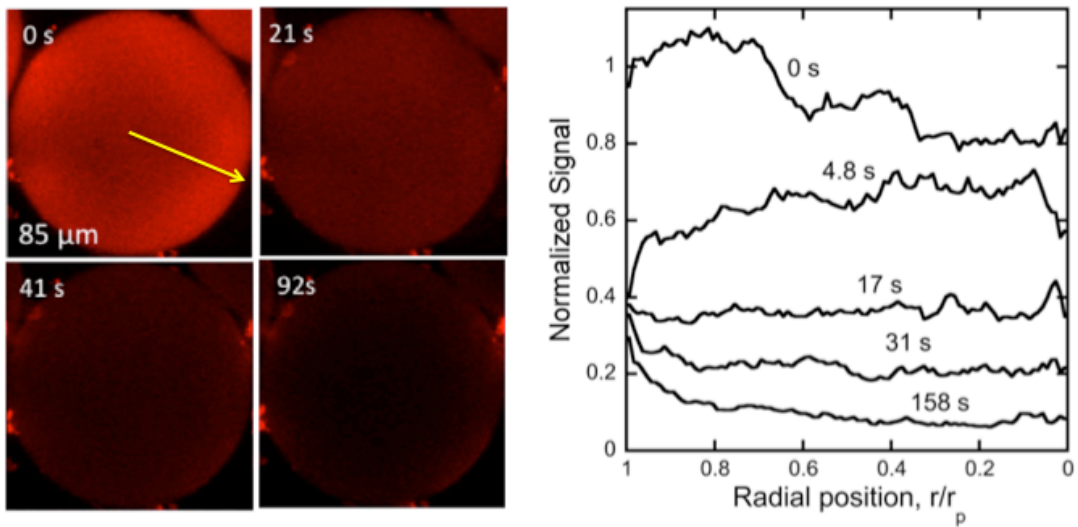


Figure 2.7. Representative CLSM images of a virgin resin bead (a) and of a bead from the bottom 1/3 sample of the cycled resin (b) during desorption at pH 3.5 following incubation with 5 mg/mL mAb in PBS. The bead diameters are 72 and 85  $\mu\text{m}$  for the virgin and cycled bead, respectively. The graphs on the right show the digitized fluorescence intensity at the bead centerline from the bead surface to the bead center as indicated by the arrow in the left image.

the cycled samples showed significant deviations from a circular front and exhibited rates significantly slower than those observed for the virgin resin particles.

Figure 2.7 shows representative CLSM images obtained in the flow cell for a virgin (a) and a cycled resin bead (b) during desorption at pH 3.5 following incubation with 5 mg/mL mAb in PBS for 3 h for the virgin sample and for 1 h for the cycled sample. The fluorescence intensity profiles, normalized based on the fluorescence intensity profile of the virgin saturated bead as discussed by Perez-Almodovar et al. [12] and Tao et al. [13], are also shown along the bead centerline for both the virgin and the cycled bead. As seen from this figure, the CLSM results for the virgin bead are consistent with the batch desorption measurements with desorption essentially complete in less than 90 s. The intensity profiles, in this case, follow the pattern expected for a diffusion-controlled process with the intensity dropping to near zero after a very short time following exposure to the desorption buffer. Longer times are obviously needed for the cycled bead. In this case, both the images and the digitized profiles show that the fluorescence intensity at the bead surface drops quickly upon initial exposure to the desorption buffer, but then settles to a value that remains about constant for the rest of the duration of the experiment. Even after 158 s, the fluorescence intensity at the bead surface is still more than 30% of the initial value indicating that essentially irreversibly bound protein persists near the bead surface. Although some residual mAb appears to exist throughout the bead even after a relatively long time in the desorption buffer, accumulation of the mAb seems to be greatest near the bead surface where accumulation of foulants during process cycling is also greatest.

#### **2.4 Discussion and conclusions**

The results obtained in this work show that cycling the Protein A MabSelect resin through a standard process for mAb capture from a clarified cell culture supernatant results in some significant changes in resin structure and properties that appear to be correlated with declining process performance. Macroscopically, the cycled resin particles have a strong tendency to adhere to each other and have a “clumpy” appearance, which makes it difficult to disperse the particles in a homogeneous slurry and repack them into a column and is likely caused by accumulation of hydrophobic foulants. The cycled resin samples show reduced porosity and apparent pore size and contain a dense residue both as a film at the bead surface and as granules through the bead interior. With regards to performance properties, the cycled resin samples exhibit mAb binding capacities that are fairly close to that of the virgin resin and adsorption rates of the purified mAb which differ only for short times from the rates observed for the virgin resin. Based on the rate measurements and consistent with the TEM results, the nature of the foulant film at the bead outer surface appears to be heterogeneous thereby still allowing the protein to diffuse into the beads, albeit at a reduced rate. This reduction is evident from the much lower apparent Biot numbers for the fouled beads (see Table 2.2), which suggest the addition of a “fouling resistance” associated with a solid film analogous to that often seen in heat transfer equipment. This fouling resistance is in addition to the ordinary boundary layer resistance on the fluid side of the bead-fluid interface and results in a lower apparent  $Bi$ . Desorption rates were more significantly affected by cycling with the time required for desorption becoming significantly longer for the cycled resin. Microscopic examination by CLSM confirms that both adsorption and desorption are diffusion-limited for both virgin and cycled resin. Different beads

from the virgin resin sample behaved in a consistent manner under both adsorption and desorption conditions, indicating that structural and chemical characteristics are initially homogeneously distributed. This was not the case, however, for the cycled resin samples for which different beads exhibited dramatically different behaviors under both adsorption and desorption conditions. The reasons for this heterogeneity are not known. One possibility is that the extent to which the beads are fouled depends on the existence of locally areas exposed to minimal or no flow in the packed bed actually used for the capture process. Corbett et al. [10] and Close et al. [21], have shown that fouling of an anion exchanger resin used in a mAb polishing step was heterogeneously distributed which was shown to be correlated with the highly compressed nature of the packed bed that created areas with little or no flow of the mobile phase.

A final consideration is whether some of the techniques used in this work can be used to assess the effectiveness of modified cleaning protocols. Figure 2.8 shows TEM images of resin beads taken from the top 2/3 and bottom 1/3 of a different column that was cycled with the same clarified cell culture supernatant for the conditions described in the Materials and Methods section, but replacing the 50 mM NaOH/1 M NaCl cleaning step with a different, improved cleaning protocol. A discussion of the nature of the improvements made is beyond the scope of this paper and the results above are shown only to provide an example where some of the techniques developed in this work were used to validate a successful cleaning protocol. As shown in this figure, even after 40 cycles there is no evidence of accumulation of foulants of the type seen with the original protocol. This new protocol resulted in a process that did not exhibit significant changes

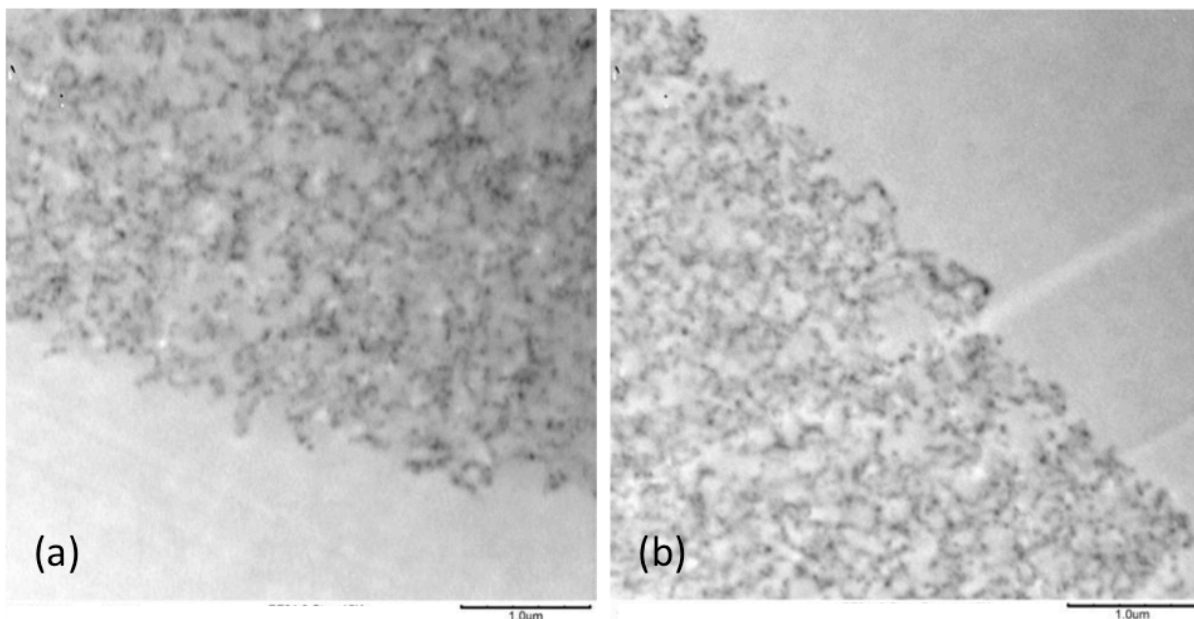


Figure 2.8. TEM images of cycled resin from: (a) the top 2/3; and (b) the bottom 1/3 of a column after 40 cycles used with the protocol described in the Materials and Methods section but with an improved 3-step cleaning procedure. Magnification was 15k. Scale bar is 1  $\mu\text{m}$ . No stain was used.

in performance suggesting that absence of the dense deposits from the TEM is correlated with stable process performance.

Two aspects not specifically considered in this work are the potential effects of the low pH strip that was included in the process protocol and the nature of the mAb on the fouling behavior observed with the original cleaning protocol. With regards to the effect of the low-pH strip, although consistent with operating protocols provided by the resin manufacturer, a possibility is that this step could potentially lead to degradation of protein molecules left in the resin at the end of the elution step. With regards to the effects of the nature of the mAb, the results presented in this work are specific to the specific mAb used, which is more hydrophobic in nature compared to other mAbs. In either case, it is clear that further research is needed to generalize our findings.

## **2.5 References**

- [1] Gagnon P. Purification tools for monoclonal antibodies. Validated Biosystems, Tucson, AZ (1995).
- [2] Fahrner R.L., Whitney D.H., Vanderlaan M., Blank, G.S. Performance comparison of Protein A affinity-chromatography sorbents for purifying recombinant monoclonal antibodies. *Biotechnol. Appl. Biochem.* 30 (1999) 121-128.
- [3] Shukla A.A., Hubbard B., Tressel T., Guhan S., Low D. Downstream processing of monoclonal antibodies: application of platform approaches. *J. Chromatogr. B*, 848 (2007) 28-39.
- [4] Kelley B. Very large scale monoclonal antibody purification: The case for conventional unit operations. *Biotechnol. Progr.* 23 (2007) 995–1008.

- [5] Hober S., Nord K., Linhult M. Protein A chromatography for antibody purification. *J. Chromatogr. B*, 848 (2007) 40-47.
- [6] Hahn R., Shimihara K., Steindl F. Jungbauer A. Comparison of Protein A affinity sorbents. III Life time study. *J. Chromatogr. A*, 1102 (2006) 224-231.
- [7] Jiang C., Liu J., Rubacha M., Shukla A.A. A mechanistic study of Protein A chromatography resin lifetime. *J. Chromatogr. A*, 1216 (2009) 5849-5855.
- [8] Grönberg A., Eriksson M., Ersoy M., Johansson H.J. A tool for increasing the lifetime of chromatography resins. *MABS*, 3 (2011), 192–202.
- [9] Hagel L., Ostberg M., Andersson T. Apparent pore size distributions of chromatography media. *J. Chromatogr. A*, 743 (1996) 33-42.
- [10] Corbett R., Carta G., Iskra T., Gallo C., Godavarti R., Salm J. R. Structure and protein adsorption mechanisms of clean and fouled tentacle-type anion exchangers used in a monoclonal antibody polishing step. *J. Chromatogr. A*, 1278 (2013) 116–25.
- [11] Carta G., Ubiera A.R., Pabst T.M. Protein mass transfer kinetics in ion exchange media: Measurements and interpretations. *Chem. Eng. Technol.* 28 (2005) 1252-1264.
- [12] Perez-Almodovar E.X., Tao Y., Carta G. Protein adsorption and transport in cation exchangers with a rigid backbone matrix with and without polymeric surface extenders. *Biotechnol. Progr.* 27 (2011) 1264-1272.
- [13] Tao Y., Perez-Almodovar E.X., Carta G., Ferreira G., Robbins D. Adsorption kinetics of deamidated antibody variants on macroporous and dextran-grafted

- cation exchangers. III. Microscopic studies. *J. Chromatogr. A*, 1218 (2011) 8027-8035.
- [14] Hahn R., Bauerhansl P., Shimara K., Wiznieski C., Tscheliessnig A., Jungbauer A. Comparison of Protein A affinity sorbents. II. Mass transfer properties. *J. Chromatogr. A*, 1093 (2005) 98-110.
- [15] Bankston T.E., Stone M.C., Carta G. Theory and applications of refractive index-based optical microscopy to measure protein mass transfer in spherical adsorbent particles. *J. Chromatogr. A*, 1188 (2008) 242-254.
- [16] Stone M.C., Carta G. Protein adsorption and transport in agarose and dextran-grafted agarose media for ion exchange chromatography. *J. Chromatogr. A*, 1146 (2007) 202-215.
- [17] LeVan M.D., Carta G., Adsorption and Ion Exchange in Gree D.W. Perry's *Chemical Engineers' Handbook*, 8<sup>th</sup> Ed., Section 16, McGraw-Hill, New York (2007).
- [18] Ruthven D.M. *Principles of adsorption and adsorption processes*. Wiley, New York (1985).
- [19] Ubiera A.R., Carta G. Particle-size distribution effects in batch adsorption. *AIChE J.* 49 (2003) 3066-3073.
- [20] Hahn R., Bauerhansl P., Jungbauer A. Novel high capacity and high alkaline stable Protein A affinity chromatography media: characterization and engineering considerations. Paper presented at Affinity 2005, Uppsala, Sweden (2005).

- [21] Close E. J., Salm J. R., Iskra T., Sørensen E., Bracewell, D.G. Fouling of an anion exchange chromatography operation in a monoclonal antibody process: visualization and kinetic studies. *Biotechnol. Bioeng.* 110 (2013) 2425-2435.

### **3 Chapter 3**

#### **Nature of Foulants and Fouling Mechanism in the Protein A MabSelect Resin Cycled in a Monoclonal Antibody Purification Process**

---

##### **3.1 Introduction**

Protein A resins are used extensively in the purification of monoclonal antibodies (mAbs) at manufacturing scale [1][2][3][4]. Due to their high cost, the ability to reuse these resins is critical for economic reasons [5][6][7]. Sodium hydroxide is often the cleaning agent of choice for many Protein A resins as it has the ability to hydrolyze proteinaceous residues and simultaneously sanitize the resin [4][8][9]. Its use, however, has to be balanced against the limited stability of the Protein A ligand. Although more expensive resins containing engineered Protein A ligands are now available with the ability to sustain prolonged exposure to relatively concentrated NaOH [4][10], concentrations around 50 mM NaOH are recommended and are typically used as a compromise between cleaning effectiveness and minimum damage to the ligand for more traditional recombinant Protein A resins [6]. Although many processes can be operated successfully for an extended number of cycles (>100) with such conditions without major loss of performance, situations exist where substantial resin fouling occurs even after a relatively small number of cycles. In such cases, the ability to monitor the accumulation of foulants within the resin and on the resin surface is critical in order to assess the effectiveness of cleaning protocols or to develop strategies to prevent fouling in the first place. In prior work [11], we have shown that recovery of a mAb from a clarified CHO cell culture supernatant with the Protein A MabSelect resin declined substantially in fewer than 20

cycles. Resin removed from the process column showed clear evidence of fouling demonstrated by a strong tendency of the resin beads to adhere to each other forming resin aggregates that were difficult to disperse and prevented the effective re-packing. In our work we showed that the cycled resin had smaller porosity and apparent pore size compared to the virgin resin. Moreover, electron microscopy showed the accumulation of foulants both on the external surface of the resin beads as well as in the resin interior. The presence of these foulants was related to the reduced binding capacity and slower mass transfer kinetics observed when a purified version of the mAb was adsorbed and desorbed from the cycled resin samples. Further investigation by confocal laser scanning microscopy (CLSM) showed that the effects of fouling were not the same for all beads in the same sample and that even within individual resin beads the fouling was heterogeneously distributed.

In principle, various types of foulants can accumulate on Protein A resins during the load step as a result of non-specific, irreversible interaction of either the product or media components with the resin [12][13][14]. However, fouling can also potentially occur during the elution step. Since elution generally occurs at low pH where certain proteins can be destabilized, precipitation of large product aggregates can potentially occur on and within the resin resulting in fouling that can be recalcitrant to ordinary cleaning protocols. A few different methods have been proposed to determine the nature of foulants accumulated on Protein A resins. Hahn et al. [5], for example, boiled resin samples that were used in a lifetime study in a SDS buffer and then performed SDS-PAGE analysis of the species extracted from the resin. The results showed that some of the Protein A resins tested contained residual IgG, IgG fragments, and BSA, which was present in the protein

mixture loaded on to the column. Grönberg et al. [7] also used the approach of boiling the resin in SDS but they analyzed the extract in a high-throughput screening mode using chip-based electrophoresis to determine the presence of proteinaceous foulants. This approach was used to assess the effectiveness of more robust cleaning protocols.

Although boiling in SDS provides semi-quantitative information about the types of foulants that may be present in cycled resins, it does not provide information about their physical nature or their spatial distribution within the resin beads. The analysis is also lengthy and subject to difficulties in quantitation when silver staining is necessary for high sensitivity [5]. Thus, in this work we apply a combination of electron microscopy and confocal microscopy tools to (1) characterize the composition of foulants in the Protein A MabSelect resin for a mAb that resulted in substantial losses of product recovery with cycling; (2) determine the physical nature and spatial distribution of foulants within resin beads cycled in this process; and (3) help determine the mechanisms that lead to the accumulation of foulants during the process. These approaches are also tested by comparing fouling in resins used for different mAbs, with different resins, and for different operating conditions that did not result in significant fouling.

## **3.2 Materials and Methods**

### **3.2.1 Materials**

The monoclonal antibody (mAb A) principally used in this work is the same as that used in our prior work [11] and is a glycosylated IgG2 antibody with a molecular mass of about 160 kDa. It was provided by Pfizer (St. Louis, MO) both in highly purified form (>99% purity by SDS-PAGE and <1% of aggregated species by SEC) and as produced, in a conditioned CHO cell culture supernatant. Two additional purified mAbs (mAb B

and mAb C) that exhibited fouling behaviors different from that of mAb A, as well as anti-CHO-HCP polyclonal antibodies were also obtained from Pfizer. Other proteins, including BSA,  $\alpha$ -lactalbumin, cytochrome-C, and BSA labeled with 10 nm gold were obtained from Sigma-Aldrich (St. Louis, MO). Protein A was obtained from Repligen Corporation (Waltham, MA). Protein A labeled with 10 nm gold was obtained from Electron Microscopy Science (Hatfield, PA). Sodium phosphate, sodium bicarbonate, acetic acid, sodium hydroxide, sodium chloride, and SDS were purchased from Fisher Scientific (Pittsburgh, PA) and Sigma-Aldrich (St. Louis, MO). Rhodamine Red<sup>TM</sup>-X and Rhodamine Green<sup>TM</sup>-X succinimidyl ester amine-reactive dyes were purchased from Invitrogen Corporation (Carlsbad, CA). All experiments were conducted at room temperature.

The MabSelect resin used in this work was obtained from GE Healthcare (Piscataway, NJ). The resin was packed in a 60 cm diameter, 20 cm long column from Pall Life Sciences (Resolute® Chromatography Column, Port Washington, NY) according to manufacturer specifications and used in the mAb A purification process over multiple cycles comprising the following steps:

Equilibration: Tris buffer with high NaCl at pH 7.5 for 5 CV

Load: Conditioned CHO cell culture supernatant with a mAb load of 25 to 38 mg/mL of column volume

Wash: First equilibration buffer for 3 CV, then Tris buffer with low NaCl at pH 7.5 for 3 CV

Elute: 25 mM sodium acetate at pH 3.5 for 4 CV

Strip: 250 mM acetic acid and 250 mM NaCl for 4 CV

Clean: 50 mM NaOH with 1 M NaCl for 4 CV

As described previously [11], after 20 cycles, the column was unpacked and the resin divided in two samples – one from the top 2/3 of the column and one from the bottom 1/3. Small differences were seen between the two cycled samples. For example, the particles in both samples were highly aggregated and could be dispersed in buffer only with vigorous agitation. Both samples were stored in 20% ethanol at 4 °C. Our prior work describes the physical characterization of these samples by inverse size exclusion chromatography and by TEM along with their antibody binding capacity and adsorption/desorption kinetics.

Two additional MabSelect resin samples were obtained for resin cycled with the same protocol described above except that the cell culture supernatant in one case was replaced by the purified mAb A dissolved in PBS while in the other it was replaced by a null cell culture supernatant containing no mAb. The null cell culture was conducted following the same process conditions as the product expressing culture, while producing commensurate peak cell density and viability data. Both of these samples were obtained with laboratory scale columns. A 1.1-cm diameter, 20-cm long column, cycled for 33 times was used with the purified mAb feedstock while a 0.66-cm diameter, 19-cm long column, cycled for 20 times was used with the null cell culture supernatant.

A final sample was obtained by cycling the MabSelect resin in a scaled-down column with the conditioned CHO cell culture supernatant spiked with both fluorescently-labeled mAb A and with fluorescently-labeled BSA. Two different fluorophors were used, rhodamine red for the mAb and rhodamine green for BSA, in order to monitor the accumulation of each in the resin beads. For this purpose, the virgin resin was packed in a

0.5 diameter x 5 cm long HR chromatography column from GE Healthcare (Piscataway, NJ) fitted with two adapters to obtain a packed bed height of 0.5 cm (corresponding to a 0.1 mL column volume) and subjected to 30 cycles of the steps described above at a flow rate of 0.1 mL/min. A Model A-60-S pump (Eldex Laboratories, Inc., Napa, CA) with a Model E12 electrically actuated rotary valve (Valco Instruments Co. Inc., Houston, TX), with a computer-based control system was used for this purpose. The molar ratios of labeled mAb and labeled BSA to the mAb contained in the cell culture supernatant were 1:240 and 1:20, respectively. After 30 cycles, the column was unpacked and the resin re-suspended in PBS.

The strong cation exchanger SP-Sepharose-FF was also obtained from GE Healthcare and was used in a few control experiments.

### **3.2.2 Methods**

#### **3.2.2.1 Transmission electron microscopy**

Transmission electron microscopy (TEM) was performed as described in detail by Corbett et al. [15]. Briefly, the resin samples were dehydrated in a water-ethanol gradient, embedded in an acrylic resin (LR-White, London Resin Company, Ltd., London, UK), and ultramicrotomed. The sections were then observed with a model 1230 electron microscope from JEOL Ltd. (Tokyo, Japan). Images were taken by a SIA CCD camera with 4K×4K resolution.

Gold-labeled Protein A and gold-labeled BSA were used to determine the association of these proteins with the foulants present in the cycled resin samples and the spatial location of such interactions in the beads. For this purpose, 10 mg of each resin sample were first mixed for 2 h with 300 µL of either gold-labeled Protein A or gold-labeled

BSA, both of which had been diluted 10-fold in PBS. The samples were then washed with PBS, fixed by mixing them with 2% glutaraldehyde for 20 min, washed again with PBS, and finally embedded, ultramicrotomed, and imaged by TEM as described above.

#### **3.2.2.2 Confocal laser scanning microscopy**

Confocal laser scanning microscopy (CLSM) was used to determine the association of fluorescently labeled Protein A, BSA,  $\alpha$ -lactalbumin, cytochrome-C, and anti-CHO-HCP antibodies with the foulants present in the cycled resin beads. Fluorescent labeling was achieved for each protein as previously described [16][17]. Briefly, each protein was mixed for 1 h with the chosen rhodamine reactive dye in a 3:1 molar ratio in 500 mM sodium bicarbonate buffer at pH 8.5. Econo-Pac 10 DG desalting columns (Bio-Rad Laboratories, Hercules, CA) were then used to separate the labeled protein from any unreacted dye. Molar labeling ratios between 0.2 and 0.3 were obtained as determined with a NanoVue Spectrophotometer (GE Healthcare, Piscataway, NJ).

CLSM imaging was conducted with a Zeiss LSM 510 microscope using a Plan-Apochromat 63  $\times$ /1.4 NA oil objective (Carl Zeiss MicroImaging, LLC, Thornwood, NY). For this purpose, the resin particles were mixed with each labeled protein solution for 30 min in a microcentrifuge filter tube, then filtered, washed with PBS, re-suspended in PBS, and observed by CLSM. The excitation wavelength was 561 nm and 488 nm for red and green lasers. Emission wavelength greater than 575 nm was collected for red channel and emission wavelength between 490 and 510 nm was collected for green channel. All images were taken at the equator of the beads.

#### **3.2.2.3 Quantification of BSA binding to mAb**

Since microscope-based experiments indicated that fluorescently-labeled BSA associates with mAb A when this species is adsorbed on the MabSelect resin, size exclusion chromatography (SEC) was used as a tool to quantify the extent of association. SEC was performed with a Model BEH200 SEC 1.7  $\mu\text{m}$  UPLC column from Waters Corporation (Milford, MA) with an ACQUITY UPLC system also from Waters Corporation operated at 0.2 mL/min in 100 mM sodium phosphate at pH 6.8. The signal was monitored at both 280 nm and 570 nm, the latter corresponding to the absorbance maximum of the dye conjugated to BSA.

### **3.3 Results**

#### **3.3.1 Resin cycled with conditioned CHO cell culture supernatant**

Figure 3.1 shows representative TEM images of beads from a resin sample cycled with the mAb A-containing cell culture supernatant and incubated with 10 nm gold-labeled Protein A. Fouling is evidenced by denser bodies present both as a film on the bead outer surface and inside the matrix of cycled beads, which are not present in TEMs of the virgin resin [11]. As shown previously, these foulants are heterogeneously distributed with individual beads and different beads from the same cycled samples showing different degrees of fouling. Sections from two different beads are shown in Fig. 3.1, one with a heavily fouled bead surface and the other one with a less fouled surface, but still exhibiting evidence of dense bodies in the bead interior. Similar results were obtained for beads from the top or bottom sections of the column. As seen from these images, accumulation of gold-labeled Protein A is visible both near the outside bead surface and in its interior around the denser bodies. Because of the high specificity of Protein A for mAbs, the result suggests that the foulants in the cycled resin are mAb-related. However,

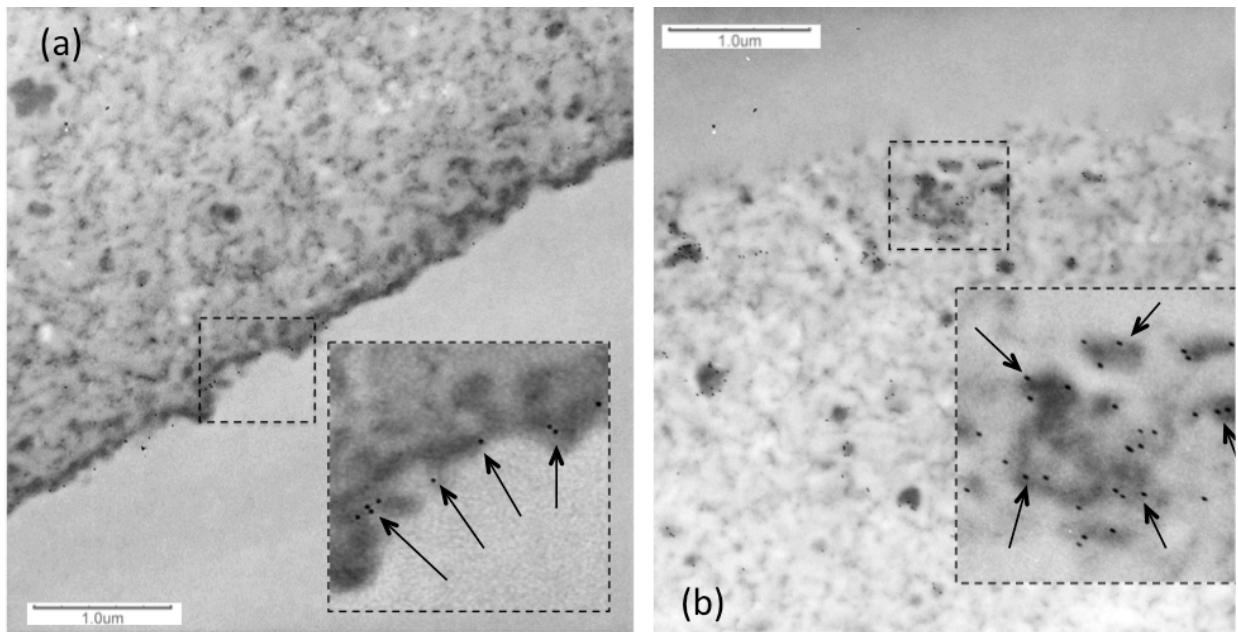


Figure 3.1. TEM images of beads taken from the bottom 1/3 of the column cycled with conditioned CHO cell culture supernatant after incubation with gold-labeled Protein A. Both images were taken near the resin bead surface. The larger box shown in each image is an enlarged view of the smaller box of (a) near the heavily fouled bead surface and (b) inside the bead. Arrows highlight some of the gold nanoparticles for better clarity.

in a control experiment, no gold-labeled Protein A was seen to accumulate either at the surface or in the interior of the beads of virgin MabSelect resin (data now shown).

Figure 3.2 shows the TEM image of a bead from the resin cycled with the mAb A cell culture supernatant and incubated with gold-labeled BSA. As seen in this image, the BSA accumulates both at the fouled bead outer surface and on the dense bodies present in the bead interior. No evidence of accumulation of gold-labeled BSA was seen for the virgin resin (data not shown) suggesting that BSA also has an affinity for the foulants.

Figure 3.3 shows representative CLSM images of three different resin particles taken from the bottom 1/3 of the column cycled with the mAb A-containing CHO cell culture supernatant followed by incubation in PBS containing a mixture of rhodamine green-labeled Protein A (RG-PA) and rhodamine red-labeled BSA (RR-BSA). As seen in the images, substantial fluorescence is seen at both wavelengths indicating that both RG-PA and RR-BSA associate with the cycled resin. CLSM images of virgin resin beads incubated with the same labeled protein mixture (data not shown) exhibited no fluorescence at either of the two wavelengths, suggesting that both Protein A and BSA associate with foulants accumulated in the cycled resin and do not interact with either the resin backbone or with the immobilized Protein A ligand. As seen in Fig. 3.3, both green and red fluorescence are heterogeneously distributed throughout the fouled beads, but follow the same pattern in each suggesting that both Protein A and BSA interact with the same foulant species. A few particularly bright areas exist in all three particles shown, mostly at the particle outer surface, but also concentrated in a few spots in the bulk of the beads, suggesting that these are regions where greater concentrations of foulants have accumulated.

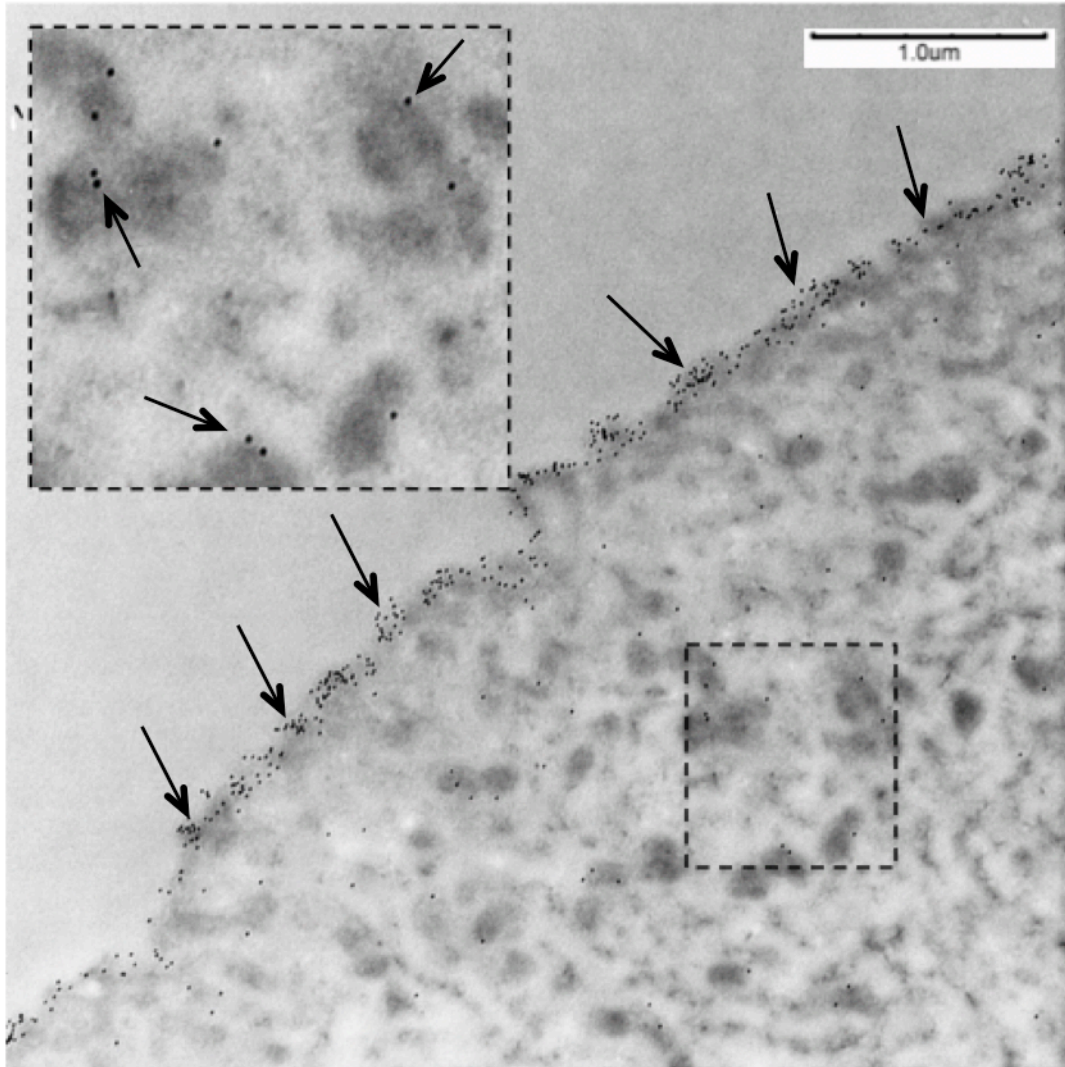


Figure 3.2. TEM image of a bead taken from the bottom 1/3 of the column cycled with conditioned CHO cell culture supernatant after incubation with gold-labeled BSA. The image was taken near the outside surface of the bead. The larger box is the enlarged view of the smaller box in the image. Arrows highlight some of the gold nanoparticles for better clarity.

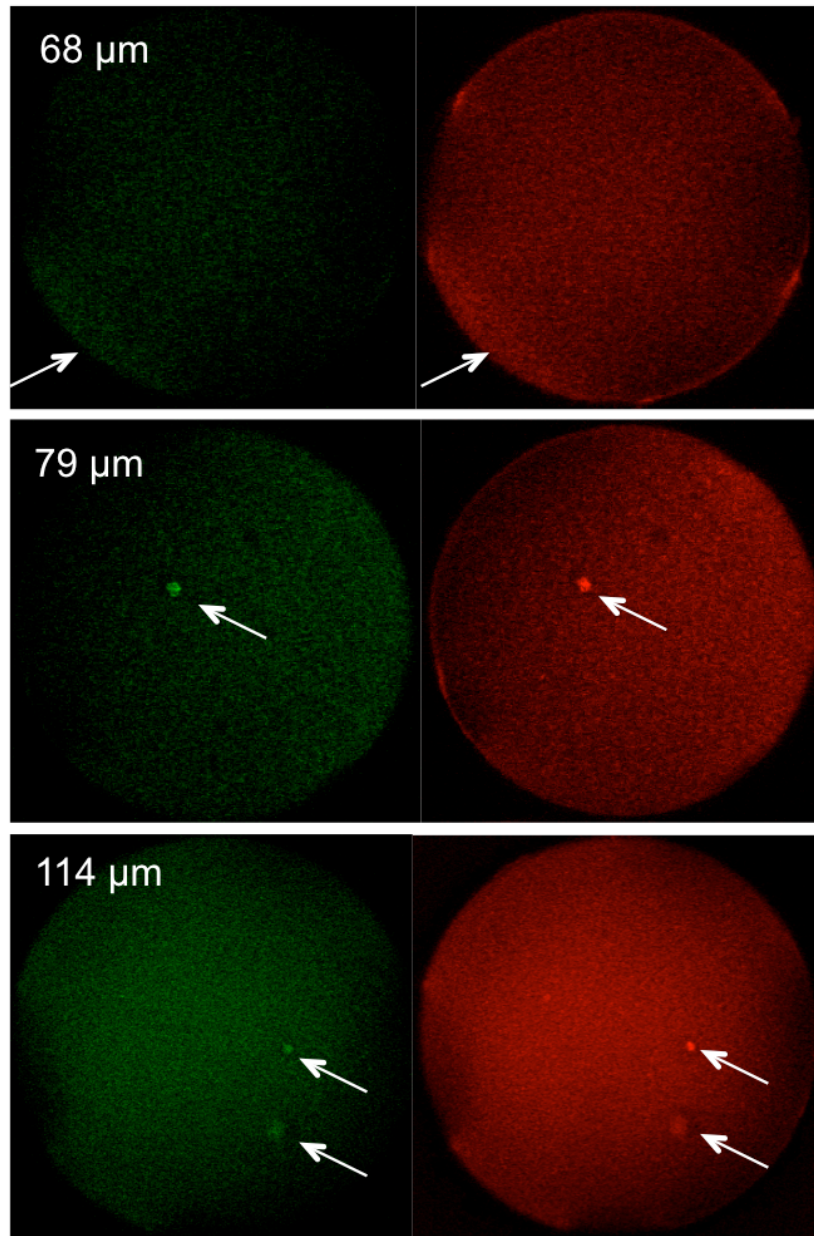


Figure 3.3. CLSM images of three different beads taken from the bottom 1/3 of the column cycled with clarified cell culture supernatant after incubation with a mixture of rhodamine green-labeled Protein A and rhodamine red-labeled BSA. The actual diameter of each bead is shown in each image. Arrows indicate for clarity some of the areas of concentrated fluorescence at the two wavelengths used to detect the rhodamine green and red dyes.

Control experiments were done with rhodamine green-labeled  $\alpha$ -lactalbumin and with rhodamine green-labeled cytochrome-c in place of BSA.  $\alpha$ -lactalbumin, which, like BSA, is lipophilic [18], gave fluorescence patterns in the cycled beads similar to those obtained with BSA, while cytochrome-c gave no fluorescence at all (results not shown). These results suggest that the observed association is common to lipophilic proteins and that it is not dependent on the fluorescent label. A further control experiment was done by adding an excess of octanoic acid to the rhodamine green-labeled BSA solution and then diafiltering the solution to remove the excess acid prior to incubation with the fouled resin beads. Little fluorescence is seen in the beads in this case, suggesting that the association of BSA with the foulants is lipophilic in nature (results not shown).

Figure 3.4 shows the CLSM images of a bead from a virgin resin sample (a) and of three different beads taken from the bottom 1/3 of the column cycled with the mAb A-containing CHO cell culture supernatant (b, c, d) taken after incubation with rhodamine green-labeled anti-CHO-HCP antibodies (RG-anti-CHO-HCP-Abs) in 25 mM sodium acetate at pH 3.5. This pH value was selected to prevent binding of the anti-CHO-HCP-Abs to the Protein A ligand while preserving their ability to bind to HCPs that may be present in the fouled resin. Since the anti-CHO-HCP-Abs were raised specifically against the CHO-HCPs found in the actual process, we hypothesize that binding of these antibodies to CHO-HCPs present in the resin would be stronger than binding to the Protein A ligand. As seen from Fig. 3.4, there is no fluorescence for the virgin bead, but some fluorescence is clearly visible at the outer surface of the bead indicating that some residual HCPs are indeed present in the cycled beads. Interestingly, however, the

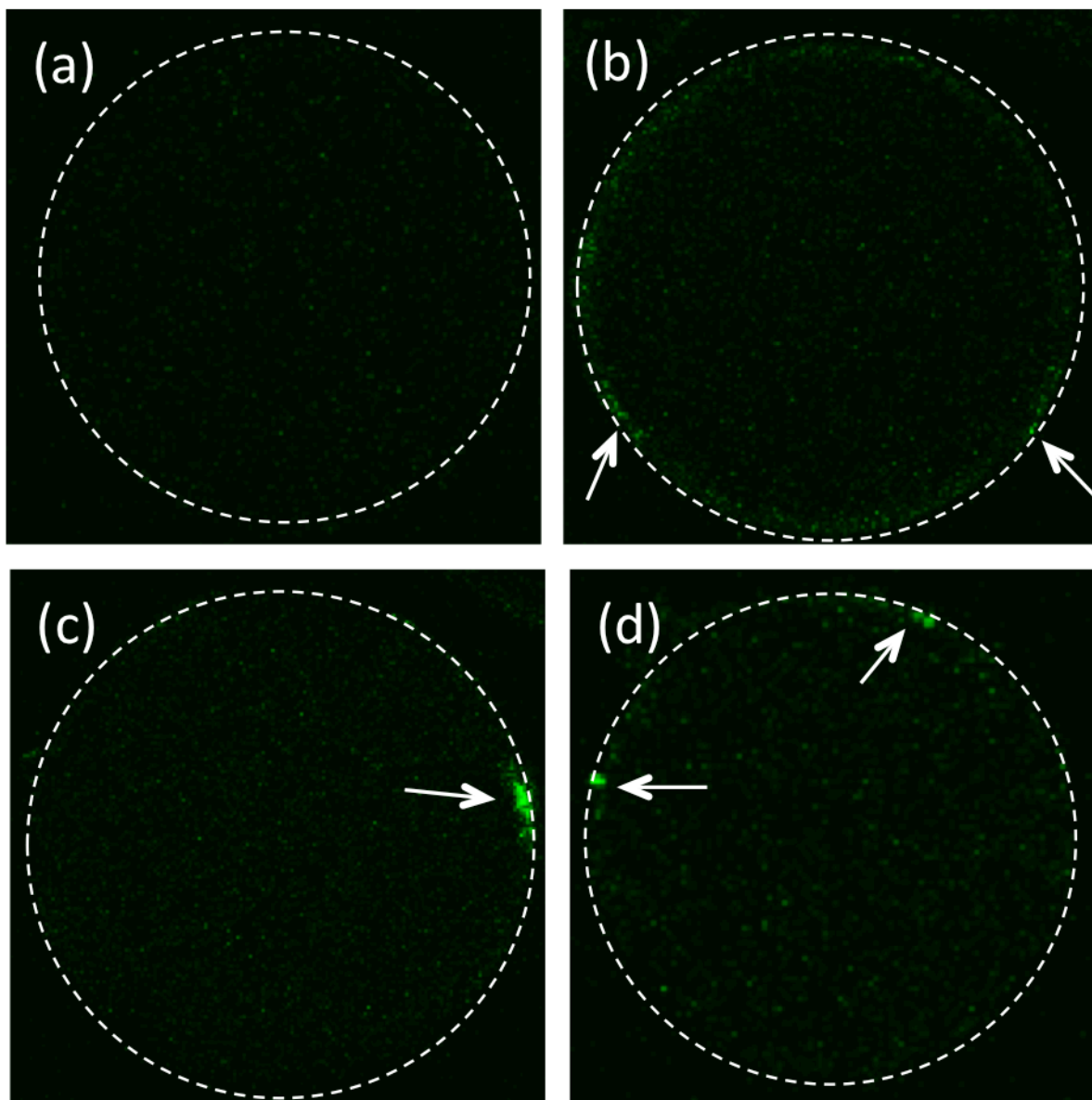


Figure 3.4. CLSM images of a virgin resin bead (a) and three different beads taken from the bottom 1/3 of the column cycled with conditioned cell culture supernatant (b, c, d) following incubation with rhodamine green-labeled anti-CHO-HCP antibodies. Actual particle diameters were 73, 78, 88, and 53  $\mu\text{m}$  in a, b, c, and d, respectively. The dashed lines show the outline of each bead. Arrows indicate for clarity some of the areas of concentrated fluorescence.

presence of HCPs in the fouled beads seems to be limited primarily to areas near the bead external surface.

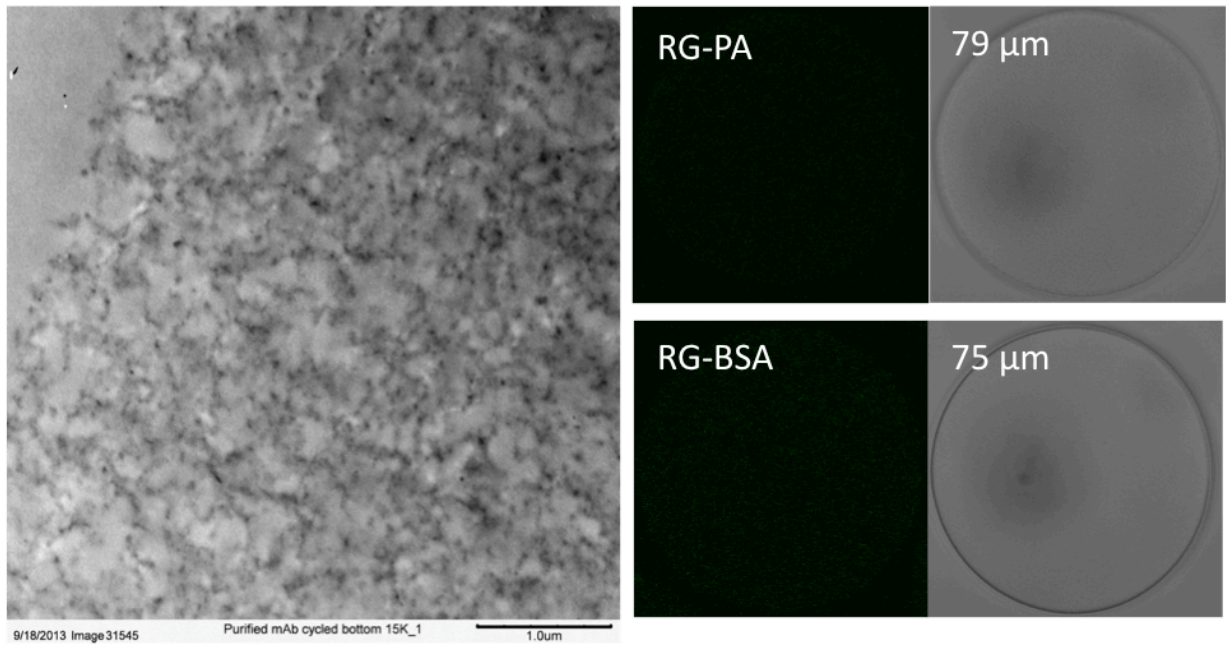
### **3.3.2 Resin cycled with purified mAb A and with null cell culture supernatant**

Figure 3.5 shows representative results for resin samples taken from the bottom section of the columns cycled with the purified mAb A in PBS and with the null CHO cell culture supernatant containing no mAb for conditions otherwise identical to the steps described in Section 3.2.1. As seen in Fig. 3.5a, TEM shows no evidence of any significant fouling. In particular, the bead outer surface shows open pores without significant accumulation of foulants. The CLSM images for beads from the same sample incubated with either rhodamine green-labeled Protein A or rhodamine green-labeled BSA also show no fluorescence. Figure 3.5b shows a similar result for beads taken from the column cycled with the null (i.e. mAb-free) conditioned CHO cell culture supernatant. As seen in this figure, incubating these beads in rhodamine green-labeled BSA resulted in no fluorescence in the beads. Similar results (not shown) were obtained for beads taken from the top sections of the respective columns. These results indicate that accumulation of foulants in the cycled resin depends on the presence of the mAb in the cell culture supernatant as neither the purified mAb A in PBS nor the mAb-free supernatant resulted in any evidence of fouling.

### **3.3.3 Virgin resin saturated with purified mAb A**

In order to understand what is responsible for the apparent association of Protein A and of BSA with the foulants present in the cycled resin and help explain the mechanism leading to fouling, a series of experiments was done with virgin resin beads initially saturated with the purified mAb A in PBS. For this purpose, samples of the virgin

(a) Resin cycled with purified mAb



(b) Resin cycled with null cell culture supernatant

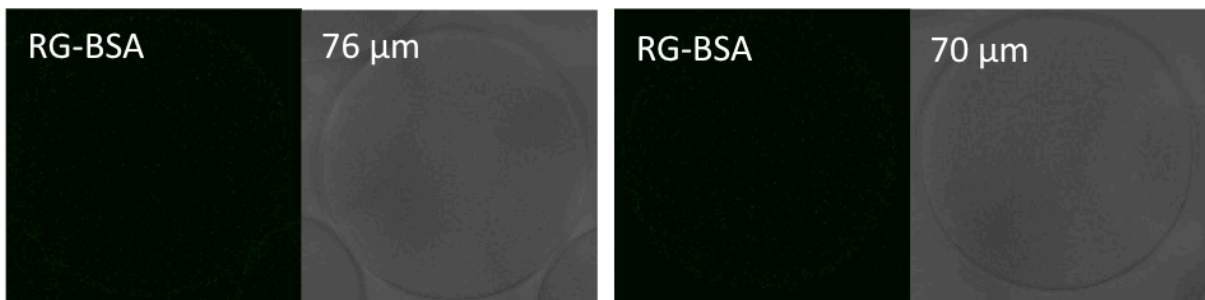


Figure 3.5. Images of beads taken from a column cycled with (a) the purified mAb A and (b) the column cycled with the null cell culture supernatant. (a) shows a TEM image (left) and CLSM images with the corresponding optical images of the beads (right) for resin samples incubated in RG-PA (top) and in RG-BSA (bottom). (b) shows CLSM and optical images for two beads incubated in RG-BSA. The diameter of each bead is indicated in each image.

MabSelect resin were first incubated for 2 h in an excess amount of 5 mg/mL purified mAb A in PBS with or without the addition of rhodamine red-labeled mAb A in a 1 to 200 molar ratio. In either case, the beads were then washed with PBS, incubated with rhodamine green-labeled BSA for at least 0.5 h, and imaged by CLSM. As a control, the same experiment was repeated with a sample of SP-Sepharose-FF initially saturated with mAb A for otherwise identical conditions. Figure 3.6 shows the results of these experiments for the case where the resin samples were incubated with a mixture of labeled and unlabeled mAb A. The same results with regards to the level of green fluorescence were obtained using the unlabeled mAb A only (results not shown for brevity). As seen from this figure, the mAb is, as expected, uniformly distributed in both resins, although the fluorescence intensity is greater for SP-Sepharose-FF as a result of its higher binding capacity for the mAb (about 190 mg/mL of bead volume for SP-Sepharose-FF, as determined by material balance, and about 90 mg/mL of bead volume for MabSelect, as shown previously [11]). The green fluorescence intensity due to the accumulation of labeled BSA is, however, very different in the two cases. As seen in this figure, BSA appears to associate very strongly with the mAb-saturated virgin MabSelect resin, while little or no association is seen with the mAb-saturated SP-Sepharose-FF suggesting that this association depends on the mAb being bound to the Protein A resin and does not occur when the mAb is bound to a cation exchange resin. The same results were obtained by incubating the mAb-saturated MabSelect resin with rhodamine green-labeled  $\alpha$ -lactalbumin, with even stronger fluorescence visible throughout the particles. In order to test the specificity of the mAb A/BSA association observed with mAb-saturated virgin MabSelect resin, the same experiment described above and shown in Fig.

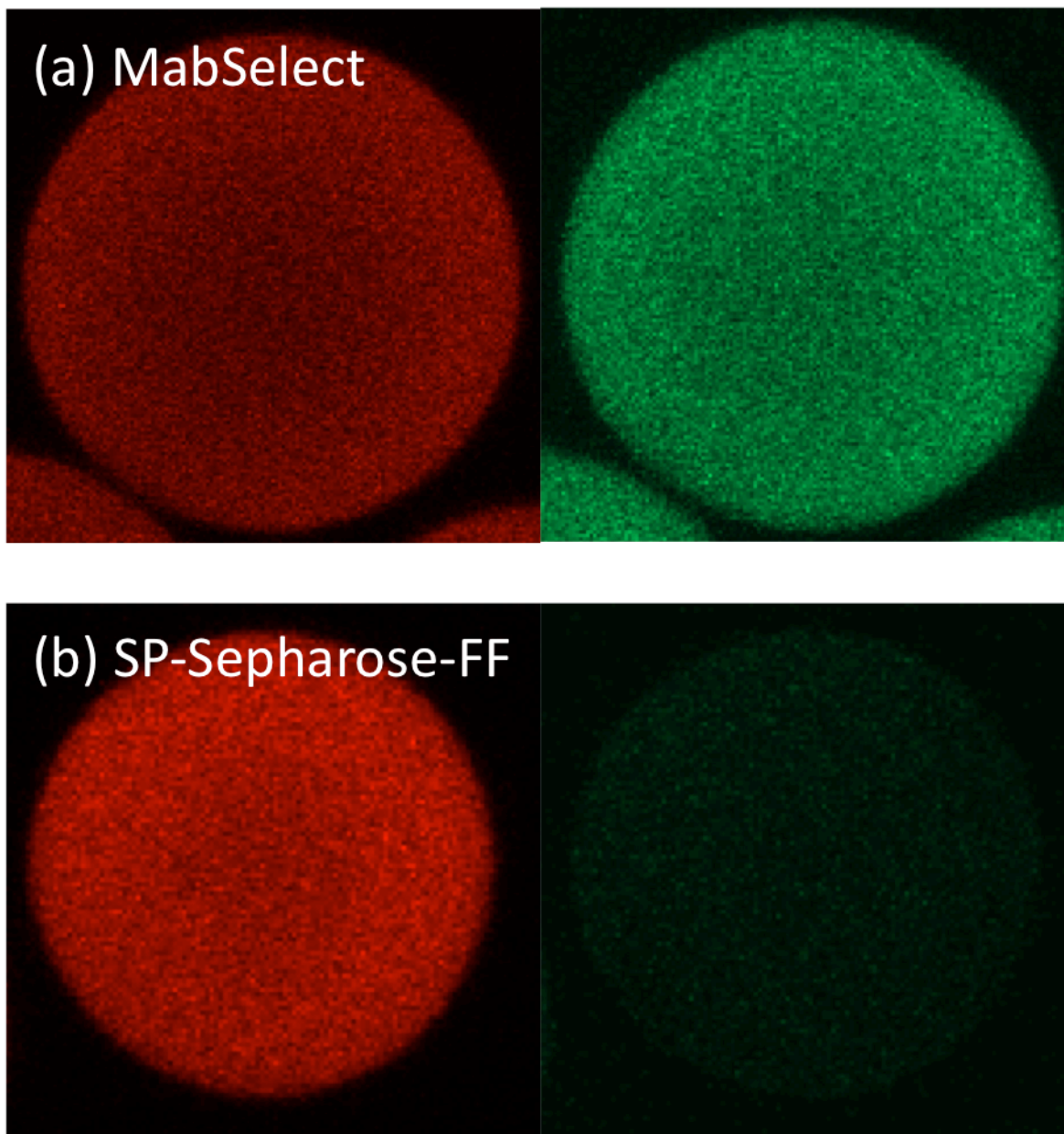


Figure 3.6. CLSM images of beads from virgin resin samples pre-saturated with a mixture of unlabeled and rhodamine red-labeled mAb A in PBS and then incubated in rhodamine green-labeled BSA. (a) MabSelect and (b) SP-Sepharose-FF. Actual bead diameters were 80 and 57  $\mu\text{m}$ , for (a) and (b) respectively. Identical CLSM settings were used in both cases.

3.6 was repeated with two additional purified mAbs (B and C). The results are shown in Fig. 3.7. As seen from this figure, even though the binding capacity of the three mAbs on MabSelect resin was essentially the same, the green fluorescence intensity due to BSA accumulated in the beads was dramatically different in the three cases. In separate experiments we measured the retention of the three mAbs on a Toyopearl PPG-600 hydrophobic interaction chromatography (HIC) column (obtained from Tosoh Bioscience LLC, King of Prussia, PA) with an ammonium sulfate gradient at pH 7.4. These experiments showed that mAb A had stronger retention than both mAb B and C, indicating that mAb A, which led to extensive fouling, is either more hydrophobic or more prone to unfolding on the HIC surface compared to mAb B or mAb C, which did not lead to significant fouling. For example, using an 18 CV gradient from 1 M to 0 M ammonium sulfate, mAb A eluted at 13.5 CV while mAb B and C eluted at 11.5 CV. Overall, these results indicate that association of BSA is specific to the particular mAb and that the extent of this association is correlated, at least in part, with the mAb hydrophobic character as measured by HIC.

Finally, SEC was used to determine the extent of association of fluorescently-labeled BSA with the MabSelect-bound mAb A. For this purpose, 20 mg of virgin MabSelect resin was first incubated for 2 h with 5 mg/mL of purified mAb A and then washed with PBS. 200  $\mu$ L of a solution containing 2.8 mg/mL of rhodamine red-labeled BSA was then added to the washed resin sample and incubated for 30 min. After washing again with PBS, 200  $\mu$ L elution buffer at pH 3.5 was added and after 3 min, 10  $\mu$ L of the supernatant was analyzed by SEC as described in Section 3.2.3. The results gave a molar ratio of

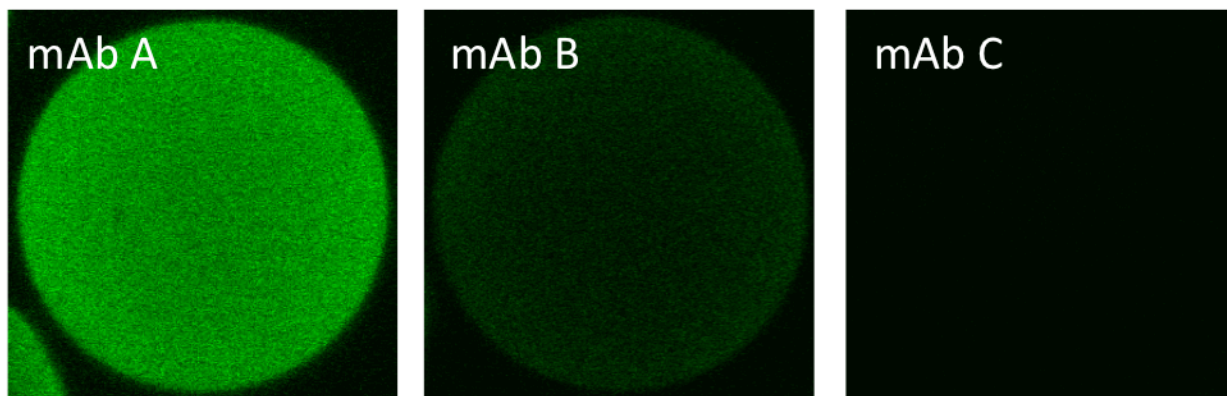


Figure 3.7. CLSM images of beads from virgin resin samples pre-saturated with three different mAbs in PBS and then incubated in rhodamine green-labeled BSA. Actual bead diameters were 64, 73, and 79  $\mu\text{m}$  for mAb A, B, and C, respectively. Identical CLSM settings were used in all three cases.

mAb to BSA of 7:1 in the desorbate, indicating that about 14% of the MabSelect-bound mAb is associated with BSA.

### **3.3.4 Resin cycled with conditioned CHO cell culture supernatant spiked with labeled mAb A and labeled BSA**

Figure 3.8 shows representative CLSM images of virgin MabSelect resin beads taken from the 0.1 mL-column that had been cycled 30 times with the mAb A conditioned CHO cell culture supernatant that had been spiked with rhodamine red-labeled mAb A and with rhodamine green-labeled BSA following process steps otherwise identical to those described in the Materials and Methods section. This experiment was designed to probe any accumulation of the mAb and BSA during cycling. After 30 cycles, the resin was removed from the column and stored in PBS with no further contact with fluorescently labeled species. As was the case for the sample taken from the large-scale column cycled with conditioned CHO cell culture supernatant, the resin beads removed from this scaled-down model also tended to adhere to each other. As seen from these images, both the mAb and BSA accumulate in the resin beads during cycling. Although both red and green fluorescence are seen throughout the beads, a pattern of areas with concentrated fluorescence consistent with those obtained by incubating the resin fouled in the actual process cycle with fluorescently labeled Protein A and BSA is evident. This consistency suggests that the mAb and BSA are comingled in these heavily fouled areas.

### **3.3.5 Discussion and conclusions**

The experimental results obtained in this work indicate that a combination of electron microscopy and confocal microscopy techniques is useful to assess the composition, physical nature, and spatial distribution of foulants in a cycled Protein A resin. While the

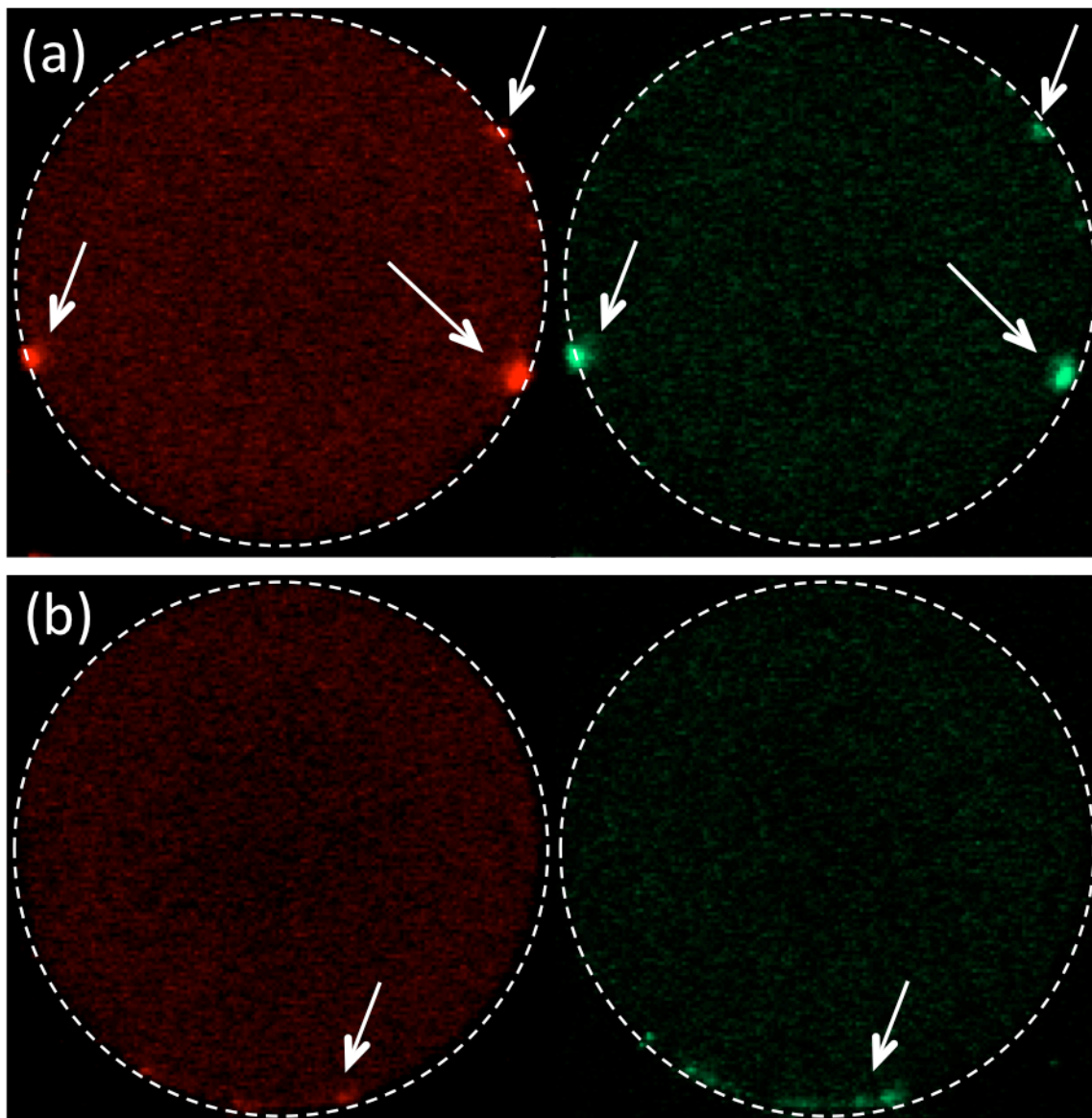


Figure 3.8. CLSM images of two resin beads taken from the MabSelect column that was cycled 30 times with mAb A conditioned CHO cell culture supernatant spiked with rhodamine red-labeled mAb A and rhodamine green-labeled BSA. The molar ratios of labeled mAb and labeled BSA to the mAb contained in the cell culture supernatant were 1:240 and 1:20, respectively. Actual particle diameters are 71 and 65  $\mu\text{m}$  for (a) and (b) respectively. The dashed circles show the outline of each bead. Arrows indicate for clarity some of the areas of concentrated fluorescence.

approach is potentially of general utility, the experimental results obtained are specific to mAb A. This mAb has been demonstrated to have a strong tendency to foul the resin during cycling, resulting in foulants that are not removed by standard cleaning procedures with dilute NaOH. The same approaches have been used to test the fouling behavior of the same mAb with alternative cleaning protocols and with other Protein A resins as well as the effects of cycling MabSelect resin with conditioned CHO cell culture supernatants containing different mAbs that did not result in recovery losses such as those seen with mAb A. As shown in our prior work [11], the removal of foulants from MabSelect resin used for the capture of mAb A employing a different cleaning protocol could be shown by TEM. A discussion of the nature of the improved protocol is beyond the scope of this work. However, it is evident that probing the effectiveness of this cleaning method by CLSM with fluorescently labeled Protein A, BSA, and anti-CHO-HCP antibodies, yields results that are consistent with those obtained based on electron microscopy suggesting that the molecular interactions observed in this work by CLSM are correlated with the structural features observed by EM. We also utilized these methods to test whether cycling with the mAb A CHO cell culture supernatant also results in the accumulation of foulants in the Protein A MabSelect SuRe resin, also from GE Healthcare (Piscataway, NJ). Since more aggressive cleaning (100 mM NaOH) could be used for this more alkali-resistant Protein A resin, no evidence of accumulation of foulants was seen even after 20 cycles by either TEM or CLSM using the same fluorescent probes used for MabSelect resin (results not shown for brevity). Finally, the methods were applied to the resin cycled with another mAb on MabSelect resin. In this case too, we could verify that insignificant

fouling occurred, ultimately resulting in a stable process over 40 cycles (results not shown for brevity).

A final consideration regards the mechanism leading to the fouling of the MabSelect resin used in the mAb A purification process. Our results show that the main foulants in the cycled resin beads are product-related and accumulate in the resin only when the mAb is present in the conditioned CHO cell culture supernatant. Further, our results show that the MabSelect-bound mAb associates with BSA and with  $\alpha$ -lactalbumin, both of which are lipophilic proteins. Finally, our results show that the mAb and BSA concentrate simultaneously in certain fouled areas of resin beads. We thus propose the fouling mechanism illustrated in Fig. 3.9, which assumes that the behavior of BSA is representative of that of actual lipophilic CHO proteins. In the first step of the proposed process, a fraction of the mAb molecules are assumed to undergo conformational changes upon binding to the Protein A ligand, which, in turn, facilitate association with lipophilic proteins. The result is a bound mAb complex associated with lipophilic proteins. Upon desorption at low pH, this destabilized complex detaches from the Protein A ligand in part refolding to the native conformation and in part forming aggregates that deposit on and within the resin. Without aggressive cleaning conditions, these deposits grow with each successive cycle leading to heavily fouled resin that has the reduced porosity, pore size, and mAb binding capacity and kinetics, shown in our prior work.

A remaining question is whether the fouling behavior observed is correlated with the HCP level in the Protein A elution pool, which could be assumed to be higher when association with the bound mAb is more pronounced. In our case, the amount of HCP found in the MabSelect elution pool for the particular mAb process used was within the

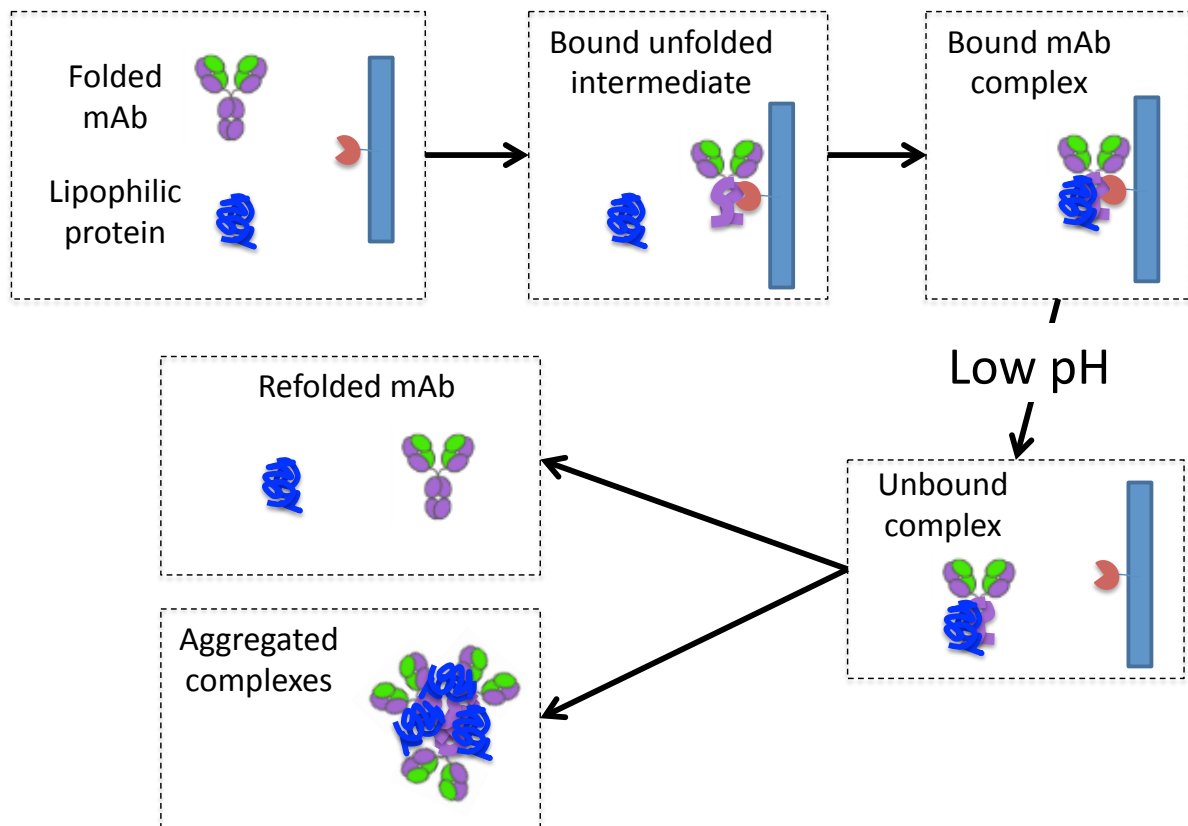


Figure 3.9. Proposed fouling mechanism of MabSelect resin by mAb A. When the mAb molecules bind to the Protein A ligands, a fraction of the mAb molecules undergo a conformational change, which exposes the hydrophobic patches at the surface of mAb molecules. Lipophilic proteins associate with these mAb molecules. During elution, most of these complexes are detached from the Protein A ligand in part refolding to the native form and in part precipitating out on and within the resin under the combined conditions of low pH and high local concentration. Once formed, unless remove by aggressive cleaning, these precipitates continue to grow as a result of cycling.

typical range, albeit on the higher side. Unfortunately, however, our data are not sufficient to establish a direct correlation, which should be investigated in further work.

### 3.4 References

- [1] Boschetti E., Jungbauer A. in: S. Ahuja (Ed.), Handbook of Bioseparations. Academic Press, San Diego, (2000), p. 535.
- [2] Kelley B. Very large scale monoclonal antibody purification: The case for conventional unit operations. *Biotechnol. Progr.* 23 (2007) 995–1008.
- [3] Shukla A.A., Hubbard B., Tressel T., Guhan S., Low D. Downstream processing of monoclonal antibodies: application of platform approaches. *J. Chromatogr. B*, 848 (2007) 28-39.
- [4] Hober S., Nord K., Linhult M. Protein A chromatography for antibody purification. *J. Chromatogr. B*, 848 (2007) 40-47.
- [5] Hahn R., Shimihara K., Steindl F., Jungbauer A. Comparison of Protein A affinity sorbents. III Life time study. *J. Chromatogr. A*, 1102 (2006) 224-231.
- [6] Jiang C., Liu J., Rubacha M., Shukla A.A. A mechanistic study of Protein A chromatography resin lifetime. *J. Chromatogr. A*, 1216 (2009) 5849-5855.
- [7] Grönberg A., Eriksson M., Ersoy M., Johansson H.J. A tool for increasing the lifetime of chromatography resins. *MABS*, 3 (2011) 192–202.
- [8] Girot P., Moroux Y., Duteil X.P., Nguyen C., Boschetti E. Composite affinity sorbents and their cleaning in place. *J. Chromatogr.* 510 (1990) 213-223.
- [9] Burgoyne R.F., Priest M.C., Roche K.L., Vella, G. Systematic development and validation of sanitization protocols for a chromatographic system designed for biotherapeutics purification. *J. Pharm. Biomed. Anal.* 11 (1993) 1317–1325.

- [10] Linhult M., Gulich S., Graslund T., Simon A., Karlsson M., Sjoberg A., Nord K., Hover S. Improving the tolerance of a Protein A analogue to repeated alkaline exposures using a bypass mutagenesis approach. *Proteins*, 55 (2004) 407-416.
- [11] Zhang S., Daniels W., Iskra T., Salm J., Glynn J., Martin J., Gallo C., Godavarti R., Carta G. Structural and performance characteristics of virgin and fouled MabSelect resin cycled in a monoclonal antibody process.
- [12] Shukla A.A., Hinckley P. Host cell protein clearance during Protein A chromatography: development of an improved column wash step. *Biotechnol. Prog.* 24 (2008) 1115–1121.
- [13] Nogal, B., Chhiba, K., Emery, J. C. Select host cell proteins coelute with monoclonal antibodies in Protein A chromatography. *Biotechnol. Prog.* 28 (2012) 454–458.
- [14] Sisodiya, V. N., Lequieu, J., Rodriguez, M., McDonald, P., Lazzareschi, K. P. Studying host cell protein interactions with monoclonal antibodies using high throughput Protein A chromatography. *Biotechnol. J.* 7 (2012) 1233–1241.
- [15] Corbett R., Carta G., Iskra T., Gallo C., Godavarti R., Salm J. R. Structure and protein adsorption mechanisms of clean and fouled tentacle-type anion exchangers used in a monoclonal antibody polishing step. *J. Chromatogr. A*, 1278 (2013) 116–25.
- [16] Perez-Almodovar E.X., Tao Y., Carta G. Protein adsorption and transport in cation exchangers with a rigid backbone matrix with and without polymeric surface extenders. *Biotechnol. Progr.* 27 (2011) 1264-1272.

- [17] Tao Y., Perez-Almodovar E.X., Carta G., Ferreira G., Robbins D. Adsorption kinetics of deamidated antibody variants on macroporous and dextran-grafted cation exchangers. III. Microscopic studies. *J. Chromatogr. A*, 1218 (2011) 8027-8035.
- [18] Cawthern, K.M., Narayan, M., Chaudhuri, D., Permyakov, E.A., Berliner, L.J. Interactions of  $\alpha$ -lactalbumin with fatty acids and spin label analogs. *J. Biol. Chem.* 272 (1997) 30812-30816.

## 4 Chapter 4

### Structural and Performance Characteristics of Representative Anion Exchange Resins Used for Weak Partitioning Chromatography

---

#### 4.1 Introduction

The purification of monoclonal antibodies (mAbs) at manufacturing scale continues to pose significant challenges resulting from the large molecular size, exquisite purity requirements, and the projected increases in scale that are anticipated for some mAbs [1]. As a result, efficient downstream processing schemes that can be deployed as a platform for multiple mAb products are desirable. Three sequential chromatographic steps are used in a typical mAb purification platform: a Protein A step for capture and initial purification; an anion exchange (AEX) step for the removal of acidic host cell proteins; and other negatively charged impurities, and a cation exchange (CEX) step for the removal of basic host cell proteins and basic product variants, including aggregates [2]. Since each step is costly, normally requires intermediate buffer exchanges, and results in a yield loss, reducing the number of steps is desirable. Weak partitioning chromatography (WPC) was introduced by Kelley et al.[3] as a way of achieving simultaneous removal of both acidic and basic impurities in one step using an AEX resin operated for conditions where the product interacts only weakly with the resin while the impurities are strongly bound. These conditions are usually determined from high-throughput screening (HTS) experiments where multiple resin candidates are tested over broad ranges of salt concentration and pH. The motivation of this work is to help reduce the number of these

experimental determinations by providing an understanding of how AEX resins with different structures perform in a WPC step.

The selection of conditions suitable for WPC operation is typically based on the value of the product partition coefficient,  $K_p$ , defined as:

$$K_p = \frac{\bar{q}}{C} \quad (1)$$

where  $\bar{q}$  is the protein concentration in the resin averaged over the resin volume and  $C$  is the protein concentration in solution obtained after incubating the AEX resin with the protein solution. The quantity used to define the “resin volume” varies dependent on the method of measurement as is either the settled resin volume excluding any extraparticle mobile phase or the volume of particles. The former is obtained from the latter simply by multiplying the latter times  $1 - \varepsilon_b$  where  $\varepsilon_b$  is the extraparticle porosity of the settled resin bed. Since  $\varepsilon_b$  is usually in the range 0.3-0.4, the difference between the different resin volume bases is not very large. As suggested by Kelley et al., values of the product  $K_p$  between 0.1 and 20 are usually desirable and, based on practical experience, often lead to conditions where both acidic impurities and mAb aggregates are strongly bound and can be effectively removed in one step [3].

The interaction between AEX resins and acidic proteins and the effects of resin structure on both binding capacity and binding kinetics have been studied by many authors [4][5][6][7][8][9][10][11]. Less is known however, about the interaction of AEX resins with mAb monomers, which are typically basic, and with mAb aggregates, including soluble dimers, which usually retain the monomer’s basic character but that are much larger in size. Burchiel et. al. [12], for example, used an AEX HPLC resin to capture mouse monoclonal antibodies with salt gradient elution. Vetter et al. [13] used medium-

pressure AEX resins to separate deamidated mAbs with induced pH gradients between pH 9 and 7. At these pH values, which bracketed the mAb pI, mAb binding was relatively weak allowing elution for relatively mild conditions. Ansaldi and Lester [14] separated mAb aggregates from monomeric species using salt steps or linear gradients with several AEX resins. Wan and Wang[15] also separated aggregates using the AEX resin Q Sepharose FF noting that aggregates are generally more charged than the monomer when the pH is close to the pI of the mAb resulting in stronger binding. Finally, Suda et al. [16] used dextran-grafted AEX resins to separate monomer-aggregate mixtures based in part on the ability of the grafts to exclude aggregates while allowing the monomer to diffuse in and bind.

The specific goal of this work is to investigate for three commonly used AEX resins having widely different structures the partitioning and mass transfer behavior of mAb monomeric species along with that of (a) mAb dimers and mAb multimeric species, and (b) BSA, both as a model of typical acidic impurities. The three resins considered are the tentacle-type, polyacrylate-based TMAE HiCap from EMD Millipore (Billerica, MA, USA), hereinafter referred to as TMAE, the relatively small-pore, agarose-based Q Sepharose FF from GE Healthcare (Piscataway, NJ, USA), hereinafter referred to as QFF, and the large-pore, polystyrene-based POROS 50 HQ from Thermo Fisher Scientific (Waltham, MA, USA), hereinafter referred to as POROS. The structure of the three resins is determined by transmission electron microscopy, their pore accessibility by inverse size exclusion chromatography, and their charge density by potentiometric titrations. Protein partitioning between solution and resin phase and transport characteristics are

then obtained for these resins based on chromatographic and confocal laser scanning microscopy experiments for conditions similar to those typically used for WPC.

## **4.2 Materials and Methods**

### **4.2.1 Materials**

TMAE is based on cross-linked polymethacrylate backbone having, according to the manufacturer, a pore diameter of about 80 nm, functionalized with charged polymers, referred to as “tentacles”, with trimethylaminoethyl groups. QFF is based on cross-linked, 6% agarose beads functionalized with quaternary ammonium ion groups [17][18].

POROS is based on a cross-linked poly (styrene-divinylbenzene) backbone surface-coated with quarternized polyethyleneimine and a bimodal pore size distribution including both small and large pores [19][20]. The particle size distribution of each resin sample was obtained from microphotographs and gave volume-averaged particle diameters of 76, 99, and 49  $\mu\text{m}$  for TMAE, QFF and POROS, respectively.

The proteins used in this work include two purified mAb monomers (mAbA and mAbB), mAbB dimers, a mAbB multimeric species, and BSA. Both mAbs were produced in recombinant CHO cell culture and purified by Protein A chromatography followed by hydroxyapatite chromatography. mAbA is an IgG2 antibody with a pI of 7.6 while mAbB is an IgG1 antibody with a pI of 8.6. Because of the lower pI and, thus, less basic character than mAbB, mAbA tends to interact more strongly with AEX resins requiring lower pH and higher salt concentration to achieve conditions favorable for WPC.

Conversely, because of the higher pI, mAbB interacts more weakly with AEX resins requiring higher pH and lower salt for WPC. The buffers actually used in this work were determined from HTS screening experiments according to Kelley et al. [21] and are 50

mM HEPES, 65 mM NaCl at pH 7.0 for the stronger binding mAbA and 22 mM Tris at pH 8.1 for the weaker binding mAbB. For simplicity, the same buffers were used for all three resins and gave product  $K_p$ -values between 0.1 and 3, well within the range of typical WPC conditions.

Dimeric and multimeric forms of mAbB were obtained from a process stream rich in high molecular weight species using first a hydroxyapatite column (CHT Type I from Bio-Rad Laboratories, Hercules, CA, USA) with a salt gradient to generate fractions enriched in dimeric and multimeric forms. The enriched fractions were then further purified by SEC with a 1 cm x 30 cm Superdex 200 column from GE Healthcare (Piscataway, NJ, USA) using stacked injections to maximize productivity. The purity of the resulting dimeric and multimeric species was greater than 95% based on HPLC SEC analysis with a GW3000<sub>XL</sub> column from Tosoh (King of Prussia, PA, USA). Both purified dimer and multimer samples were stable for long periods of time at 4 °C.

The identity of the purified species was confirmed by dynamic light scattering (DLS) with a Wyatt Dynapro Nanostar instrument from Waters Corporation (Milford, MA, USA) which gave hydrodynamic radii of  $5.5 \pm 0.1$ ,  $7.2 \pm 0.1$ , and  $16.3 \pm 0.4$  nm for monomer, dimer, and multimeric species, respectively. The monomer and dimer radii are consistent with those obtained experimentally by Reck et al. [22]. The large radius determined for the multimer suggests that this species is comprised of several mAb monomer units as reported by Ahere et al. [23]

BSA was obtained from Sigma-Aldrich (St. Louis, MO, USA) and was purified using the Superdex 200 column described above to remove the dimeric and oligomeric forms found in the sample. Rhodamine Red<sup>TM</sup>-X and Rhodamine Green<sup>TM</sup>-X Succimidyl ester amine

reactive dyes and DyLight 488 Sulfhydryl-reactive dye were obtained from Thermo Fisher Scientific (Waltham, MA, USA).

## **4.2.2 Methods**

### **4.2.2.1 Potentiometric titration**

The charge density of the AEX resins was obtained from potentiometric titration following Stone et al. [24] Briefly, about 1 g of hydrated resin was washed with distilled, deionized water and centrifuged at 5000 rpm for 15 min and then incubated with 120 mL 0.1 N NaOH for 3 h. Resin sample was then washed with DI H<sub>2</sub>O in a Buchner funnel until the pH of the filtrate reached 7. 25 mL of 0.5 M NaCl/0.05 M HCl was added to the sample. After 1 h agitation, 15 mL of the supernatant was back titrated with 0.1 N NaOH. The charge densities of the three resins, calculated from the amount of NaOH consumed by each, were found to be 260, 340 and 230  $\mu\text{mol/mL}$  particle for TMAE, QFF, and POROS, respectively.

### **4.2.2.2 Inverse size exclusion chromatography**

Inverse size exclusion chromatography (iSEC) was used to determine the accessible intraparticle porosity and the apparent pore radius of each resin. For this purpose, each resin was packed in 0.5 cm-diameter, 15 cm-long Tricorn columns from GE Healthcare, which were used to determine the isocratic retention volume of different dextrans at a flow rate of 0.5 mL/min with an Alliance e2695 HPLC system from Waters Corporation (Milford, MA, USA) with a refractive index detector. Glucose and dextran polymers with 4, 10, 40, 70, and 2,000 kDa molecular mass, obtained from GE Healthcare and Sigma-Aldrich, were used for these determinations. The corresponding molecular radii are 0.4, 1.7, 2.6, 5.3, 7.0, and 37 nm, respectively [25][26]. The values of the distribution

coefficient were calculated as  $K_D = (\overline{CV} - \varepsilon) / (1 - \varepsilon)$  where  $\overline{CV}$  is the retention volume of each probe at the peak maximum and  $\varepsilon$  is the extraparticle porosity. The latter was obtained either based on the retention of 2,000 kDa dextran, for TMAE and QFF, or by fitting the column pressure-flow curve to the Blake-Cozeny equation [27] for POROS. The total intraparticle porosity,  $\varepsilon_p$ , and the pore radius,  $r_{pore}$ , of each resin were then determined by fitting the experimental  $K_D$ -values with a cylindrical pore model, [25] using either a monomodal (for TMAE and QFF) or a bimodal pore size distribution (for POROS) [20][25].

#### **4.2.2.3 Transmission electron microscopy**

Transmission electron microscopy (TEM) was performed with a JEOL 1230 instrument (JEOL Ltd., Tokyo, Japan). Small aliquots of each resin sample were first saturated with BSA in 20 mM bis-tris propane at pH 7.0. After dehydrating the BSA-saturated resin with increasing ethanol concentrations from 0 to 100% anhydrous ethanol, samples were embedded in LR-White resin (London Resin Company, Ltd., London, UK) following the procedure outlined by Corbett et al. [11] and ultramicrotomed into 80 nm sections. The sections were then stained with lead citrate followed by uranyl acetate. Images were taken by a SIA CCD camera with 4K×4K resolution. Pre-saturating the resins with BSA provided an excellent uptake of the uranyl/lead stain, which resulted in superior resolution compared to virgin resin [28].

#### **4.2.2.4 Isocratic elution**

Isocratic elution (IE) experiments were used to determine the  $K_p$  values and intraparticle diffusivities for both mAb monomers and for the mAbB dimer for each resin using the columns described above. The mAbB multimer as well as BSA were very strongly bound

and could not be eluted isocratically under WPC conditions. Thus, confocal microscopy experiments were used to characterize the uptake behavior of these two species. For the IE experiments, 100  $\mu\text{L}$  samples containing 2 to 5 mg/ml of monomer or mAbB dimer were injected and eluted isocratically either in WPC buffers or in 2 M NaCl at different flow rates. Since in most cases the experimental chromatograms exhibited substantial tailing, the retention factor,  $k'$ , and the apparent intraparticle diffusivity,  $D_e$ , were determined for each case by fitting the analytical solution for pore diffusion in spherical particles with a linear isotherm obtained by Carta [29]. The isotherm linearity for both mAb monomers and for the mAbB dimer was checked by increasing the feed concentration by a factor of two and verifying that it did not affect the shape of the chromatograms.

$K_p$ , defined by eq. 1 based on the resin particle volume is obtained from  $k'$  from the following relationship

$$K_p = \frac{\varepsilon}{1 - \varepsilon} k' \quad (2)$$

where  $\varepsilon$  is the extraparticle void fraction of the columns used in the IE experiments, which was determined as described above.

#### **4.2.2.5 Confocal microscopy**

Confocal laser scanning microscopy (CLSM) was performed to determine the penetration of the mAbB multimeric species and BSA within the resin particles. For this purpose, the mAbB multimeric species was conjugated with either Rhodamine Red or Rhodamine Green amine reactive dyes with a previously described procedure [30][31]. Briefly, each protein was mixed with dye in a 3:1 molar ratio and incubated in 500 mM sodium bicarbonate buffer at pH 8.5 for 1 h. A 10-PG desalting column (Bio-Rad Laboratories,

Hercules, CA, USA) was then used to separate the labeled protein from unreacted dye. The labeled protein was further diluted with unlabeled protein to yield a final molar ratio of labeled to unlabeled protein of 1:50. The ensuing CLSM results were the same, regardless of the dye used for all three resins. BSA was conjugated with DyLight 488 Sulfhydryl-reactive dye, which reacts readily with the lone free –SH residue in this protein. A protein to dye molar ratio of 2:1 in PBS with a 2 h reaction time were used in this case. Diafiltration was then used to remove unreacted dye. A 1:200 labeled protein to unlabeled protein ratio was used for the CLSM experiment.

CLSM experiments were conducted with a Zeiss LSM 510 microscope with a Plan-Apochromat 63 ×/1.4 NA oil objective (Carl Zeiss MicroImaging, LLC, Thornwood, NY, USA). The excitation wavelength was 561 nm and 488 nm for red and green lasers. Emission wavelength greater than 575 nm was collected for red channel and emission wavelength between 490 and 510 nm was collected for green channel. All images were taken at the equator of the beads. Batch measurements were made to determine the adsorption kinetics by adding less than 1 mg of resin to a tube containing 3 mL of the labeled protein at a total concentration of 0.5 mg/mL for mAbB multimer and BSA. 250 μL of the sample was periodically pipetted out, and rapidly filtered in a microcentrifuge filter to remove the extraparticle solution. Because of their opacity, prior to imaging, the TMAE and POROS particles were re-suspended in 50% (w/v) sucrose buffer and benzyl alcohol, respectively, in order to provide an approximate match of each resin's refractive index and, thus, give sharper images [11][32]. QFF, on the other hand, was sufficiently transparent to enable imaging in the working buffer.

#### **4.2.2.6 BSA adsorption isotherms**

Adsorption isotherms were also obtained for BSA by a batch equilibration method, following a previously described procedure [27] with a 24 h equilibration time.

## 4.3 Results

### 4.3.1 Resin Structure

Figure 4.1 shows representative TEM images taken near the bead surface of TMAE (a), QFF (b), and POROS (c) particles at 15,000x magnification. In each image, the uniform light grey area outside the bead outer surface (marked as 1 in the figure) is the embedding matrix. It can be seen that below the outer surface the structure is very different for each material. TMAE (Fig. 4.1a) shows very dark, heavily stained areas (marked as 2), which correspond to the bound BSA, as well as areas of an intermediate shade of grey (marked as 3), which correspond to the resin backbone. Resin samples without BSA did not show the dark grey areas (data not included). The presence of these areas in the BSA-saturated sample suggests that the tentacles form a charged gel-layer where the protein binds.

Based on the image, this layer appears to be as thick as 0.2  $\mu\text{m}$ , thereby filling a large fraction of the backbone porosity. A number of open areas that appear to be filled with the embedding matrix (marked as 4) are also visible. It is not clear, however, to what extent, if any, these areas correspond to open pores that are connected to each other and with the bead outer surface and actually present in the fully hydrated state of the resin or whether these are artifacts of the drying and embedding process used to produce these samples. QFF (Fig. 4.1b) shows instead a fibrous structure (marked as 2) that defines a fairly uniform network of relatively small pores (most below 0.1  $\mu\text{m}$  in size). These fibrous structures are heavily stained because of the bound BSA. In fact, QFF samples without BSA (results not included) showed very little staining and, thus, very poor image

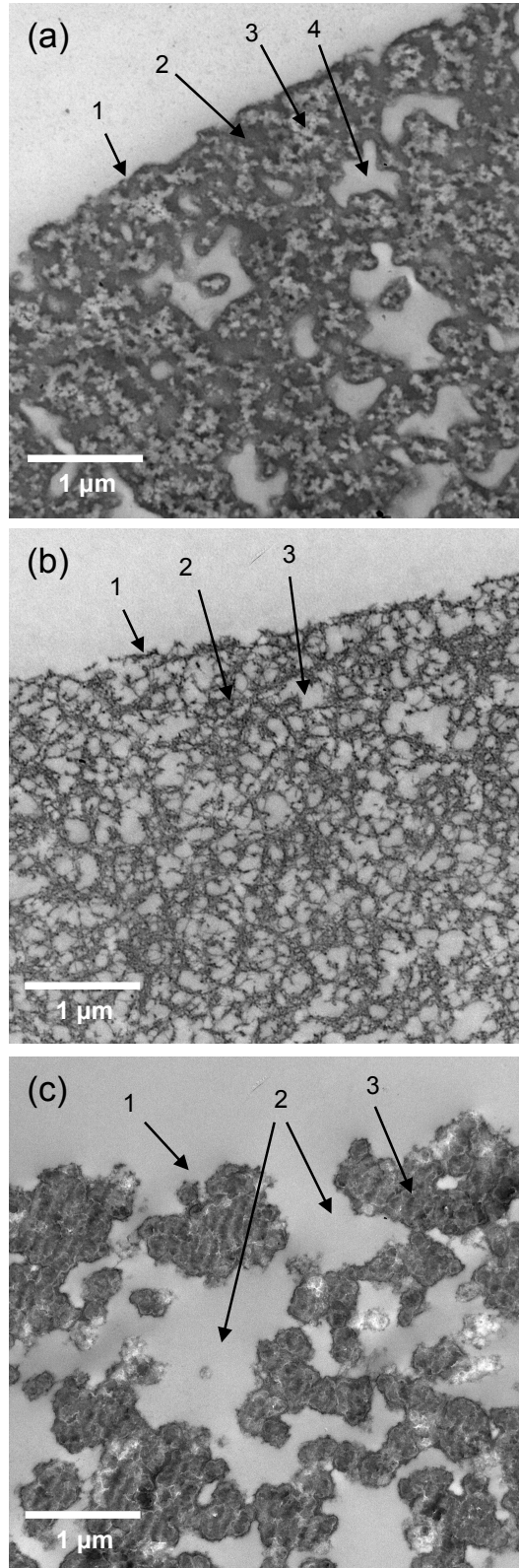


Figure 4.1. Transmission electron micrographs of TMAE (a), QFF (b), and POROS (c) resins. The arrow point to different structural characteristics as indicated in the text.

resolution compared to the BSA-saturated sample. Finally, POROS (Fig. 4.1c) shows a “granular” structure with large pores (marked as 2) as large as 1  $\mu\text{m}$  in size, as well as smaller pores within the granules (marked as 3) where most of the BSA appears to be bound, resulting in heavy staining. POROS samples without BSA gave images similar to Fig. 4.1c, suggesting that the bound BSA is mostly held within the granules and does not affect the large pores. The structure observed for POROS 50 HQ, used in this work, is similar to that of cation exchange resin POROS 50 HS as reported by Wu et al. [32]. Figure 4.2 shows the  $K_D$  values obtained from iSEC experiments with dextran standards (open symbols) in the mAbB WPC buffer along with those obtained from the isocratic elution experiments with the mAb monomers and the mAbB dimer in a buffer containing 2 M NaCl (solid symbols). No binding of these molecules is expected for these conditions and retention is due exclusively to diffusion within the empty pore space of the resin. Thus, in this case,  $K_D$  is related to the retention factor by  $k' = (1 - \varepsilon)K_D / \varepsilon$ . The lines shown in Fig. 4.2 are fitted to the dextran standards data according to the following equation: [20][25]

$$K_D = \sum_{i=1}^n \varepsilon_{p,i} \left( 1 - \frac{r_s}{r_{pore,i}} \right)^2 \quad (3)$$

which is based on a cylindrical pore geometry assuming a discrete distribution of pore sizes. The  $K_D$ -data were fitted with a monomodal distribution ( $n=1$ ) for TMAE and QFF and with a bimodal distribution ( $n=2$ ) for POROS. Assuming  $n=2$  for either TMAE or QFF did not alter the quality of the fit, while a value of  $n=2$  was needed to obtain a good fit for POROS. The fitted parameter values,  $\varepsilon_p$  and  $r_{pore}$  are summarized in Table 4.1 for each resin. As seen in this table, the apparent pore radius of TMAE is very small (in fact,

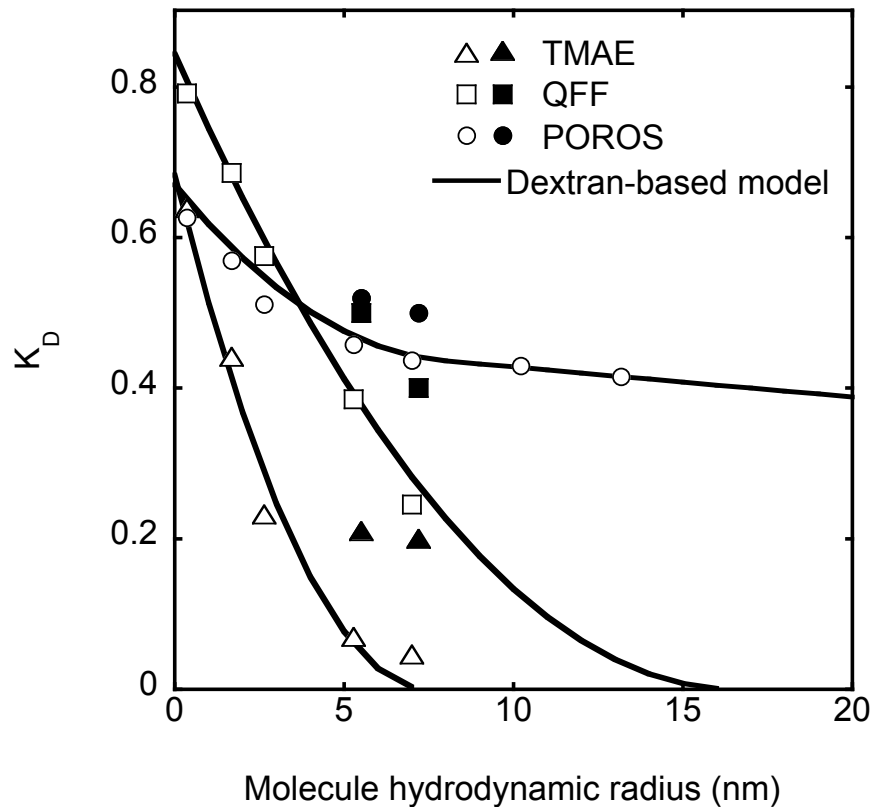


Figure 4.2.  $K_D$ -values obtained from dextran standards in the mAbB WPC buffer (open symbols) and for mAb monomer and dimer species under non-binding conditions in 2 M NaCl (filled symbols). Lines are based on eq. 3 with  $n=1$  for TMAE and QFF and  $n=2$  for POROS. Parameter values are given in Table 4.1.

Table 4.1. Structural properties of the resins used in this work.

	TMAE	QFF	POROS	
Particle diameter, $d_p$ ( $\mu\text{m}$ )	76	99	49	
Column extraparticle porosity, $\varepsilon$	0.37	0.28	0.36	
Total intraparticle porosity, $\varepsilon_p$	0.68	0.84	0.67	
Pore radius obtained assuming a monomodal distribution, $r_{pore}$ (nm)	7.5	17.0	-	
Intraparticle porosities obtained assuming a bimodal distribution, $\varepsilon_{p,i}$	-	-	0.20	0.47
Pore radii obtained assuming a bimodal distribution, $r_{pore,i}$ (nm)	-	-	7.9	220

only slightly larger than the mAb's hydrodynamic radius), rather large for the larger pores in POROS, and intermediate for QFF. These results are consistent with the corresponding TEM images. For TMAE, the iSEC results show that the large, isolated "pores" visible in Fig. 4.1a are indeed either artifacts of the embedding procedure or are actual pores not connected to the bead outer surface. Thus, we conclude that the observed size exclusion properties of this resin are mainly due to interactions with the tentacles. As seen in Fig. 4.2, although the general trends of the  $K_D$ -values obtained for the monomers and mAbB dimer species are consistent with those observed for the dextran standards, the protein  $K_D$ -values are higher than those for the dextrans. The relative difference between these values is small for POROS, but becomes fairly large for TMAE. It is likely that this is a result of the high salt concentration used for the protein measurements (2 M NaCl), which, in turn, is likely to have caused changes in the tentacle structure resulting in somewhat greater accessibility by the unbound proteins. Additionally, the different shape of the proteins and dextran may have contributed to the difference.

#### **4.3.2 Isocratic Elution Behavior**

Figure 4.3 shows the isocratic elution behavior of mAbA and mAbB monomers, and mAbB dimer, both for non-binding conditions (2 M NaCl) and for WPC conditions, as defined in the Methods section. The experiments were done at a flow rate of 0.5 mL/min, corresponding to a superficial velocity of 150 cm/h. Similar results (not shown) were also obtained at 1, 2, and 3 mL/min and showed trends similar to those in Fig. 4.3 but, as expected, with broader and more tailing elution profiles. The vertical dashed line in each graph corresponds to the extraparticle porosity. For non-binding condition, TMAE (Figs.

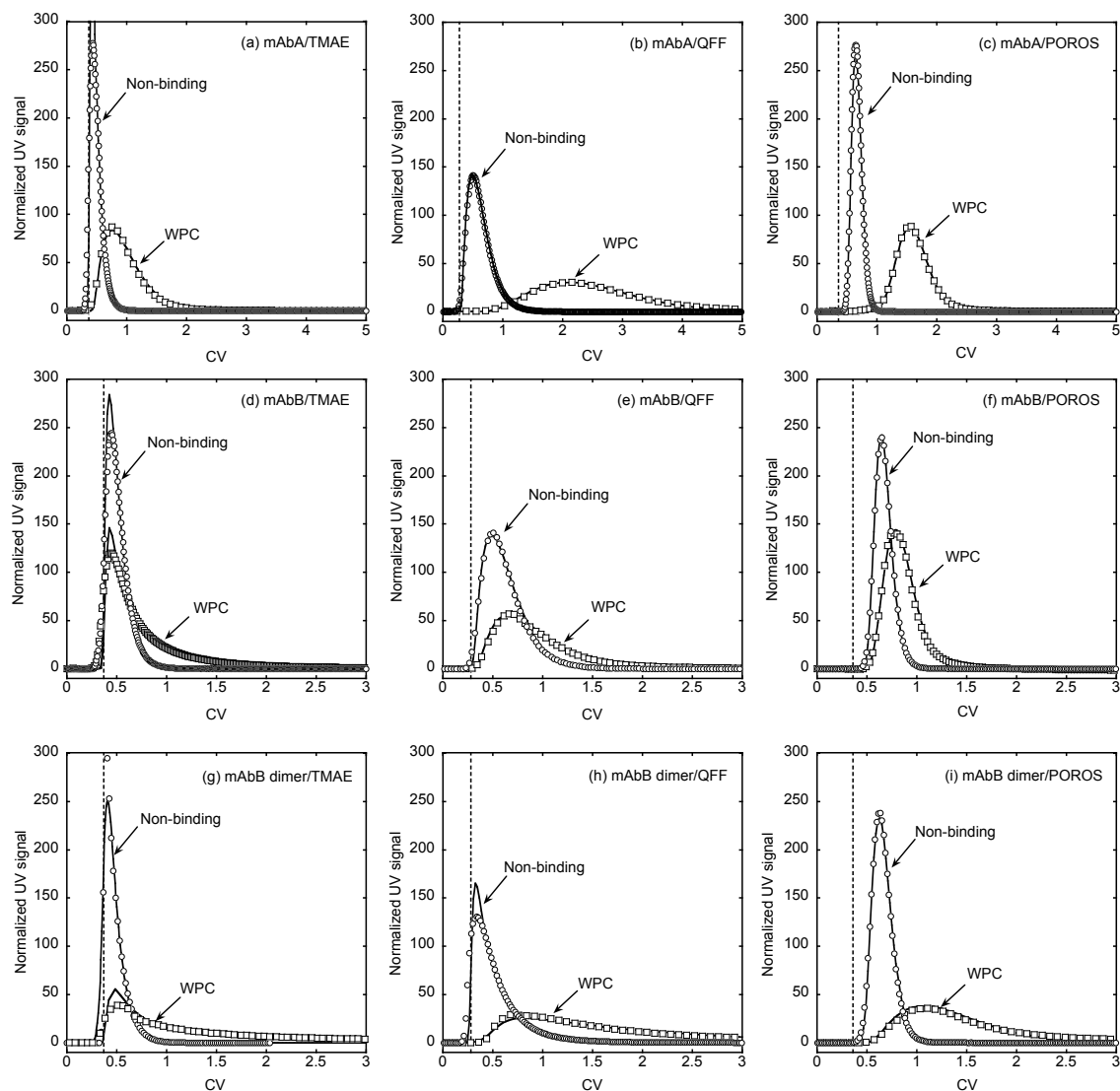


Figure 4.3. Chromatographic elution profiles obtained under WPC conditions (squares) and non-binding conditions in 2 M NaCl (circles) for mAbA and mAbB monomers and mAbB dimer. Note the different CV-axis scale in (a), (b), and (c) for the mAbA monomer data.

4.3a, d, and g), shows the same elution behavior for all three species as all three are almost completely excluded from the resin. Under WPC conditions, the TMAE elution peaks become highly skewed especially for mAbB monomer and mAbB dimer, indicating that mass transfer becomes severely limiting. The results for QFF (Fig. 4.3b, e, and h) under non-binding conditions show broader and more tailing peaks, especially for the mAbB dimer, compared to those obtained for TMAE. This occurs because of the greater accessible intraparticle porosity, relatively small pore size, and large particle diameter, which limit the rate of diffusion in and out of the QFF particles. Under WPC conditions, QFF shows substantial retention of both mAb monomers and for mAbB dimer. A broad, but nearly symmetrical peak is obtained for the more strongly retained mAbA, a more skewed peak for the more weakly retained mAbB, and a broad, highly tailed peak is obtained for mAbB dimer. Finally, the results for POROS (Fig. 4.3c, f, and i) show relatively narrow and symmetrical peaks for the monomers under both non-binding and WPC conditions and a relatively narrow and moderately tailing peak for the mAbB dimer. The POROS behavior is explained by its relatively large pore size and small particle diameter that facilitate diffusion in and out of the particles.

Table 4.2 summarizes the  $K_p$  and  $D_e$ -values obtained by fitting the isocratic elution peaks as discussed in the Methods section. For non-binding conditions, the  $K_p$ -values are close to the  $K_D$ -values of dextran standards of corresponding size for QFF and, especially, for POROS (*cf.* Fig. 4.2). On the other hand, the non-binding  $K_p$ -values for TMAE is somewhat larger than those obtained for correspondingly size dextrans, probably because, as discussed earlier, the 2 M NaCl concentration used for the protein experiments affected the TMAE tentacle structure. In any case, because all three proteins eluted very

Table 4.2.  $K_p$ -values, based on the resin particle volume, and effective pore diffusivities,  $D_e$  in  $10^{-8}$  cm<sup>2</sup>/s, obtained from isocratic elution experiments under non-binding conditions and under WPC conditions as defined in the text. Error margins for the  $K_p$ -values are  $\pm 10\%$ .

Non-binding conditions (2 M NaCl)						
	TMAE		QFF		POROS	
	$K_p$	$D_e$	$K_p$	$D_e$	$K_p$	$D_e$
mAbA	0.21	ND	0.51	4.0±0.5	0.52	8.0±2.9
mAbB	0.20	ND	0.48	4.0±0.5	0.52	8.0±2.9
mAbB dimer	0.20	ND	0.40	1.9±0.6	0.45	6.8±2.2
WPC conditions						
	TMAE		QFF		POROS	
	$K_p$	$D_e$	$K_p$	$D_e$	$K_p$	$D_e$
mAbA	1.1	2.5±0.7	2.9	8.8±0.9	1.8	12.0±4.2
mAbB	0.41	0.52±0.2	0.86	5.1±1.0	0.72	6.0±2.6
mAbB dimer	2.9	2.7±0.9	1.9	2.5±0.6	1.7	2.8±1.0

close to the extraparticle void volume, it was not possible to determine the value of  $D_e$  with any accuracy for this resin under non-binding conditions. Even under WPC conditions and for all three resins, only approximate values could be determined because of the very extensive tailing. Thus, only an approximate comparison of the  $D_e$ -values is possible. As seen in Table 4.2, the  $D_e$ -values for TMAE vary substantially with conditions, generally being larger when  $K_p$  is larger, indicating that the tentacles affect the diffusion process. Larger  $D_e$ -values are obtained for QFF and POROS with a relatively small difference between the values determined under non-binding conditions and those obtained under WPC conditions. This small difference suggests that the dominant transport mechanism is pore diffusion and that the resin matrix only affects transport through the ordinary hindered diffusion mechanism [33]. The smallest  $D_e$ -values are obtained for the mAbB dimer in QFF as a result of its larger molecular size and, hence, greater diffusional hindrance.

### 4.3.3 Adsorption Isotherms

Figure 4.4 shows the adsorption isotherms for BSA on the three resins for WPC conditions plotted as mg of protein bound per mL of particle volume. BSA binding is stronger in the WPC buffer used for mAbB because the ionic strength is lower and the pH is higher compared to the WPC buffer used for mAbA. The requirement for WPC is that conditions must be such that basic impurities, including dimer and higher order aggregates are bound along with acidic impurities (here represented by BSA). As a result a lower ionic strength and higher pH are needed for mAbB, which binds more weakly to the AEX resins studied. As seen in Fig. 4.4, for all three resins the BSA binding capacity is much higher in mAbB-WPC buffer, is highest for TMAE and generally lowest for

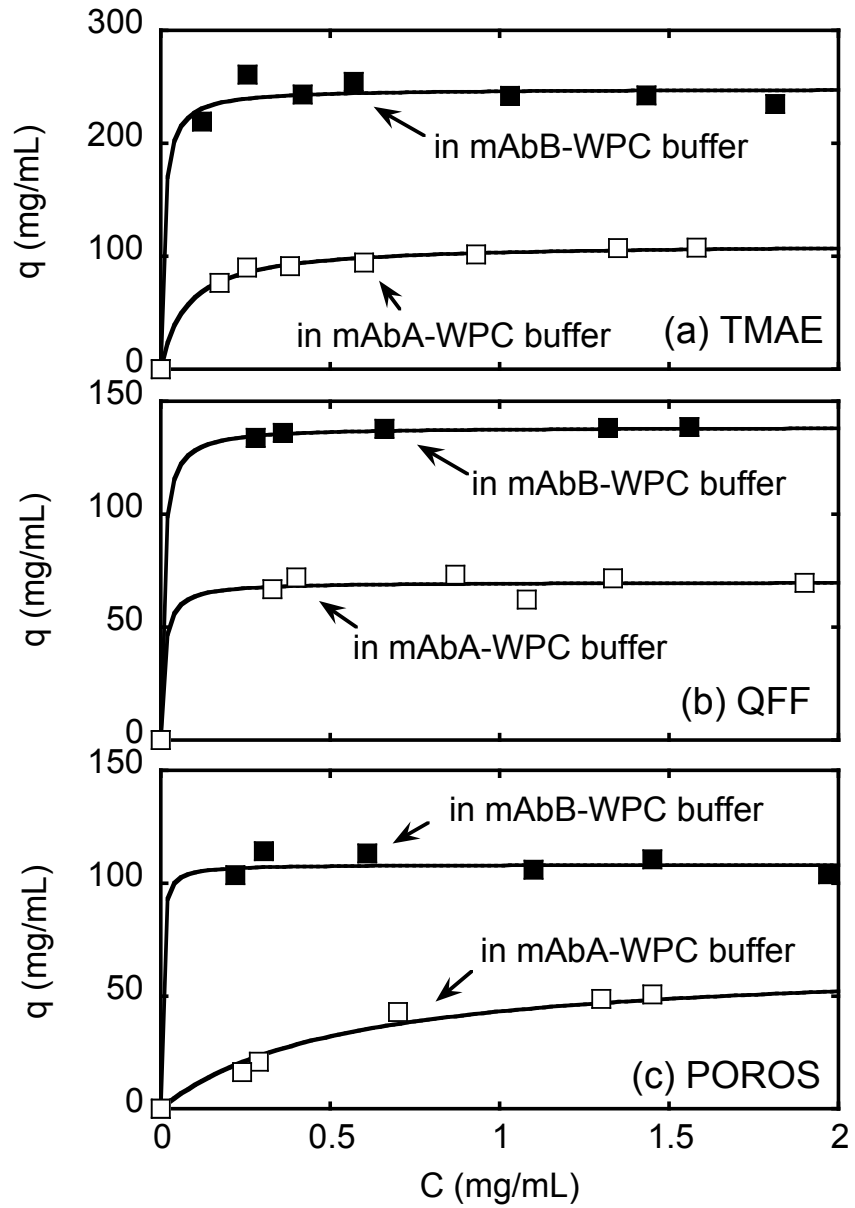


Figure 4.4. Adsorption isotherms for BSA in the buffers selected for WPC of mAbA (open squares) and WPC of mAbB (filled squares). Lines are based on the Langmuir isotherm. Note the different  $q$ -axis scale in (a).

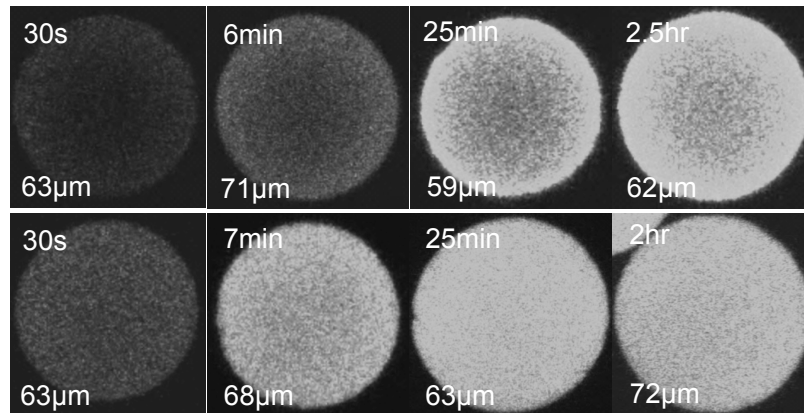
POROS. This result is likely a consequence of the tentacle structure of TMAE, which facilitates interactions between the resin's charged groups and the protein.

#### 4.3.4 CLSM Imaging

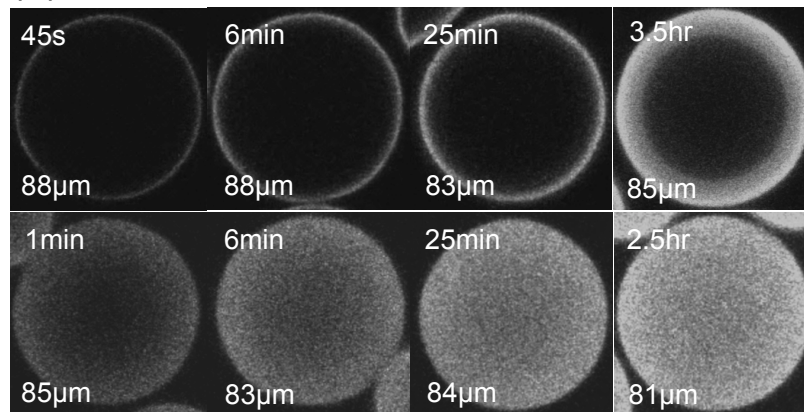
The goal of the CLSM experiments was to elucidate the spatial distribution of protein within the particles during transient adsorption of BSA and of the mAbB multimeric species. Results are given in Figs. 4.5 and 4.6 as gray scale images which more faithfully reproduce the observed fluorescence intensity patterns than the color microscope pictures. Figure 4.5 shows the CLSM images for BSA binding to the three resins for the conditions of Fig. 4.4 at a total (labeled plus unlabeled) BSA concentration of 0.5 mg/mL for all three resins. For each resin, the top row corresponds to the mAbB WPC buffer (i.e. lower ionic strength and higher pH), which leads to stronger BSA binding, while the bottom row corresponds to the mAbA WPC buffer (i.e. higher ionic strength and lower pH), which leads to weaker BSA binding. As seen in Fig. 4.5a, BSA binding occurs rapidly on TMAE in both WPC buffers. Moreover, the protein appears to be distributed spatially in a fairly uniform manner within the particles starting very early on during transient adsorption, which is especially evident on the mAbA WPC buffer (bottom row in panel a). This result is consistent with prior results by Corbett et al. [11] at pH 8.5 and suggests that a solid-diffusion mechanism where the protein migrates while interacting with the charged tentacle ligands is likely responsible for the fast transport kinetics observed in our experiments.

The results for QFF (Fig. 4.5b) are quite different dependent on the buffer. In the mAbB WPC buffer (top row in panel b), when conditions favor very strong binding and a high binding capacity is observed (*cf.* Fig. 4.4b), transport is very slow and even after 3.5 h,

(a) TMAE



(b) QFF



(c) POROS

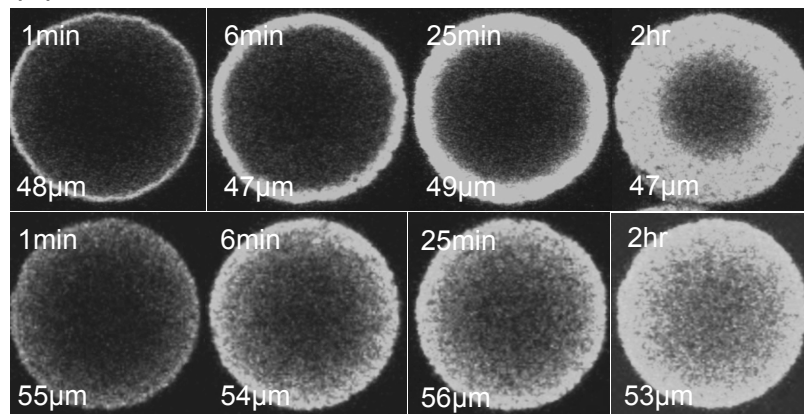


Figure 4.5. CLSM images of particles of TMAE (a), QFF (b) and POROS (c) during adsorption of 0.5 mg/mL BSA in the mAbB WPC buffer (top row in each panel) and in the mAbA WPC buffer (bottom row in each panel). The time and actual particle diameter are shown in each image.

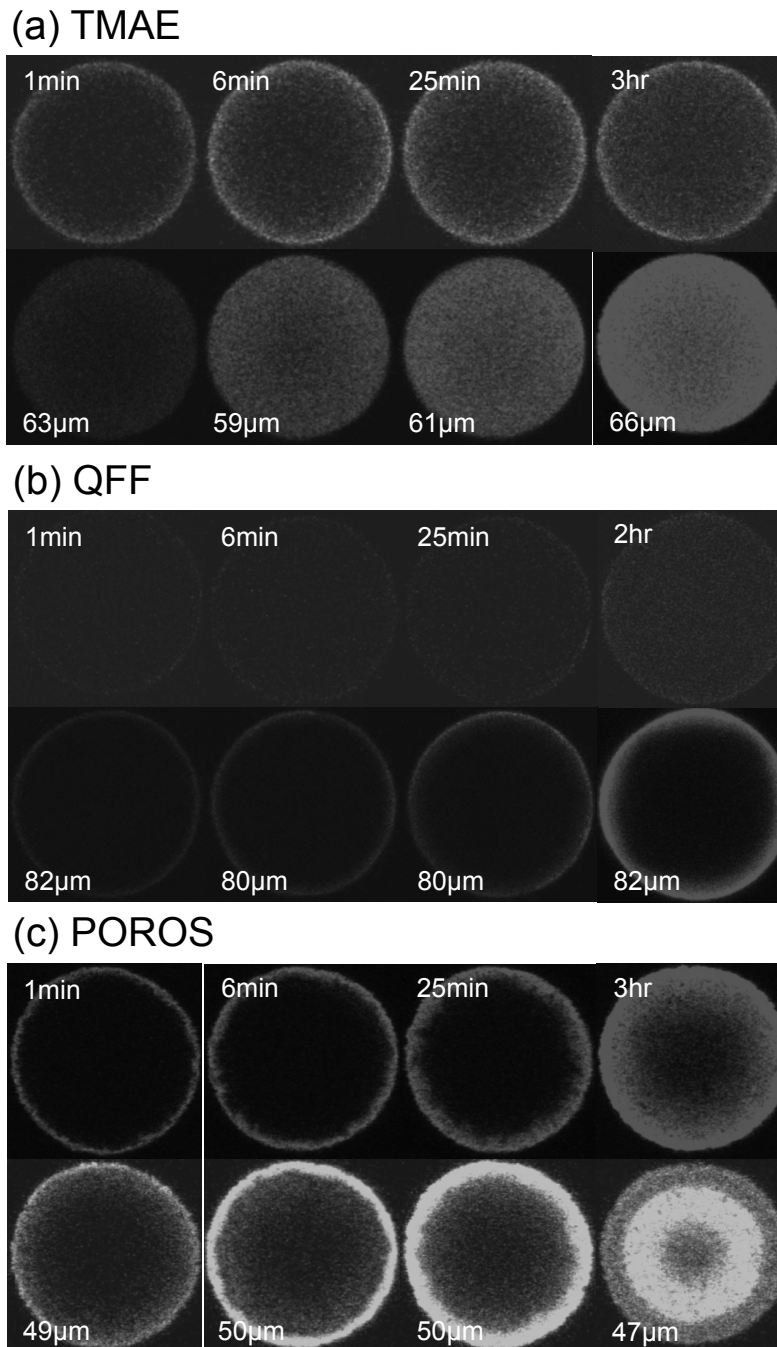


Figure 4.6. CLSM images of particles of TMAE (a), QFF (b) and POROS (c) during co-adsorption of 0.5 mg/mL BSA and 0.5 mg/mL of mAbB multimeric species in the mAbB WPC buffer. The top row in each panel shows the multimeric species while the bottom row in each panel shows BSA for the same particle at the time indicated. The actual particle diameter is shown in each image.

the bound BSA is confined to a relatively thin layer near the particle outer surface. We believe that this is a result of the high concentration of bound BSA, which partially blocks the relative small pores in this resin, and the high binding strengths, which prevents surface diffusion. On the other hand, in the mAbA WPC buffer (bottom row in panel b), the BSA adsorption kinetics is much faster as indicated by a nearly uniform saturation of the bead at 25 min, which is likely a result of the lower BSA binding capacity and weaker interactions with the charged ligand which provide a surface diffusion contribution to the mass transfer flux [34].

The results for POROS (Fig. 4.5c) show qualitatively similar, but quantitatively different adsorption kinetics in the two buffers. In the mAbB WPC buffer (top row in panel c), where BSA binds much more strongly, the adsorption kinetics is relatively slow and is controlled by diffusion in the resin pores according to the well known shrinking core model [33]. In the mAbA WPC buffer (bottom row in panel c) the resin appears to be saturated more quickly, but this is primarily a consequence of the much smaller binding capacity at the 0.5 mg/mL BSA concentration used. Note that for these conditions, the BSA isotherm is only slightly favorable (*cf.* Fig. 4.4c), which explains the smoother concentration profiles seen for this case.

Figure 4.6 shows the CLSM images for the simultaneous adsorption of 0.5 mg/mL mAbB multimeric species (using Rhodamine-labeled multimer as a tracer, top row in each panel) and 0.5 mg/mL BSA (using DyLight 488-labeled BSA as a tracer, bottom row in each panel) for all three resins in the mAbB WPC buffer. As seen in Fig. 4.6, simultaneous adsorption of the multimeric species and BSA occurs in both TMAE (Fig. 4.6a) and POROS (Fig. 4.6c), albeit following different patterns of intraparticle concentration

profiles. Little adsorption of the multimer is seen, however, on QFF, while BSA adsorption at 25 min is confined to a thin layer near the bead surface, consistent with Fig. 4.5b for adsorption of BSA alone. This result is likely caused by the small pore size of QFF, which prevents diffusion of the multimer species into the beads in the presence of the strongly bound BSA. Although both TMAE and POROS can simultaneously adsorb the multimeric species and BSA, the differences in the binding patterns are striking. In the case of TMAE (Fig. 4.6a), while the multimer species at 25 min is mainly confined to a layer near the bead surface (top row), BSA is rapidly adsorbed and appears to have saturated the particle at the same time (bottom row). On the other hand, in the case of POROS (Fig. 4.6c), at 25 min both the multimer species and BSA are adsorbed predominantly in a layer at the bead surface indicating that their co-adsorption is strongly mass transfer limited. After 3 h, however, the bound BSA (bottom row) appears to be displaced by the incoming multimeric species and concentrates near the center of the particle. Longer times were not investigated since they would exceed the times scales that are representative of the actual process.

#### **4.4 Conclusions**

The principal finding of this work is that conditions can indeed be found where both acidic impurities (represented by BSA in this study) and basic impurities (represented by a mAb multimeric species in this study) are simultaneously strongly bound on AEX resins while the mAb monomer is only weakly retained. The behavior of the mAb dimer in this study is intermediate showing stronger chromatographic retention than the mAb monomer, but overall weak binding. It is apparent that selecting WPC operating conditions solely based on the product  $K_p$ -value in the range 0.1-3 provides only some

guidance as the overall performance is ultimately highly dependent on the structure of the particular resin used. In our study, TMAE showed slow diffusion for both mAb monomer and dimer species but rapid rates of adsorption for BSA, which uniformly saturated the resin beads. For the same conditions, in co-adsorption experiments with BSA, the multimeric species also adsorbed rapidly although binding appeared to be restricted predominately to a relatively thin layer near the resin bead surface, likely as a result of the large size of the multimeric species and its inability to quickly diffuse within the tentacle structure of this resin.

Binding of BSA on QFF was found to be highly dependent on the particular WPC buffer used with indications of different rate mechanisms prevailing under different conditions. Likely as a result of its small pore size, this resin seemed unable to effectively adsorb the mAb multimer under WPC conditions.

Finally, POROS was able to bind both the multimeric species and BSA under WPC conditions. In the mAbB WPC buffer, both of these species were strongly bound showing evidence of competitive displacement of the bound BSA by the multimeric species.

Overall, TMAE had the advantage of a very high binding capacity and fast rate of adsorption of BSA while nearly completely excluding the mAb monomer. POROS, on the other hand, seem to have the best resolution ability for the separation of mAb monomer and dimer under WPC conditions. Obviously, there seems to be no absolute best resin among the three studies and the choice will be ultimately dependent on what the main goal of the WPC step as well as on consideration of the rates of adsorption that can be obtained as a result of different resin architectures and varying buffer compositions.

#### 4.5 Reference

- [1] Kelley, B. Very large scale monoclonal antibody purification: The case for conventional unit operations. *Biotechnol. Prog.* 2007; 23: 995–1008.
- [2] Hober S, Nord K, Linhult M. Protein A chromatography for antibody purification. *J. Chromatogr. B* 2007; 848: 40-47.
- [3] Kelley BD, Tobler SA, Brown P, Coffman JL, Godavarti R, Iskra T, Switzer M, Vunnum S. Weak partitioning chromatography for anion exchange purification of monoclonal antibodies. *Biotechnol. Bioeng.* 2208; 101: 553-566.
- [4] Yamamoto S, Nakanishi K, Matsuno R. Ion-exchange chromatography of proteins. New York: Marcel Dekker, 1988
- [5] Fernandez MA, Carta G. Characterization of protein adsorption by composite silica-polyacrylamide gel anion exchangers I. Equilibrium and mass transfer in agitated contactors. *J. Chromatogr. A* 1996; 746: 169-183.
- [6] Fernandez M, Laughinghouse SW, Carta G. Characterization of protein adsorption by composite silica-polyacrylamide gel anion exchangers II. Mass transfer in packed columns and predictability of breakthrough behavior. *J. Chromatogr. A.* 1996; 746: 185-198.
- [7] Janzen R, et al. Adsorption of proteins on porous and non-porous poly (ethyleneimine) and tentacle-type anion exchangers. *J. Chromatogr. A.* 1990; 522: 77-93.
- [8] Miyabe K, Guiochon G. Kinetic study of the mass transfer of bovine serum albumin in anion-exchange chromatography. *J. Chromatogr. A.* 2000; 866: 147-171.

- [9] Staby A, Jensen IH, Mollerup I. Comparison of chromatographic ion-exchange resins: I. Strong anion-exchange resins. *J. Chromatogr. A.* 2000; 897: 99-111
- [10] Zhu M, Carta G. Adsorption of polyethylene-glycolated bovine serum albumin on macroporous and polymer-grafted anion exchangers. *J. Chromatogr. A.* 2014; 1326: 29-38.
- [11] Corbett R, Carta G, Iskra T, Gallo C, Godavarti R, Salm JR. Structure and protein adsorption mechanisms of clean and fouled tentacle-type anion exchangers used in a monoclonal antibody polishing step. *J. Chromatogr. A.* 2013; 1278: 116–25.
- [12] Burchiel SW, Billman JR, Alber TR. Rapid and efficient purification of mouse monoclonal antibodies from ascites fluid using high performance liquid chromatography. *J. Immun. Meth.* 1984; 69: 33-42.
- [13] Vetter TA, et al. Mixed-beds of strong and weak anion exchange resins for protein separations with step-induced pH gradients. *Sep. Sci. Technol.* 2014; 49: 477-489.
- [14] Ansaldi D, Lester P. Separation of polypeptide monomers. U.S. Patent 6,620,918, 2003.
- [15] Wan M, Wang GY. Enhanced aggregate removal from bulk biological using ion exchange chromatography. US Patent 6,177,548, 2001.
- [16] Suda EJ, Thomas KE, Pabst TM, Mensah P, Ramasubramanian N, Gustafson ME, Hunter AK. Comparison of agarose and dextran-grafted agarose strong ion exchangers for the separation of protein aggregates. *J. Chromatogr. A.* 2009; 1216: 5256-5264

- [17] Pezzini J, Cabanne C, Santarelli X. Comparative study of strong anion exchangers: Structure-related chromatographic performances. *J. Chromatogr. B.* 2009; 877: 2443-2450.
- [18] Shi QH, Jia GD, Sun Y. Dextran-grafted cation exchanger based on superporous agarose gel: Adsorption isotherms, uptake kinetics and dynamic protein adsorption performance. *J. Chromatogr. A.* 2010; 1217: 5084-5091.
- [19] Afeyan NB, Fulton SP, Regnier FE. Perfusion chromatography packing materials for proteins and peptides. *J. Chromatogr. A.* 1991; 544: 267-279.
- [20] Yao Y, Lenhoff AM. Pore size distributions of ion exchangers and relation to protein binding capacity. *J. Chromatogr. A.* 2006; 1126: 107-119.
- [21] Kelley BD, et al. High-throughput screening of chromatographic separations: IV. Ion-exchange. *Biotechnol. Bioeng.* 2008; 100: 950-963.
- [22] Reck JM, et al. Adsorption equilibrium and kinetics of monomer–dimer monoclonal antibody mixtures on a cation exchange resin. *J. Chromatogr. A.* 2015; 1402: 46-59.
- [23] Ahrer K, et al. Analysis of aggregates of human immunoglobulin G using size-exclusion chromatography, static and dynamic light scattering. *J. Chromatogr. A.* 2003; 1009: 89-96.
- [24] Stone MC, Carta G. Protein adsorption and transport in agarose and dextran-grafted agarose media for ion exchange chromatography. *J. Chromatogr. A.* 2007; 1146: 202-215.
- [25] Hagel L, Ostberg M, Andersson T. Apparent pore size distributions of chromatography media. *J. Chromatogr. A.* 1996; 743: 33-42.

- [26] Hagel L. In: P.L. Dubin (Ed.), *Aqueous size-exclusion chromatography*. Amsterdam: Elsevier, Amsterdam, 1988: p. 119.
- [27] Bird RB, Stewart WE, Lightfoot EN, *Transport phenomena* (2<sup>nd</sup> edition). New York: Wiley. 2006.
- [28] Zhang S, et al. Structural and functional characteristics of virgin and fouled protein A MabSelect resin cycled in a monoclonal antibody purification process. *Biotechnol. Bioeng.* 2016; 113: 367-375.
- [29] Carta G. Exact analytic solution of a mathematical model for chromatographic operations. *Chem. Eng. Sci.* 1988; 43: 2877-2883.
- [30] Perez-Almodovar EX, Tao Y, Carta G. Protein adsorption and transport in cation exchangers with a rigid backbone matrix with and without polymeric surface extenders. *Biotechnol. Prog.* 2011; 27: 1264-1272.
- [31] Tao Y, Perez-Almodovar EX, Carta G, Ferreira G, Robbins D. Adsorption kinetics of deamidated antibody variants on macroporous and dextran-grafted cation exchangers. III. Microscopic studies. *J. Chromatogr. A.* 2011; 1218: 8027-8035.
- [32] Wu Y, et al. "Protein and virus-like particle adsorption on perfusion chromatography media. *J. Chromatogr. A.* 2013; 1297: 96-105.
- [33] Carta G, Jungbauer A. *Protein chromatography: process development and scale-up*. Weinheim: Wiley VCH, 2010.
- [34] Dziennik SR, et al. Nondiffusive mechanisms enhance protein uptake rates in ion exchange particles. *Proc. Nat. Academ. Sci.* 2003; 100: 420-425.

## 5 Chapter 5

### Conclusions and Recommendations

---

This work has examined the key process parameters in a two-step monoclonal antibody purification process which includes a Protein A capture step followed by an anion exchange step operated in weak partitioning mode. For the first part of this work, macroscopic studies, including protein adsorption and desorption and inverse size exclusion chromatography, showed that cycled Protein A MabSelect resin had lower binding capacity, slower mass transfer and decreased intraparticle porosity. Foulants were imaged both as films at resin bead surface and as granules inside pores under TEM and CLSM. Further microscopic studies using molecular probes revealed that the fouling was caused by the aggregate formation mainly caused by the hydrophobic interaction between mAb and lipophilic proteins while the mAb was bound to the Protein A ligand.

It seems that in this work the resin sample taken from the bottom of the Protein A column fouled slightly more than the resin samples taken from the top of the Protein A column. Future study focusing on the difference between the top and bottom of the Protein A column could be helpful to further understand the fouling in this study.

From practical point of view, slower mass transfer for cycled resin resulted in broader chromatographic profiles and therefore increased product pool volume. Process yield loss was mainly caused by the formation of aggregates involving mAb during elution process. Although as mentioned above, a more aggressive cleaning strategy was shown to effectively remove the foulants, the process yield was still low since the mAb contained in the foulants could not be recovered in the harsher cleaning method. Further studies

based on this work could be potentially useful to increase the lifetime of Protein A MabSelect resin as well as maintain a high process yield. First, since this work elucidated that the interaction between mAb and lipophilic protein is hydrophobic driven, a wash step targeting at interrupting the hydrophobic interaction could potentially be incorporated to the process after primary wash step with loading buffer. The effects of additives in the wash buffer, such as organic solvents, could be studied for this purpose. An alternative method may be a wash step using an intermediate pH buffer or a pH gradient. Second, as mentioned above, since mAb conformational change on Protein A ligand was responsible for the binding of lipophilic proteins, method could be developed to “loosen” the binding between mAb and Protein A ligand. This could potentially be achieved by either through new engineered Protein A ligand or modification of existing Protein A ligand. Third, since hydrophobic interaction is affected by temperature, the effects of temperature on the Protein A fouling could be studied.

The second part of this work compared the structural and performance differences among three commonly used AEX resins under weak partitioning conditions. iSEC experiments were shown to be effective at predicting the accessibility of protein to ligands for open pore structured resins such as Q Sepharose FF and POROS 50HQ. iSEC, on the other hand, was less effective to predict the accessibility of protein species to ligands in tentacle typed resin such as TMAE HiCap, mainly because of the more complicated interactions involving both protein size exclusion effects with tentacles and protein charge interaction with ligands. This work showed that weak partitioning conditions could be screened for all three resins where target mAb monomer interacts least strongly and impurities including mAb dimer, multimer and more acidic proteins interact stronger

with the ligands. As a result, all three resins were shown to be effective at acidic impurity capturing represented by BSA batch and CLSM adsorption studies. Q Sepharose FF, however, showed very poor capturing of mAb multimer species mainly because of the relatively small pore size of this resin. The mass transfer for BSA adsorption was shown to be very fast and least dependent on conditions on TMAE HiCap while more dependent on conditions on both Q Sepharose FF and POROS 50HQ. On the other hand, POROS 50HQ demonstrated best resolution between mAb monomer and dimer probably because of the relatively smaller bead sized of this resin. Therefore, although TMAE HiCap showed most potential to be a platform candidate for the AEX step because of its exclusion of mAb monomer, high impurity binding capacity and fast mass transfer rate, the ultimate decision should still be made based on the impurity contents in Protein A pool and the purpose of the AEX step. A further consideration for this work is that other impurities should also be considered to decide which resin to choose for a certain product. For example, DNA and most virus partials are negatively charged at pH above 7, the mAb multimer studied in this work probably indicates that the size of these two species may be too large to be effectively captured by Q Sepharose FF. Other resins with different structural characteristics could be considered for the extension of this work. For example, open pore structured resin with larger pore size than Q Sepharose FF and resin with intermediate length of tentacles could both be potentially good candidates.